Simulation of High Strain Rate Deformation in Structural Polymeric Foam: Innovation Report

by

Craig Robert Carnegie

A thesis submitted in partial fulfilment of the requirements for the degree of Doctor of Engineering

University of Warwick, WMG

December 2016

Declaration

This Innovation Report is submitted to the University of Warwick in support of my application for the degree of Doctor of Engineering. It has been composed by myself and has not been submitted in any previous application for any degree.

The work presented (including data generated and data analysis) was carried out by the author.

Acknowledgements

Academic Mentors: Professor Richard Dashwood, Dr Richard Beaumont and Professor Darren Hughes

Industrial Mentor: Dr Mark Blagdon

Funding Body: EPSRC and Jaguar Land Rover

Firstly I would like to thank the University of Warwick, EPSRC and Jaguar Land Rover for supporting this project, in particular Professor Richard Dashwood for giving me the opportunity and Professor Darren Hughes for taking up the reins toward the end. Both of which helped guide the project into the portfolio it has become. A thanks also goes to Dr Mark Blagdon for providing an insight into Jaguar Land Rover and helping to identify areas of improvement.

A very special thanks goes to my supervisor Richard Beaumont ("The confusion is there to guide you") who took on the role exceptionally well and has been approachable and considerate throughout. To the people that made the experience a fun one; Sanjeev Sharma, Scott Taylor, Elspeth Keating and Neill Wrath. To Dave Williams for taking an interest and having my back.

A massive thanks goes to Sarah, to whom I owe a lot of time; especially in the final few months. To my family, who were always there when I needed them; Mum, Dad and especially Duncan for carrying me when I was having an off day. And finally to Alice, whom without I may not have taken the path of Engineering, but having done so I am eternally grateful.

Abstract

Passenger safety within vehicles is a priority for automotive companies in order to meet both the regulations and customer expectations. The safety critical materials, those used for absorbing energy during a crash, are simulated with FEA in order to design and improve components and to reduce the requirement for physical testing, which in turn saves on development time and cost.

The simulation capabilities of Jaguar Land Rover were identified as lacking in accuracy for energy absorbing materials. Quasi-static and dynamic testing of expanded polypropylene as coupon samples and vehicle components was carried out to assess their stress-strain responses, energy absorption capabilities and strain rate effects. Using the properties within FEA the mechanical behaviour of the material was predicted and validated against the physical testing. Updated material models were implemented back into Jaguar Land Rover that fully incorporate strain rate effects and contain reliable, traceable input data. The material models require stress-strain curves, density, material modulus and un-loading characteristics.

A test methodology has been implemented into Jaguar Land Rover for characterising energy absorbing materials, something that was previously unavailable. This includes the use of three machines, a low strain rate Instron 5800R, a high strain rate Drop Tower and a Very High Strain rate (VHS) testing rig; each used to understand the effect of compression testing at a range of strain rates and under decelerating/constant velocity impact conditions.

Energy absorbing materials were sourced from two foam manufacturers. It was shown that different manufacturer's material performed differently, even when supplied to the same requirement and manufactured from the same precursor. Computed tomography under synchrotron radiation was utilised to inspect material differences, identifying possible causes for stress-strain changes under compression. From the images a 3D mesostructural model was created to predict the material performance during deformation.

As a result Jaguar Land Rover procedures were changed, increasing FEA capabilities and increasing the utilisation of foam within the vehicle. New test procedures were implemented for characterising future energy absorbing materials.

The simulation and computed tomography work will help towards the understanding of foam compression mechanisms.

Table of Contents

1 Introduction to Energy Absorbing Materials in the Automotive Industry, Objectives of the Project and Portfolio Layout 1

1.1 Project Specification and Objectives 1

1.2 Research Question 2

1.3 Innovation Summary 3

1.4 Contribution to Knowledge 4

1.5 Portfolio Layout 5

1.6 Structure of the Innovation Report 6

2 Literature Review: Characterisation, Testing and Simulation of Energy Absorbing Materials (Submission One) 7

2.1 Material Characterisation and Selection 7

2.1.1 Sample Orientation 9

2.1.2 Density Distribution 9

2.1.3 Sample Preparation 10

2.2 Analytical Solutions for Predicting Material Performance 10

2.3 Test Methods and Strain Rate Effects 13

2.3.1 Strain Rate Effects 13

2.4 Simulation: Selection of Material Models 16

2.4.1 Continuum Modelling 16

2.4.2 3D Mesostructural Modelling 18

2.5 Review of Current Practices within Jaguar Land Rover 19

2.5.1 Testing 19

2.5.2 Simulation 19

2.6 Identification of Gap in Knowledge and Industrial Need 20

3 Simulation of Expanded Polypropylene: The Review and Improvement of JLR Practices (Submission Two) 22
3.1 Review of Previous Methodologies 22
3.2 Model Creation and Recommended Simulation Methods 24
3.2.1 Element Formulation and Mesh Size 25
3.2.2 Surface Contacts 26
3.3 Selection of Material Models 27
3.4 Manufacturers of EPP and Supplier to JLR 27
3.4.1 EUEPP 27
3.4.2 UKEPP 28
3.5 Incorporating a Material Dataset: EUEPP Drop Tower 28
3.6 Validation of Material Models 30
3.6.1 Quantifying a Vehicles Safety 35
3.7 Summary 37
4 Geometry Investigation: Stress-Strain Response of Expanded Polypropylene, Strain Rate Effect and Production Variation (Submission Three) 39
4.1 Material Selection and Sample Preparation 40
4.2 Test Methodologies: Strain Rate Sensitivity Investigation 41
4.2.1 Quasi-Static Compression Test Methodology 43
4.2.2 Drop Tower Test Methodology 45
4.2.3 VHS Test Methodology 47
4.3 Procedures for Data Processing 49
4.4 Test Specification Comparison 51
4.5 EUEPP Dataset Validation 54
4.6 Material Performance across Manufacturers 55
4.6.1 Strain Rate Effect 57

4.7 Final Review of Material Models with Validation 60
4.7.1 Strain Distribution using Digital Image Correlation 62
4.8 Effect of Production Methods 64
4.8.1 Density Distribution 65
4.8.2 Exterior Skin Layer 68
4.8.3 Multiple Layers of Material 68
4.8.4 Sample Size 71
4.9 Summary 72
5 Micromechanics of Expanded Polypropylene: Computed Tomography and 3D Simulation (Submission Four) 75
5.1 Internal Structure of EPP 75
5.1.1 Predicting the Effect of Material Distribution 76
5.2 Computed Tomography at WMG 77
5.3 International Placement: ESRF (Submission Five) 79
5.4 X-Ray Technology and its Utilisation 80
5.5 Experimental Procedure for the use of Synchrotron Radiation 81
5.6 Differences between Manufacturers Foam 82
5.7 In-situ Compression of Foam 84
5.8 3D Mesostructural Simulation 87
5.9 Summary 90
6 Review of Research Impact 92
6.1 Research within Submissions 92
6.2 Informative Documentation 92
6.3 Material Testing and Database 93
6.3.1 Test Methodology 93
6.3.2 Expanded Polypropylene Test Data 94

6.4 Simulation of Foam 94
6.4.1 LS-DYNA models 94
6.4.2 Material Models for Simulation 95
6.5 Spreadsheet for Data Extrapolation 95
6.6 Additional Contributions outside of Jaguar Land Rover 95
6.6.1 ESRF User Documentation 96
6.6.2 EUEPP Data validation 96
7 Conclusions and Recommendations 97
7.1 Characterisation 98
7.2 Simulation 99
7.3 Material Testing 101
7.4 EPP Microstructure 103
7.5 Summary of Key Achievements and Contributions to Innovation 105
7.6 Further Work 107
7.6.1 Material characterisation 107
7.6.2 Utilising EPP 107
7.6.3 Material Testing 108
7.6.4 Production 108
7.6.5 Simulation 109
7.6.6 Computed Tomography 109
7.6.7 Review for Jaguar Land Rover 110
References 111

Table of Figures

Figure 1: Typical stress-strain curve for polymer foam (Goga 2010) 7
Figure 2: a) Open Cell Foam and b) Closed Cell Foam (Goga 2010) 8
Figure 3: Cell collapse mechanics. a) Free body diagram with failure mechanics of b) buckling, c) yielding and d) fracture (Ashby 2006) 10
Figure 4: Stress–strain curves for two different EPP foam microstructures. (Bouix et al 2009) 14
Figure 5: Foam Characterisation Equipment. a) Testing fixture and b) Foam dimensions 19
Figure 6: Stress - strain response for a sample of 170 kg.m^{-3} EPP compared to the two material models that represent it within JLR. Showing the use of a ramped value for stability 24
Figure 7: Cube Validation Model within LS-DYNA 25
Figure 8: Simulation output with varied FEA Elements 26
Figure 9: Original material card data compared to quasi-static and drop tower testing for 60 kg.m^{-3} EPP. Circles indicate areas of missing curve accuracy for EPPFOAM60 ... 29
Figure 10: a) JLR's drop tower configuration and b) LS-DYNA Simulation 31
Figure 11: Component Testing carried out by JLR Compared to their original material inputs for simulation titled “ARPRO” 31
Figure 12: Component Testing carried out by JLR Compared to their original material inputs for simulation titled “EPPFOAM” 32
Figure 13: Replacement Material input used in the validation simulation 33
Figure 14: Simulation of Head Impact block using most recent Material 83 input 34
Figure 15: Cross section of a full vehicle model for HIC analysis 35
Figure 16: Block location within a Land Rover vehicle 35
Figure 17: Comparison between a) original, b) new MAT_57 and c) new MAT_83 material definitions against the HIC test 36
Figure 18: Instron 5800R Compression Rig 43
Figure 19: Velocity Profile of a 200 mm.min^{-1} compression test on the Instron 5800R 43
Figure 20: Compression plates for the 5800R testing rig 44
Figure 21: Instron Drop Tower 45

Figure 22: Custom made impactors for the Drop Tower. Flat plate (Left) and Cylindrical (Right) 46
Figure 23: Instron VHS 47
Figure 24: Compression plates on the VHS testing rig 48
Figure 25: The a) raw Load/Time and b) Displacement/Time data from a drop tower test of 60 kg.m^{-3} EPP at 3.5 m.s^{-1} 49
Figure 26: Post processed a) Load/Time and b) Displacement/Time data from a drop tower test of 60 kg.m^{-3} EPP at 3.5 m.s^{-1} 50
Figure 27: Load/Displacement Curve from a drop tower test having been filtered and zeroed for a 60 kg.m^{-3} EPP compressed at 3.5 m.s^{-1} 50
Figure 28: Velocity - Displacement and Load -Displacement for a sample of EPP 30 kg.m^{-3} under the three test conditions available from the Drop Tower and VHS 51
Figure 29: Stress-Strain curves for 30 kg.m^{-3} EPP at 5m.s^{-1} on the Drop Tower and VHS 52
Figure 30: Stress-Strain curves for 60 kg.m^{-3} EPP at 2.5m.s^{-1} on the Drop Tower and VHS 53
Figure 31: Manufacturer and Validation stress-strain data for 30 kg.m^{-3} EPP..... 54
Figure 32: VHS testing of two supplier's material at three different velocities; a) 0.1, b) 2.5 and c) 5 m.s^{-1} 56
Figure 33: Drop Tower velocity outputs for 60 kg.m^{-3} EPP 58
Figure 34: VHS stress-strain outputs for 60 kg.m^{-3} EUEPP EPP with an increasing velocity..... 59
Figure 35: Materials Young's Modulus and Yield Stress with an increase in Strain rate for 60 kg.m^{-3} EUEPP EPP 59
Figure 36: FEA models used for testing and validating test data; a) Coupon and b) Cylindrical Impactor..... 60
Figure 37: Material Model input curves used to compare the cylindrical impact simulations..... 61
Figure 38: Cylindrical impact response from testing and simulation of 50 kg.m^{-3} 61
Figure 39: Strain distribution from a compression test using DIC (top row) and the simulated test in LS-DYNA (bottom row); at 0, 10 and 20 % engineering strain. 63

Figure 40: Strain mapping using DIC for a cylindrical impactor on EPP with an initial energy of 100J 63
Figure 41: Strain mapping from LS-DYNA for a cylindrical impactor on EPP 64
Figure 42: Cross section of 20 kg.m^{-3} part with samples taken from the corner to the centre of the block..... 65
Figure 43: Density variation within a block of foam. The dotted line represents the layers average density 66
Figure 44: Average Stress-Strain response of Layer A and Layer B..... 66
Figure 45: Yield and Densification stage of Layer A and Layer B showing the maximum and minimum responses. a) Yield of Layer A, b) densification of Layer A, c) yield of Layer B, d) densification of Layer B. 67
Figure 46: Strain calculations for the skin layer taking into account only the foamed material..... 68
Figure 47: Stress-strain response for a block of 60 kg.m^{-3} and a layered equivalent 70
Figure 48: Stress-strain response for each layered combination..... 71
Figure 49: Sample variation for a block of 60 kg.m^{-3} EPP at 2 m.s^{-1}..... 72
Figure 50: X, Y and Z axis cross section of a sample of 80 kg.m-3 EPP using the Nikon CT system with a 50 µm voxel resolution..... 78
Figure 51: Schematic of the building layout; showing the individual beamlines (ESRF, 2016)..... 79
Figure 52: Novitom5K Compression Fixture on ID19 81
Figure 53: Scans during experimental procedures that show the corresponding strain during each compression test 82
Figure 54: XY slice from a sample of unloaded EUEPP (left) and UKEPP (right) 80 kg.m^{-3} EPP 83
Figure 55: Cell Structure of an unloaded EUEPP (left) and UKEPP (right) 80 kg.m^{-3} EPP83
Figure 56: EUEPP 80 kg.m^{-3} under Macro B conditions: a) Stress Response b) 0, c) 0.2, d) 0.4, e) 0.6 and f) 0.8 strain. Highlighting the displacement and collapse of a bead (yellow) 85
Figure 57: EUEPP 80 kg.m^{-3} under Macro C conditions: a) Stress response, b) 0, c) 0.02, d) 0.05, e) 0.07 and f) 0.1 strain. 86

Figure 58: FEA models from a a) 50 micron resolution scan and b) a 5 micron resolution scan 88
Figure 59: Size and resolution comparison between the two scans; ESRF - red, WMG - blue 88
Figure 60: LS-DYNA Model of 80 kg.m^{-3} EPP at a) 0, b) 0.2, c) 0.4 and d) 0.6 Strain 89
Figure 61: Strain distribution for a slice of 80 kg.m^{-3} EPP compressed in LS-DYNA..... 89
Figure 62: Material Model input curves used to compare the cylindrical impact simulations..... 100
Figure 63: Comparison between material models used for cylindrical impact simulations of 50 kg.m^{-3} EPP; created using Original JLR Data, ARPRO Data and Validation Data 101

Table of Tables

Table 1: Portfolio submissions and subchapters therein 5
Table 2: Original Material Input Data for Simulation of Expanded Polypropylene..... 23
Table 3: Data Acquired from EUEPP of their EPP analysis 30
Table 4: Residual error comparison between iterations of material models 34
Table 5: Material Specifications for Testing 40
Table 6: 5800R Machine Specification 44
Table 7: 5800R Sample Preparation 44
Table 8: 5800R Test Setup 44
Table 9: Drop Tower Machine Specification 45
Table 10: Drop Tower Sample Preparation 46
Table 11: Drop Tower Test Setup 46
Table 12: VHS Machine Specification (Compression)..... 47
Table 13: VHS Sample Preparation..... 48
Table 14: VHS Test Setup..... 48
Table 15: Specifications for an investigation into the effect of stacked material..... 69
Table 16: Comparison between contributing foam features with different fractions of material within cell edges..... 76
Table 17: Experimental Procedures created for executing the required scan conditions 82

List of Abbreviations

CAE	-	Computer Aided Engineering
DIC	-	Digital Image Correlation
EPP	-	Expanded Polypropylene
ESRF	-	European Synchrotron Radiation Facility
FEA	-	Finite Element Analysis
HIC	-	Head Injury Criterion
JLR	-	Jaguar Land Rover
MAT_57	-	LS-DYNA Material Model: Low Density Foam
MAT_83	-	LS-DYNA Material Model: Fu Chang Foam
MAT_63	-	LS-DYNA Material Model: Isotropic Crushable Foam
MAT_75	-	LS-DYNA Material Model: Bilkhu/Dubois Foam
PU	-	Polyurethane
PUR	-	Rigid Polyurethane
VHS	-	Very High Strain Rate
µCT	-	Micro Computed Tomography
TPJLR	-	Test Procedure for Jaguar Land Rover

1 Introduction to Energy Absorbing Materials in the Automotive Industry, Objectives of the Project and Portfolio Layout

This project is centred on the safety of passengers within automotive vehicles. Using energy absorbing materials to decelerate and protect an occupant during a crash is paramount to road safety. Through evaluating and understanding the material it is possible to develop their use within the automotive industry. High strain rate deformation is the dominant load case experienced during said crash; the simulation of which must be accurate and robust in order to both improve predictability and reduce physical testing required to validate their use. Improving the fidelity of simulation is therefore the goal of this investigation.

This document is an executive summary of the work that has progressed the topic. The project was broken down into sections; a review of previous investigations into energy absorbing materials, the physical response of these materials at a range of strain rates, the use of simulation within an automotive company to replicate them and finally the microstructural features that contribute to their mechanical behaviour. Each area of focus is supported by a primary document that evaluates it in detail; the executive summary will highlight the key methodologies and findings from them with references to further discussions where required.

1.1 Project Specification and Objectives

Jaguar Land Rover (JLR) is the leading premier automotive manufacturer in the UK. This project was formulated on the premise that the JLR methodology for the simulation of polymer foam during high speed deformation was not fit for purpose, especially for energy absorption. Energy absorbing foams are critical for passenger and pedestrian safety, due to their soft properties that decelerate occupants without exhibiting harmful stresses. Parts that employ the material include interior trim, door pusher blocks, seat pusher blocks and head-rests. They are designed to meet legal and consumer safety standards.

The JLR CAE (Computer Aided Engineering) foam database had last been updated in 2006 and required both validation and rework where issues were identified. Issues included the traceability of the data in order to prevent problems arising in the future, inaccurate models that lead to incorrect responses and therefore the unsafe design of components.

The following tasks were identified at the onset in collaboration with JLR and were used to define the EngD project.

- Research and deliver improved material characterisation and CAE techniques for simulating the behaviour of energy absorbing foams when subjected to high deflection, dynamic loading, specifically those that occur during vehicle crash events.
- Understand JLRs current foam material usage and functionality, CAE methodology and foam material models.
- Understand the important characteristics of current foams and identify weaknesses in current CAE methods. Investigate processing and environmental variability.
- Using DYNA CAE code, improve current modelling methods and develop a correlation test to validate improvements.

1.2 Research Question

The proposal to investigate the accuracy of polymer foam simulation requires the full characterisation of the material. This includes differences between cell structures, density change caused by manufacturing methods, the stress-strain responses that arise from said differences and the effect a wide range of test conditions has on them.

Crash events mean that the materials will deform at a high strain rate and it is therefore important to test the material in these conditions and hence to reflect this effect within the simulation; ready for accurate representation and characterisation within JLR.

Focus was put on the polymer foam expanded polypropylene (EPP), due it its energy absorption properties, as well as its ability to undergo hysteresis. JLR currently use EPP within their vehicles, so a supply chain is already in place. The material densities that were used within this project range from 20 to 170 $kg.m^{-3}$.

The following areas were investigated:

- Importance of the accuracy of the foam stress-strain behaviour used during simulation
- Compression mechanisms of the foams
- Internal Structure of polymeric foam and its influence on energy absorption
- High strain rate deformation and simulation of coupons and components

Throughout the investigation the following questions were considered in order to achieve the objectives discussed above.

- How does a foam absorb energy during compression
- Is the material strain rate sensitive and how does the strain rate affect its ability to absorb energy
- What is the effect of a decelerating mass and a constant velocity impact on foamed material deformation
- Does the manufacturing process change the foam performance
- Do suppliers achieve the same performance, based on the density that is specified
- Which material model best represents the polymer foam within CAE
- What is the distribution of mass within a sample as the density is increased
- Can a 3D mesostructural model be used to predict the compressive behaviour of a material

1.3 Innovation Summary

The deliverables that were requested by JLR have been supplied. This includes an extensive polymer foam characterisation, incorporating material knowledge and previous research completed. The literature review has become a source of

information for JLR on the manufacturing methods and consequent structural responses. It also showcases where investigations have taken place into the material, highlighting where their research can be directed.

New test methodologies for characterising energy absorbing materials have been developed; this includes a range of strain rate machines tested using different load cases. The methodologies were used to investigate the effect of compression testing on EPP. JLR can use both the test procedure and datasets to characterise new materials in the future and benchmark against them.

Using the datasets a full consolidation of EPP material models for simulation were provided, incorporating features that were previously missing, such as strain rate effects. The validated simulation methodology that represents them will provide the information for creating new geometric and material models in the future.

The original simulation methodology was poor, the development of an updated methodology significantly improved the accuracy of simulation, with a residual error reduction of 93 %.

The full process has been documented, from test design, experimentation, post-processing, validation and implementation. They represent guidelines for accurate and robust simulations which promotes occupant safety within JLR vehicles.

JLR run their simulations using the material models developed and analysed within this report. A recent system within their database allows them to access the models easily and remotely. This ensures each employee is sourcing their data from the same location and increases the reliability of their results.

1.4 Contribution to Knowledge

A high resolution FEA (Finite Element Analysis) model of a bead of Expanded Polypropylene was created and compressed within LS-DYNA for stress-strain analysis. This model was created with images collected from in-situ compression of Expanded

Polypropylene using synchrotron radiation. Analysis of the compression mechanisms under quasi-static compression has been presented.

An in depth analysis of two LS-DYNA material models (MAT_LOW_DENSITY_FOAM_57/MAT_57 and MAT_FU_CHANG_FOAM_83/MAT_83) for simulating Expanded Polypropylene has been conducted. Original validation tests were used to correlate the material data to its simulated counterpart.

A comparison between the deceleration of the typical drop tower testing and the constant velocity compression on the VHS machine for a number of material variations has been conducted. Experimental work includes density change, sample size and strain rate effects.

Two suppliers of EPP to the automotive industry have had their foams compared under a range of test conditions; including dynamic testing and µCT analysis. The change in material performance has been related to analytical solutions used to predict their performance.

1.5 Portfolio Layout

Table 1 is a list of submissions from which this report is developed and the chapters in which they are referred to is highlighted.

Table 1: Portfolio submissions and subchapters therein

Submission No.	Submission Title and Content Topics	Chapter Discussed
1	Literature Review: Material Characterisation, Manufacturing Processes, JLRs procedures	2
2	Simulation Development: Finite Element Analysis, Validation, Documentation	3
3	Geometry Investigation: Material Database, Compression Testing, Digital Image Correlation	4
4	Micromechanics of Polymer Foam using Computed Tomography: Internal Structure, In-situ Compression, Mesostructural Model	5

5	International Placement: The ESRF: Introduction to the ESRF, Synchrotron Radiation, ID19 Beamline	5

1.6 Structure of the Innovation Report

From this point forward a review into previous research is carried out on cellular solids (Chapter 2, supported by Submission One). Using this information an initial characterisation was developed for the material. As well as focussing the research into areas that were missing in both physical testing and simulation.

Having identified how the material can be simulated correctly, an investigation into JLR methods was carried out (Chapter 3, supported by Submission Two). The following section will demonstrate how this was done, and the resulting changes required to their methods in order to improve their database and resources.

Once the simulations were created, they required further validation (Chapter 4, supported by Submission Three). This involved testing on a drop tower and a Very High Strain rate machine. Manufacturers foam were compared, showing the importance for JLR in their selection of material and suppliers.

Having tested the material, it became apparent that internal mechanisms for energy absorption must vary across manufacturer's material. Therefore the internal structure was analysed using non-destructive methods, i.e. computed tomography. This section looks at the use of both WMG facilities and those available at the ESRF (Chapter 5, supported by Submission Four and Five).

The deliverables from the project and alternative innovations that have been implemented into JLR are discussed in Chapter 6. This includes networking that has been established for them.

The project is then concluded (Chapter 7), showing what has been achieved with a detailed description of innovation and where there are opportunities for future development (Chapter 7.6) of the topic and from the work presented.

2 Literature Review: Characterisation, Testing and Simulation of Energy Absorbing Materials (Submission One)

Jaguar Land Rover (JLR) identified the need for foam material characterisation and simulation techniques for high deflection crash events. This requires a review of current practices and methodologies in both testing and simulation. Any issues identified will require suggestions for improvement. Particular areas of interest were sample orientation, density distribution, analytical methods for predicting performance and the effect of variations in test conditions, including strain rate. Finally the methods for simulating cellular solids in an FEA package as a continuum and mesostructure. Therefore the literature review was tailored to investigate these key areas.

2.1 Material Characterisation and Selection

Cellular Solids have been reviewed by Semerdjiev (1982), Gibson and Ashby (1999) and Mills (2007). Manufacturing processes, material responses across a range of test conditions and theoretical analysis are included. Foamed materials tend to exhibit three phases of compression as shown in Figure 1. Each phase is attributed to a different energy absorption mechanism, including cell wall bending (linear elasticity), cell collapse (plateau) and eventual expulsion of internal air (densification).

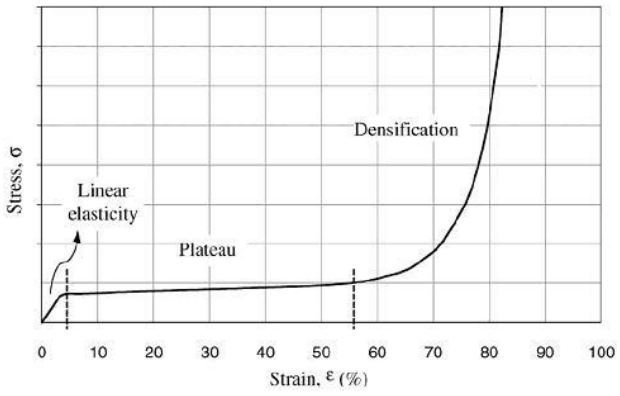

Figure 1: Typical stress-strain curve for polymer foam (Goga 2010)

Figure 2 shows the microstructure of an open and closed cell foam. An open cell foam's structure allows air to pass freely throughout the material, whereas a closed

cell encases the air within. This plays an important role in compression, especially at higher strain rates. Gibson and Ashby (1999) formulated theoretical equations for predicting the performance of polymeric foams; see Section 2.2. Closed cell foams incorporate a pressure component that applies to the gas present within the cell, it has a larger effect on foams that have a smaller Poisson's Ratio due to the reduced displacement of each cell and therefore restriction to air movement.

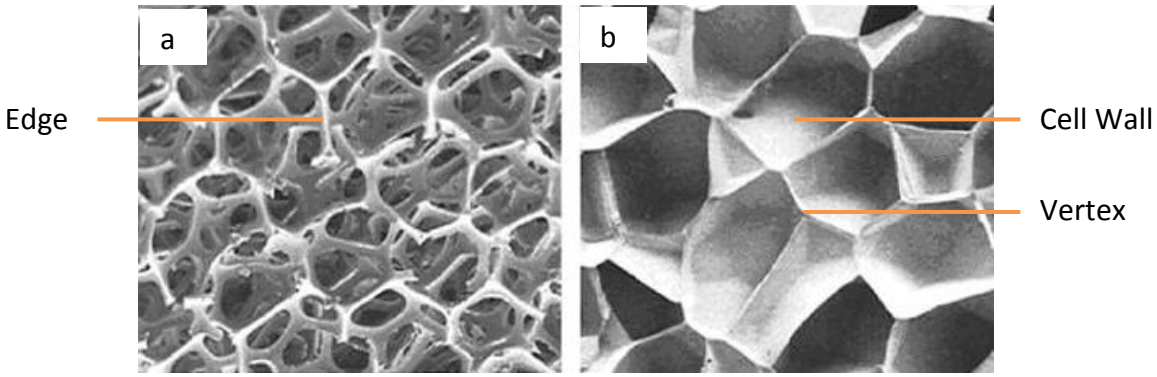

Figure 2: a) Open Cell Foam and b) Closed Cell Foam (Goga 2010)

During the manufacturing process of foams, cells expand and come into contact with adjacent cells; a pressure difference of zero between the two causes polyhedral cell shapes. Cells are made up of vertexes, edges and faces. An open cell foam experiences a collapse in the cell wall (face) during production, causing a thicker strut (edge) as the material retracts.

Polyurethane (PU) is an open cell foam, often used as a low density seat foam for comfort due to its elastic properties and hysteretic rate. An alternative, high density Polyurethane can be manufactured as a rigid foam (PUR) for energy absorption, replacing a buckling mechanism with fracture for energy absorption. Consequently, permanent damage occurs to the material during compression; which is a concern when designed for repeat loading conditions.

In order to evaluate the manufacturing process for EPP, Guo et al (2013) constructed a lab-scale autoclave system. Through increasing the saturation pressure during the annealing phase, a reduction in the melting peak for crystilinity was achieved. This resulted in a higher expansion ratio for the beads; demonstrating that the manufacturing process can affect the microstructure and therefore performance of a material.

2.1.1 Sample Orientation

PUR is formed through the mixture and chemical reaction of its two liquids counterparts; the rise direction in foam cells of polyurethane was investigated using a drop tower test by Kabir, et al (2006). Higher stresses occur when compressed in the direction of material flow, tangential to the elongation of cells. Simulation of PUR does not take into account the elongation of cells or the direction in which it happens, but it has been shown to affect its compressive properties.

Expanded polypropylene is a collection of extruded beads that are expanded in a pressure chamber and orientated within a mould randomly. The sample orientation does not affect its mechanical response.

2.1.2 Density Distribution

Mills (2007) took a deeper look into the manufacturing process of expanded polypropylene and discovered that a density distribution occurs in a single block due to the forming techniques used. Jin, et al (2007) used Digital Image Correlation (DIC) to study the density distribution effect on closed-cell polyurethane; samples from the same block can consequently have a large difference in performance. Sample preparation is discussed further in Section 4.1.

A density distribution was investigated by Bouix, et al (2009). A large block, 200 mm tall, with an optimum density of 76 $kg.m^{-3}$ had a variation between 68 and 80 $kg.m^{-3}$, for samples 23 mm cube. The exterior skin layer was recorded at 150 $kg.m^{-3}$.

Through the use of SEM imaging it has been found that cellular solids can contain irregular hexagonal or circular shaped cells; which are distributed uniformly (Chakravarty 2010). The importance of foam microstructure was discussed, having a large influence on a materials strength and ability to absorb energy. For closed cell foam a significant increase in compressive strength during high strain rate loading was attributed to the materials trapped air within each cell.

2.1.3 Sample Preparation

Raps et al (2015) conducted a large review into the manufacturing processes for a range of polymer bead foams. It was suggested that EPP has unique advantages over other foams, including energy absorption, impact resistance and flotation. The range in size of EPP bead cells was stated as being from 200 to 500 µm.

Sample preparation for rigid polyurethane was reviewed by Wijnands (2010), who found a non-destructive method of waterjet cutting had good results. However a softer material, such as expanded polypropylene has not been investigated, but could cause exterior damage due to its flexibility under high forces.

2.2 Analytical Solutions for Predicting Material Performance

Based on experimental work, Gibson and Ashby (1999) formulated equations to predict the mechanical properties of polymeric foams. These materials are either an elastomeric, elastic-plastic or brittle foam. All three exhibit a linear elastic stage, followed by a collapse plateau and finally a densification, shown in Figure 1. They attribute the linear elastic phase to cell wall bending, plus the stretching of cell walls in the case of a closed cell. Cells collapse during the plateau phase, either by buckling, yielding or fracturing as shown in Figure 3; each defining the three types of foams discussed respectively.

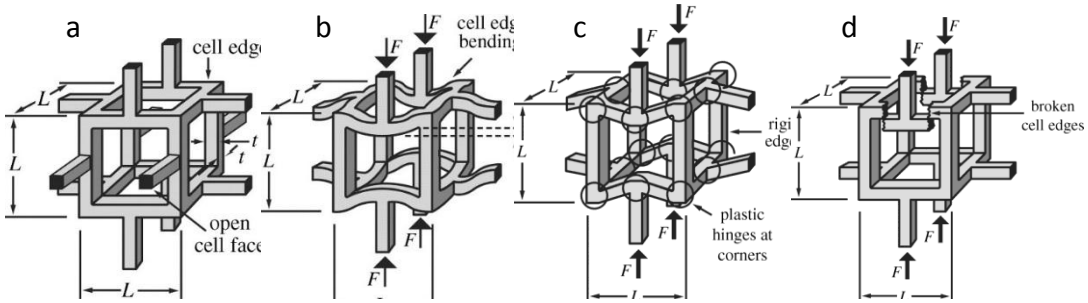

Figure 3: Cell collapse mechanics. a) Free body diagram with failure mechanics of b) buckling, c) yielding and d) fracture (Ashby 2006)

Gibson and Ashby modelled the foam cells as cubic arrays as shown in Figure 3, with strut length *l* and a square cross section *t*. The equation for Young's Modulus is derived using beam theory; a linear elastic deflection of a beam loaded at the midpoint by load

F. The deflection of a beam is proportional to Fl^3/E_sI and the compressive stress comes from $F \propto \sigma l^2$. These equations are combined with the relative density equation $(\rho^*/\rho_s) \propto (t/l)^2$ and the second moment of area $I \propto t^4$. Finally the modulus of the foam (E^*) is given by stress over strain with the strain calculated using deflection over length.

A few assumptions have been made when formulating the equations and they should therefore be applied with caution. The constant C_1 was determined using experimental data from impact tests of a range of foamed materials. The material tested by Gibson and Ashby was PU for open cell polymer foam and EPE for closed cell polymer foam. Both were found to have a C_1 value of 1; EPP is similar in internal structure to EPE and therefore the same constant will be used. In Gibson and Ashby's calculation for density cell corners were double counted. Also the material was treated as a continuum, whereas in reality cell structures will vary. The principles behind the failure mechanics still apply for all foamed materials.

The following equations are used to predict a specific area of the foams stress-strain response and are adapted to both open and closed cell. An (*) specifies a property of the foam material, whereas an (s) is the property from the solid source polymer. Equation 1 predicts the Young's modulus (*E**) of a closed cell foam, a property that increases with density.

$$\frac{E^*}{E_s} \approx \phi^2 \left(\frac{\rho^*}{\rho_s}\right)^2 + (1-\phi)\frac{\rho^*}{\rho_s} + \frac{p_0(1-2\nu^*)}{E_s(1-\frac{\rho^*}{\rho_s})}$$

A B C *Equation 1*

It contains a pressure component (p_0), to predict the effect that air pressure has on the compressive response from within each cell. The fraction of solid in the edges (ϕ) is used to equate the percentage of material within the struts versus the material in the cell walls. This isolates the contributions to modulus within a closed cell foam as the cell struts (A), cell walls (B) and air pressure (C).

Beyond the linear elastic region, an elastic collapse caused by the buckling of cell walls initiates the plateau. There are now two terms for pressure, the pressure of gas within the cell (p_0) and the external atmospheric pressure (p_{at}). The stress (σ_{el}^*) for the initiation of collapse is given by:

$$\frac{\sigma_{el}^*}{E_s} \approx 0.03\left(\frac{\rho^*}{\rho_s}\right)^2\left(1+\left(\frac{\rho^*}{\rho_s}\right)^{\frac{1}{2}}\right)^2 + \frac{p_0 - p_{at}}{E_s}$$

Equation 2

The stress is not affected by the distribution of mass in the cell walls and cell struts, instead it is the density ratio ($\frac{\rho^*}{\rho_s}$) between foam and solid material that affect the materials collapse. However an elastic-plastic foam does incorporate these components, as shown in the equation for plastic collapse (σ_{pl}^*).

$$\frac{\sigma_{pl}^*}{\sigma_{ys}} \approx 0.3\left(\phi\frac{\rho^*}{\rho_s}\right)^{3/2} + (1-\phi)\frac{\rho^*}{\rho_s} + \frac{p_0 - p_{at}}{E_s}$$

A B C *Equation 3*

If a foam shows brittle characteristics during compression, the crushing strength (σ_{cr}^*) can be used to predict the stress at yield. Upon a brittle failure, the air within the cell does not contribute to the mechanism.

$$\frac{\sigma_{cr}^*}{\sigma_{fs}} \approx 0.2\left(\phi\frac{\rho^*}{\rho_s}\right)^{3/2} + (1-\phi)\frac{\rho^*}{\rho_s}$$

A B *Equation 4*

The equations discussed demonstrate the three main features that contribute to the prediction of a foams properties; the cell struts, the cell walls and the air within each cell.

Sin and Li (2005) sought to clarify the effect of trapped gas within foam using analytical models. They attribute the strain rate sensitivity of foam to the gas and the mechanical response for the monolithic polymer. They added a new term to the Gibson and Ashby equations to incorporate a higher-order strain term. This was to improve to the analytical prediction for higher strains. Their results showed that the gas effect has a larger contribution during the densification stage of compression and is reliant on the cells morphology. They also suggest caution should be taken when applying the numerical models in order to estimate a materials performance under dynamic loads.

Four analytical models were analysed by Avalle et al (2007); Gibson, Rusch, a modified version of Gibson and their own newly developed model. Gibson's model showed a good correlation to test data.

2.3 Test Methods and Strain Rate Effects

EPP has been evaluated for reducing head injury during contact sport (Zhou et al, 2015). Using the Head Injury Criteria (HIC) calculation they assessed the specifications required to avoid damage. EPP headgear (8 – 12 mm thick) is appropriate for avoiding injury up to an impact velocity of 5 $m.s^{-1}$; where it becomes no longer suitable for protection.

Pask et al (2007) highlighted the issue with characterising polymeric foams identifying 54 test methods available for doing so. Testing therefore requires a specific testing standard for each load case as a reference for both the investigation and JLRs future work.

The recommended testing standard for the compression of rigid polymer foam are BSENISO_844_2009 (British Standards Institution, 2009); equivalent to ASTM D1621, or EN826. For low density flexible foam, below 250 $kg.m^{-3}$, BSENISO_3386_1_1997 (British Standards Institution, 1997); equivalent to ASTM D3574-C. The Test methodologies will be discussed in Section 4.2.

2.3.1 Strain Rate Effects

The strain rate effects on cellular solids has been investigated. Mills (2007) suggested that for open cell foams the air flow has limited effect on the stress during impact speeds, unless the sample has a side dimension greater than 200 mm or the impact speeds exceed 5 $m.s^{-1}$. This is due to a limitation in the distance and time in which the air can be expelled before having an influence on the resultant force.

Ouellet, et al (2006) did similar research but with a polyurethane foam, noting a reduction in stress during the plateau stage of compression as the strain rate increased. This is associated with the fracture and consequent expulsion of fractured material during compression. This apparent damage and reduction in hysteresis is an issue for automotive purposes. A repeat loading case supported this, demonstrating a single use for peak performance of the material. The selection of EPP is therefore advantageous for this application.

The same research mentioned for density distribution (Bouix et al, 2009) also varied the foaming methods of EPP, resulting in two 90 $kg.m^{-3}$ foams with different microstructures, foam B having a smaller cell size. They were analysed at high and low strain rates, as shown in Figure 4. An increase in strain rate changed the response of the material within the foam, but has had little effect on the Young's Modulus. Therefore a performance change has been achieved through enhancing the manufacturing process.

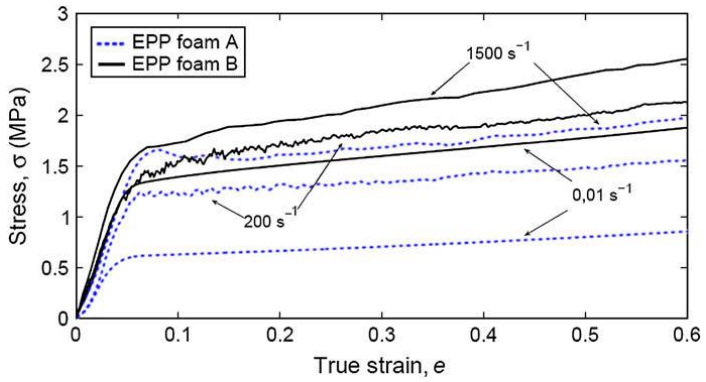

Figure 4: Stress–strain curves for two different EPP foam microstructures. (Bouix et al 2009)

Cronin and Ouellet (2016) investigated three foamed materials, low density polyethylene, expanded polystyrene and expanded polypropylene, specifically looking at the effect of strain rate during compression, sample size and sample variation. The strain rates ranged from 0.1 to 100 s^{-1}, demonstrating an increase in stress with strain rate for the three phases of compression. A large density variation was recorded across the three materials, however the samples were cut out across each sheet. A consequence of this is the incorporation of a skin layer at each end of a sample and therefore large variations in density. Three sizes of cylindrical samples were studied, 10, 17 and 35 mm diameter. For expanded polypropylene this was shown to have little

effect on the materials stress-strain response, however it is below the BSENISO_844_2009 standard and may therefore not exhibit the mechanical response that an increase in sample size might have. Larger samples were therefore investigated within this project from a much larger block of moulded material, removing the effect of manufacturing additions such as skin layer.

An Instron VHS testing machine has been used by Weiβenborn (2016) to correlate the modelling of strain rate effects on rigid polyurethane. The samples are very dense, ranging from 230 to 610 $kg.m^{-3}$; not an appropriate density for passenger safety and due to the load cell capabilities were restricted to a samples size of 25 x 25 x 25 mm^3, which does not represent vehicle components. The VHS was used for compression testing, however the set up meant the compression plate was decelerating during the final portion of the test, therefore not providing a constant velocity test condition. This is similar to a drop tower testing condition and may result in a softening effect as the strain rate changes mid test.

Koohbor et al (2017) evaluated the dynamic behaviour of foam on a meso-scale. Digital Image Correlation was utilised to view the strain patterns and therefore strain rates across a samples. It was found that strain rates were at least one magnitude greater within localised areas when compared to the overall sample. This emphasised the possibility for various failure mechanisms to occur across a sample during compression, switching between a buckling and brittle failure.

2.3.1.1 Cyclic Loading

Zhang, X., et al (2011) investigated the effect of residual strain within a sample of EPP after a compression test. It was concluded that accumulated residual strain depends on the level of strain a sample is compressed to. Although the residual strain will slowly dissipate if the sample is left for sufficient time. Andena, et al (2016) tested EPP ranging from 20 to 120 $kg.m^{-3}$. They used Gibson and Ashby's numerical models as a comparison to test data. Using SEM imaging the samples were inspected before and after the experiment, it was found that densities higher than 60 $kg.m^{-3}$ did not fully

recover their shape. However it is unclear what period of time was allocated for residual strain to be released.

Fernandes, et al (2015) looked at the effect of consecutive double loading for different polymer foams. It was found that the protection provided by a sample of EPS is minimal due to lack of elastic recovery between impacts. The recommendation was therefore made to use EPP as an alternative due to its hysteretic properties. Repeat loading was also investigated by Yang et al (2011), supporting the previous findings. Each sample was loaded to 0.25, 0.55 and 0.9 strain; with a softening effect on the material after each compression. The capability of a sample to absorb energy was dependant on the deformation history that sample had undergone. Using a full scale car bumper it was determined that the component underperformed after each load case.

Zhang, L., et al (2011) found the effect of cyclic loading on rigid polyurethane caused damage to the material which resulted in a different response after the first impact, with a drop off in stress of 70%. The effect of strain rate only became apparent when increasing the rate by a factor of 10, although strain rate effects may be present at lower intervals, the contribution of variables such as density distribution may hide it. Simulation done on the testing was defined using the LS-DYNA material model *MAT_FU_CHANG_FOAM_83*, with a good correlation to the test results.

2.4 Simulation: Selection of Material Models

For simulations within JLR a material model for continuum geometries are required. However a monolithic polymer material model would be required for simulating mesostructural samples that have been scanned using µCT.

2.4.1 Continuum Modelling

Maheo and Viot (2013) used *MAT_FU_CHANG_FOAM_83* to simulate foam in LS_DYNA. A review of a multi layered foam with varied densities was also analysed. By

incorporating many layers and material models for a single sample the run time for the model would be unnecessarily increased when compared to the accuracy of the result.

Sambamoorthy (2001) compared different material models for the characterisation of energy absorbing Polyurethane using four possible material definitions. They include *MAT_ISOTROPIC_CRUSHABLE_FOAM*_63, *MAT_BILKHU_FOAM*_75, *MAT_LOW_DENSITY_FOAM*_57 and *MAT_FU_CHANG_FOAM*_83. MAT_63 and MAT_75 do not incorporate strain rate effects and are designed to represent materials that undergo brittle failure during compression. This removes the hysteresis that is possible with MAT_57 and MAT_83. For modelling Polyurethane, MAT_57 produced the closest match to physical testing, however MAT_83 was close.

The use of MAT_83 for modelling polymeric foam was however supported by Serifi (2003) and Croop (2009), the latter of which used the material model to simulate expanded polypropylene.

For modelling EPS, Ozturk and Anlas (2011) opted for the material model MAT_57. Through analytical modelling they established the required unloading data for accurate modelling of foam. A Hysteretic Unloading (HU) value of 0.0001 and a Shape Factor (SHAPE) value of 200 were recommended. They found that the material model accurately predicted force, deceleration and displacement of the test, but only for the first loading case. For repeat loading the model required improvement. Thiyahuddin et al (2014) used MAT_83 with two input curves (0.02 and 1 $m.s^{-1}$) to simulate polymer foam; with good correlation to test data. They used a shape factor of 4.

For the application of single velocity crash testing Borazjani and Belingardi (2017) chose to simulate foam using MAT_63 within LS-DYNA. However their research suggests that for a strain rate sensitive simulation the appropriate material model is MAT_83. In order to overcome instability in foam modelling they used an exponential extrapolation of their stress-strain curves up to a strain of 1.

A drop tower configuration was simulated by Jiang, et al (2013) for a range of strain rates; 0.01 s^{-1} to 300 s^{-1}. A comparison between MAT_83 and MAT_163 showed they were both appropriate for the application.

2.4.2 3D Mesostructural Modelling

A computed tomography study by Viot, et al (2011), showed areas of localised compression for expanded polypropylene. Di Prima (2010) imported CT images into an FEA package, with a 12 µm resolution, which was found to be too big in order to capture the internal features. A finer resolution would be required in order to visualise and simulate the cell walls, which is possible with µCT capabilities. This would enable a full cell structure to be visualised and then tested within FEA to view the material response and possibly predict its physical performance.

Both Brydon (2005) and Alkhadar, et al (2008) discussed the issues with modelling polymeric foam as a homogenous model and a CT model within an FEA package. This is due to the complexity of internal structures, the difficulty to mesh a complex geometry and the range of deformation tests and strain rates that are conducted on them. The structure of the material can be split into two characteristics; the sample boundary morphology and the internal cellular topology. The structure of the material can be split into two characteristics; the sample boundary morphology and the internal cellular topology. The mechanisms for energy absorption are different for both, therefore increasing the complexity to accurately represent a material within simulation.

A lower density of rigid polyurethane was quantitatively characterised by De Pascalis (2016) using X-ray computed tomography. Software was used to analyse void count and void statistics. The capabilities have been demonstrated; however the volumetric model was not evaluated within FEA.

Lachambre (2013) and Bouterf (2017) used synchrotron radiation at the ESRF to scan polymeric foams within an in situ compression experiment. Lachambre (2013) used a hydrostatic pressure chamber to analyse expanded polypropylene. The study does not represent the unidirectional loading for energy absorption and the analysis was based on the images rather than the stress-strain data the material underwent.

2.5 Review of Current Practices within Jaguar Land Rover

2.5.1 Testing

A review of JLR's polymer foam knowledge was done during the early stages of the project; having collected information to benchmark it against. The materials characterisation department had a TPJLR (Test procedure), shown in Figure 5, for characterising materials for energy absorption. This test methodology dates back to previous owners of the organisation and does not conform to the current British Standards that have been reviewed. It has not seen use within JLR since their formation.

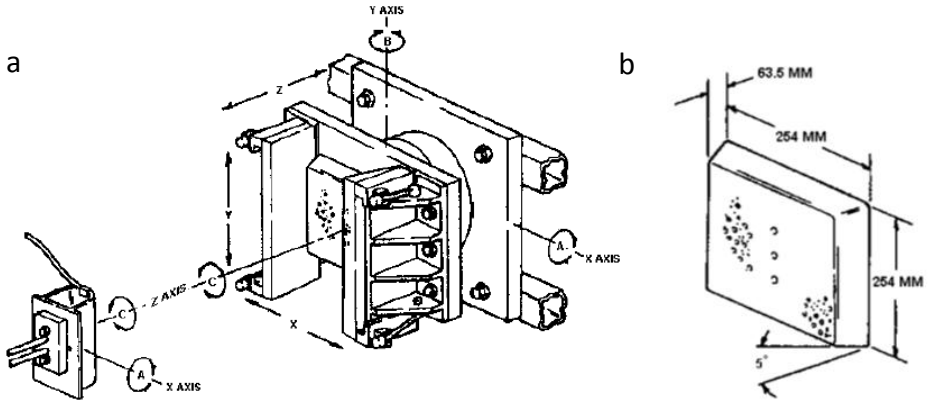

Figure 5: Foam Characterisation Equipment. a) Testing fixture and b) Foam dimensions

This test setup is specific to material validation at high strain rates, a test procedure will be required for coupon testing at a range of rates for characterisation and simulation input data.

2.5.2 Simulation

For finite element analysis JLR use LS-DYNA. Feedback from within JLR suggest there is not a process in place for establishing robust models without the requirement for iterative feedback. This highlighted the need for rigorous modelling methods as well as the material characterisation discussed. The models are made using either a hexahedron or tetrahedron mesh, with a varied element choice based on this. A

review of JLR simulation methodology and capabilities can be seen in Section 3.1, followed by recommendations for element choice and mesh size in Section 3.2.

2.6 Identification of Gap in Knowledge and Industrial Need

Testing of polymeric foam for energy absorption has been focussed on the use of expanded polypropylene. The material comes in a range of densities that allow it to be tailored for both passenger deceleration and to protect them from dangerous zones within the vehicle. Alternative foam, such as rigid polyurethane suffers in cases of repeat loading due to the damage caused during compression. JLR require a new test methodology and validated simulation for charactering these materials at a range of strain rates, due to their current lack of knowledge about the most appropriate techniques. This also includes preparation and cutting methods for getting samples ready for testing.

It has been shown that the manufacturing process of polymer foams can cause a density distribution, a thicker skin layer and variations in microstructure. These differences as well as those across manufacturers require investigation. JLR obtain their parts from third tier suppliers, making it difficult for the organisation to trace where it has come from. The implications of material variations and the effect on the simulations that represent them need to be investigated. Digital Image Correlation has been shown to be a good tool for investigating strain patterns on foamed material and can therefore be applied to the expanded polypropylene used within JLR.

Strain rate effects on cellular foams have been applied to alternative materials, but needs to be explored for expanded polypropylene, highlighting the effect of strain rates up to and beyond 50 s^{-1}, where other foams show a change in performance. Current simulation methods adopted within JLR using MAT_LOW_DENSITY_ FOAM_57 do not take into account these strain rate effects, whereas a change to MAT_FU_CHANG_FOAM_83 would. Further validation of this material model is consequently necessary.

High resolution scanning of expanded polypropylene enables the capture of cell features. This provides an input for a mesostructural model, ready for FEA compression that can represent the absorption mechanisms across a range of strain rates. It is therefore possible to estimate the effect of sample shape, density distribution and loading conditions using said model. The use of µCT also demonstrates to JLR the potential material characterisation that is available and the possibilities for full sample analysis of a third party component. This ensures specifications are being met during the component manufacture.

3 Simulation of Expanded Polypropylene: The Review and Improvement of JLR Practices (Submission Two)

The project was formulated due to the identification of an issue with the fidelity of simulating cellular solids at Jaguar Land Rover (JLR). Chapter 2 highlighted how to improve the capabilities and robustness of modelling these materials, showing which material models are most appropriate for representing Polyurethane (PU) and Expanded Polypropylene (EPP).

This chapter is a collection of the work that has been discussed in *Submission Two - Simulation Development* and it begins with a review of JLR's methods and procedures for simulating polymer foams. A new specification for setting up models within LS-DYNA is discussed, comparing the material models for representing EPP. Through a collaboration established with a manufacturer of said material, a dataset was supplied that created the foundation for material model inputs used to validate physical testing.

The aim was to fully evaluate current methods, create new procedures where appropriate and consequently implement them back into JLR. A robust simulation database will improve model reliability and reduce the requirement for further material model configuration.

3.1 Review of Previous Methodologies

JLRs material models, those used to input material information into simulations, were reviewed. Table 2 shows the expanded polypropylene definitions from within JLRs database. All are created using MAT_LOW_DENSITY_FOAM_57, of which literature showed a good correlation for PU, but was not recommended for EPP due to inaccuracy in correlation work. A full list of foam material models used for polymeric foams can be seen at the beginning of Section 2 of *Submission Two – Simulation Development*.

Table 2: Original Material Input Data for Simulation of Expanded Polypropylene

JLR Model Title	Parameters used	Density ($Kg.m^{-3}$)	Young's Modulus (MPa)	Stress-Strain Data Points
ARPRO exp PP foam 30g/l	3	30	8.202	7
ARPRO exp PP foam 45g/l	3	45	8.202	7
ARPRO exp PP foam 105g/l	3	105	8.202	7
ARPRO exp PP foam 120g/l	3	120	8.202	10
ARPRO exp PP foam 170g/l	3	170	8.202	9
Bayer exp PP foam 40g/l	3	40	8.202	37
Bayer exp PP foam 50g/l	3	50	8.202	6
Bayer exp PP foam 90g/l	3	90	8.202	6
EPP FOAM – 30g/l	8	29.8	3.0	20
EPP FOAM – 60g/l	8	60	3.0	10
EPP FOAM – 90g/l	8	90	3.0	10
EPP FOAM – 120g/l	8	128	3.0	18
EPP FOAM – 170g/l	8	170	3.0	10

The largest number of data points for an input curve was 37, this lack of curve resolution is not suitable for capturing key changes in material response, such as yielding and densification. Investment has been made into improving these material definitions previously, by implementing an abnormally high, or ramped, value to the end of each curve in order to stabilise at large compressions and prevent element inversion. It improved the numerical stability at a cost of model accuracy. However issues remained within the material definitions, such as incorrect density data, repetition of modulus values across the set of similar titled models and the number of data points used to represent the curve.

Figure 6 shows a comparison between two material model input curves and testing of an equivalent density block of EPP, for which the data was supplied by EUEPP; a foam manufacturer discussed in section 3.4.1. The set of material definitions labelled as "ARPRO" were assigned the same Young's modulus, despite the change in density that they represent and therefore a change in material properties that was suggested by Gibson and Ashby's equations (1999). Also, each input curve had 10 or less data points that represent the materials stress-strain response, which as mentioned led to key features being lost; such as the curvature of the yield. The high densification value, previously discussed, consequently misrepresents the material and its energy absorption capabilities. It was a similar case for the models labelled "EPPFOAM", which had incorrect density values as an input, the same Young's modulus for all densities

and less than 20 data points. Most of which also used a ramped value for the densification phase.

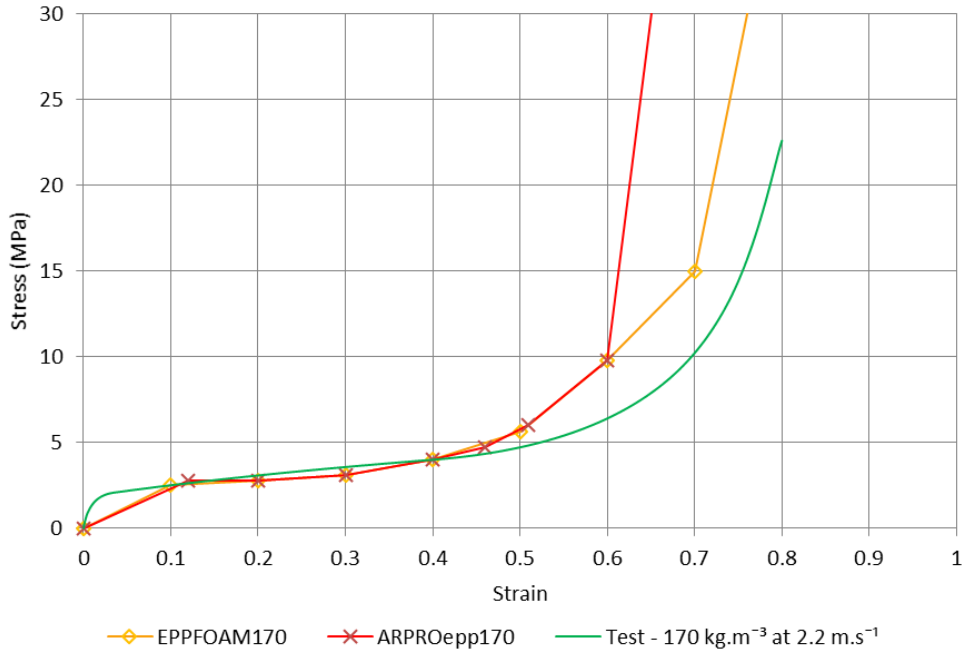

Figure 6: Stress - strain response for a sample of 170 kg.m^{-3} EPP compared to the two material models that represent it within JLR. Showing the use of a ramped value for stability

Traceability is an issue flagged by JLR when concerning their data. The test conditions, including strain rates, are unknown. This means a single density curve is applied to all strain rate conditions, when the literature has highlighted the different responses caused by this change for polymer foams with up to a factor of 2 difference in plateau stress.

Different departments have the choice of which material definitions they use, therefore a single sample could be defined under multiple different inputs. The definitions need to be consolidated into a single selection based on density, strain rate and supplier, to limit this variability.

3.2 Model Creation and Recommended Simulation Methods

This section concentrates on the implementation of foam materials in LS-DYNA, an FEA solver that is the most commonly used package within the CAE department at JLR.

A lack of validated modelling methods and techniques has resulted in a variety of formulations being used across models. For example a collection of hexahedron or tetrahedron elements with a variety of mesh sizes are present from model to model. Having investigated the effect of each, a recommendation for model setup has been presented when constructing simulations of Expanded Polypropylene, which will be transferable to alternative polymeric foams.

Figure 7 shows the model set up for simulating coupon testing. Both the top and bottom plate were limited to only a global z-axis translation. A Damper and Spring prevent the bottom plate from moving, but provide an alternative force output to compare to contact forces (See Section 3.2.2).

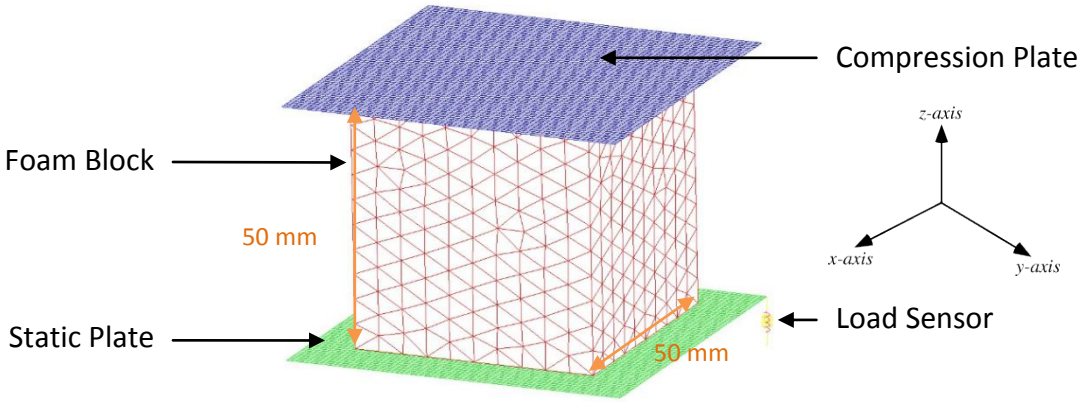

Figure 7: Cube Validation Model within LS-DYNA

3.2.1 Element Formulation and Mesh Size

Tetrahedrons showed the greatest correlation to test methods; with a mesh size of 5 mm in 1 point tetrahedron element type (ELFORM 10, or element formulation) within LS-DYNA. Figure 8 shows the comparison between three hexahedron meshes, using ELFORM 1, 2 and 3 as well as one tetrahedron mesh using ELFORM 10. Although the third hexahedron mesh had good results, the model became unstable beyond a strain of 0.8 and returned calculation errors.

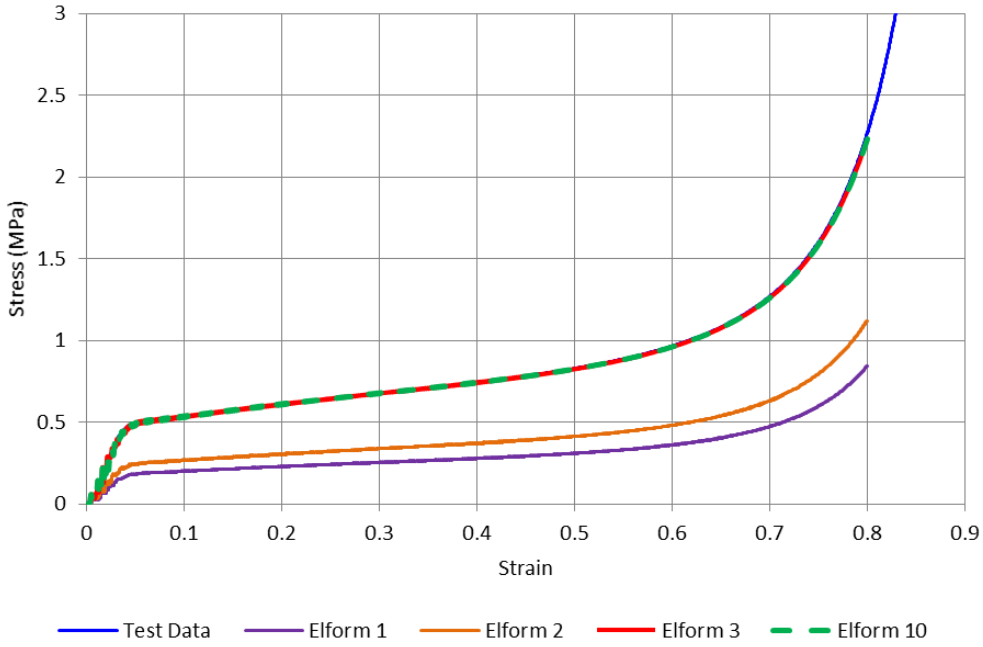

Figure 8: Simulation output with varied FEA Elements

3.2.2 Surface Contacts

The contact name used for the simulations is *AUTOMATIC_SURFACE_TO_SURFACE*, automatic contacts are the software's latest additions and are therefore the most up-to-date. They also have no specific orientation assigned to them, whereas the alternatives require it. They are suitable for non-continuous surfaces, specifically useful for JLRs full vehicle models.

As well as creating interactions between parts, the contacts also act as force transducers. The contact records forces produced through the interaction which can in turn be extracted using the output options. If an alternative contact, *AUTOMATIC_GENERAL* or *AUTO_SINGLE_SURFACE*, was used the force would not be recorded and a different means of recording it would need to be added to the simulation. However the former is suitable in a more complex model, such as a full vehicle model, where individual surface pairs are too numerous to define.

3.3 Selection of Material Models

For a possible transition from the previously used material model *MAT_LOW_DENSITY_FOAM_57* to the newly evaluated *MAT_FU_CHANG_FOAM_83* an in depth evaluation was required. The latter model has the added benefit of incorporating strain rate effects, which in turn reduces the number of material models required for the database and increases model accuracy. Both were reviewed with the required inputs from testing in order to run the model. The initial data required for the MAT_83 card includes the density, Young's modulus and an input compression stress-strain curve with a corresponding strain rate. Further data includes the unloading effects, multiple curves for different strain rates and a tensile failure point. These will be discussed in more depth in Section 3.6.

3.4 Manufacturers of EPP and Supplier to JLR

Discussions began with material manufacturers in order to help increase the knowledge available on EPP. This included production methods, the consequences of these methods to sample size and surface and the limitations that it brings.

3.4.1 EUEPP

Through connections at WMG, a relationship was established with a European manufacturer of expanded polypropylene, which at the time had few contacts through JLR. The use of an existing manufacturer that houses their own research and development team was not available through JLR. The company will be referred to as ***EUEPP*** throughout this document.

In order to begin the investigation, EUEPP supplied test data for their material; stress-strain curves for densities ranging from 20 to 170 $kg.m^{-3}$ at impact velocities between static and 11.11 $m.s^{-1}$. Their dynamic testing was carried out on a drop tower testing machine. The data received was used to create the first set of material models that could lead to the replacement of JLRs initial low quality data.

Through hosting meetings at both WMG and JLR, EUEPP became a source of information for both the project and for JLR. They have now become a key support for projects within the company and are expanding the amount of material they supply to them.

3.4.2 UKEPP

Time was also spent with an expanded polypropylene manufacturer that is based in the UK, a second tier supplier to JLR. They will be referred to as ***UKEPP*** throughout the document. UKEPP produce parts including the front bumper for a range of Jaguar models. The raw polypropylene that they use to create each part is purchased from EUEPP and then expanded on site and moulded within their own fixtures. This removes the raw material as a reason for performance differences between the companies foam; meaning any variations are caused by manufacturing processes, which can then be investigated.

3.5 Incorporating a Material Dataset: EUEPP Drop Tower

As mentioned in Section 3.4.1, the simulation data was created using EUEPP's drop tower data. Figure 9 is a comparison between the data that JLR were using to represent a foam of density 60 $kg.m^{-3}$ at an unspecified impact velocity against two blocks of EUEPP material of the same density; tested under quasi static conditions and at 2.2 $m.s^{-1}$.

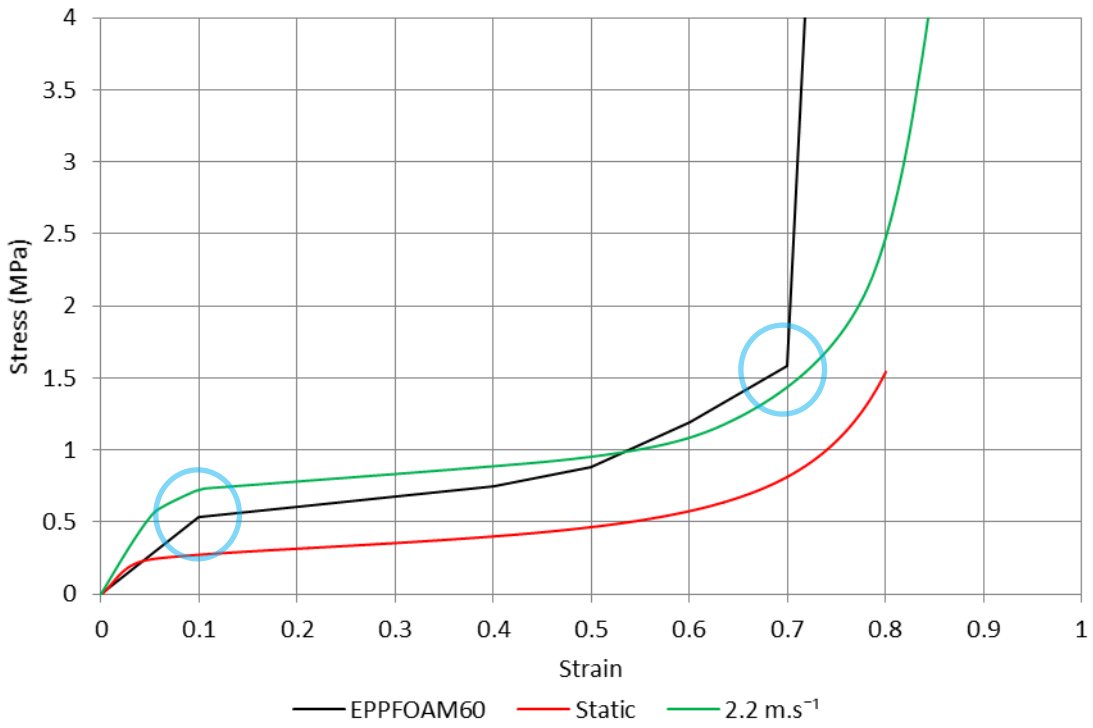

Figure 9: Original material card data compared to quasi-static and drop tower testing for 60 kg.m^{-3} EPP. Circles indicate areas of missing curve accuracy for EPPFOAM60

EPPFOAM60 does not appear to represent either velocities, and instead crosses both during the compression. The ramped value for densification has dramatically changed the response that the material would have, showing full compaction at approximately 10% lower strain. There are 10 data points used to define the curve, two areas have been highlighted to show how the lack of data points reduces the curvature that would otherwise occur.

Table 3 shows the material definitions that were created using the datasets received from EUEPP, initially using MAT_57 as a direct replacement for JLRs previous database. These and the replacement MAT_83 material models will be compared in the following section.

Table 3: Data Acquired from EUEPP of their EPP analysis

Density kg.m^{-3}:	**20**	**30**	**45**	**50**	**60**	**70**	**80**	**90**	**100**	**110**	**120**	**140**	**170**
Static 3×10^{-4} km.h^{-1} $\dot{\varepsilon}$ = 0.00189	✓	✓	✓	✓	✓	✓	✓	✓	✓	✓	✓	✓	
Impact 8 km.h^{-1} $\dot{\varepsilon}$ = 22.2222		✓	✓		✓		✓		✓		✓	✓	✓
15 km.h^{-1} $\dot{\varepsilon}$ = 41.6667		✓	✓		✓		✓						
24 km.h^{-1} $\dot{\varepsilon}$ = 66.6667		✓	✓		✓								
40 km.h^{-1} $\dot{\varepsilon}$ = 111.111		✓	✓		✓								

During a meeting hosted by JLR, EUEPP were able to demonstrate their material's capabilities and limitations. A presentation of these is now available to JLR.

The source of information and traceability was highlighted as an issue early on in the project. A process for assimilating information into the organisation was therefore produced and JLR have access to this via the database that contains the material definitions. Due to EUEPP's contribution and links that have been created through the project, their contribution to JLR has increased. It was therefore important to validate the material data that EUEPP supplied.

3.6 Validation of Material Models

An LS-DYNA simulation was created to represent the drop tower work that was performed by JLR on their own drop tower testing rig. Figure 10 shows the test setup used to validate foam material models on complex geometries and the corresponding model created to represent it.

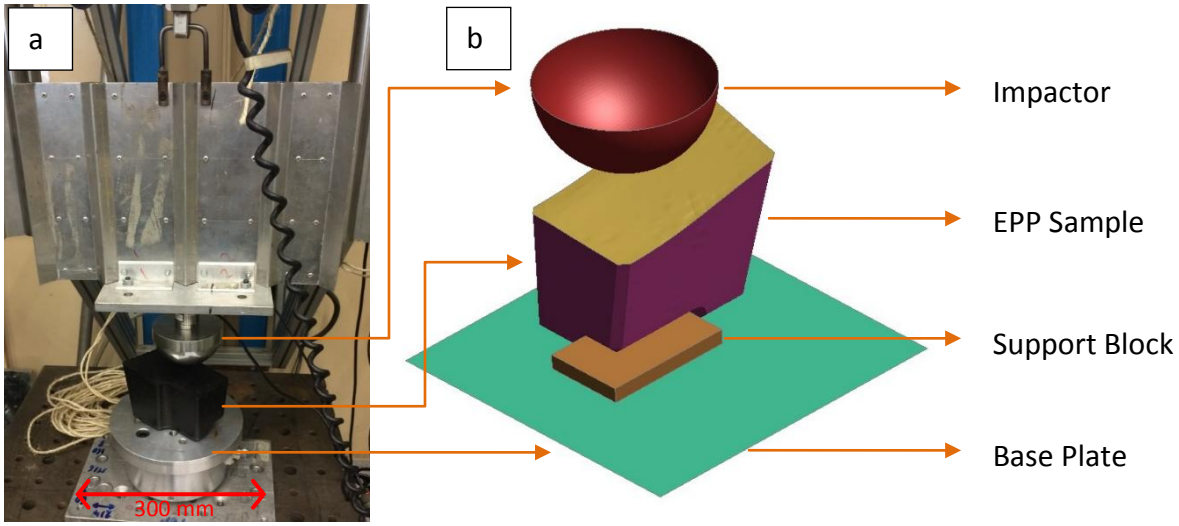

Figure 10: a) JLR's drop tower configuration and b) LS-DYNA Simulation

The sample had a density of 120 kg.m^{-3}, which was taken from the rear interior trim of a Land Rover. The drop mass was 4.5 kg, and the impact velocity was recorded at 7 m.s^{-1}. Figure 11 and Figure 12 show the results from both testing and simulation using the original material definitons that JLR had within their database; "EPPFOAM" and "ARPRO" respectively.

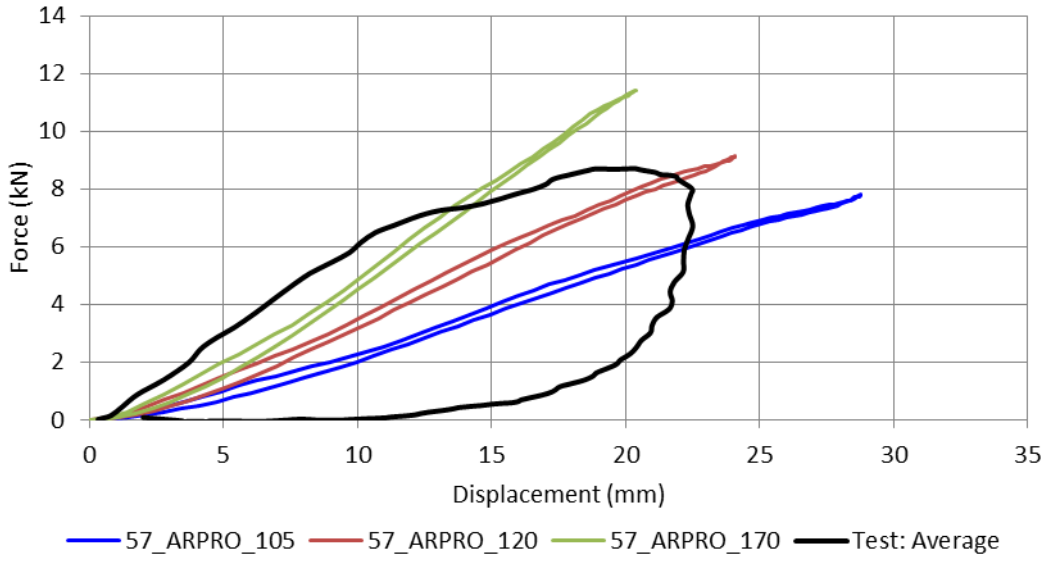

Figure 11: Component Testing carried out by JLR Compared to their original material inputs for simulation titled "ARPRO"

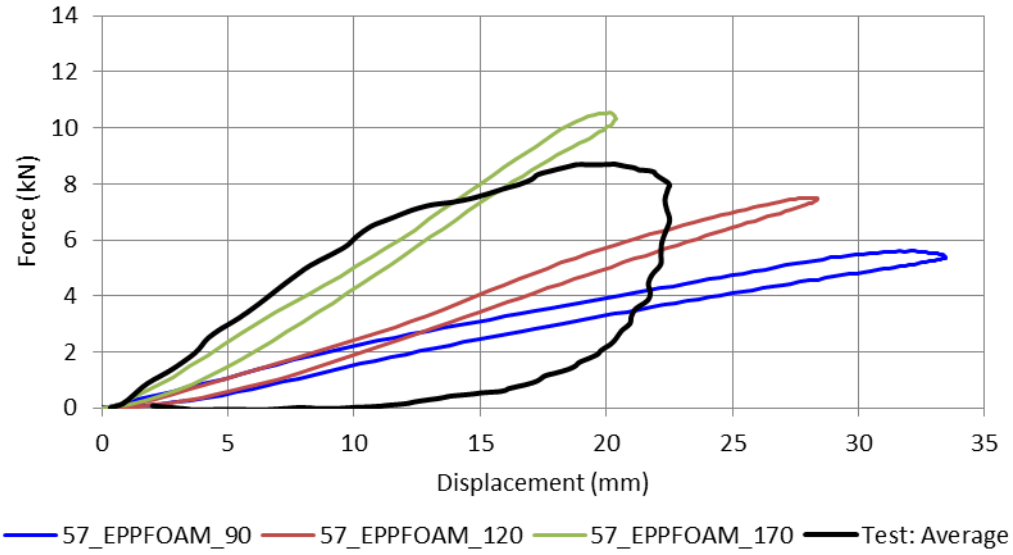

Figure 12: Component Testing carried out by JLR Compared to their original material inputs for simulation titled "EPPFOAM"

The simulation data has poor correlation to the test data, with 120 $kg.m^{-3}$ material models both having a vastly different yield slope. The unloading values did not represent the hysteresis from testing, instead having a fully elastic response. The material models may output a reasonable result on coupon test simulation, which is dominated by the plateau stress, but the incorrect linear elastic region and therefore modulus leads to an inaccurate stress distribution for more complex geometires.

Figure 13 is the initial outputs using a new MAT_57 and MAT_83 material model which were created from EUEPP's dataset. The output is the correct shape with hysteresis included. Some mass was missing from the drop weight within the model, resulting in reduced stiffness. MAT_57 shows a sharp peak at the maximum load and displacement, which was caused by a lack of strain rate effects; supported by an investigation using a MAT_83 input with strain rate sensitivity removed (see Submission Two: Section 6.2.2 for full analysis). This suggests the softening observed during testing is due to strain rate sensitivity caused by a mass decelerating as maximum displacement is approached.

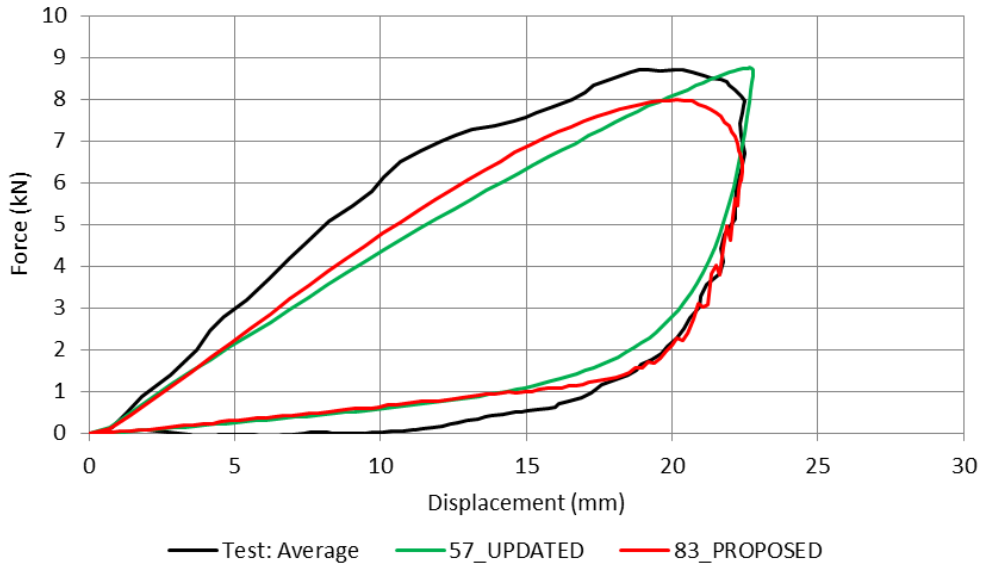

Figure 13: Replacement Material input used in the validation simulation

Figure 14 shows improvements to the simulation work with further changes to the input model, including drop weight, material stiffness and strain rate assigned to each strain rate curve. The final material model accurately simulates the initial loading of the block as well as matching the unloading. For MAT_83 the parameters used to model unloading were Hysteretic Unloading (HU) and shape factor (SHAPE). Both of these values were established through simulation testing.

Table 4 is a comparison of residual error between the test data, the original material models and those updated through the project. A residual is the difference between the observed y-value and the predicted y-value. Each curve was regularised using an equal number of data points. The vertical distance between each data point was then recorded and summed. Taking the "ARPRO" input curve as a benchmark, a reduction in residual error of 89% has been achieved for loading and 97% for unloading.

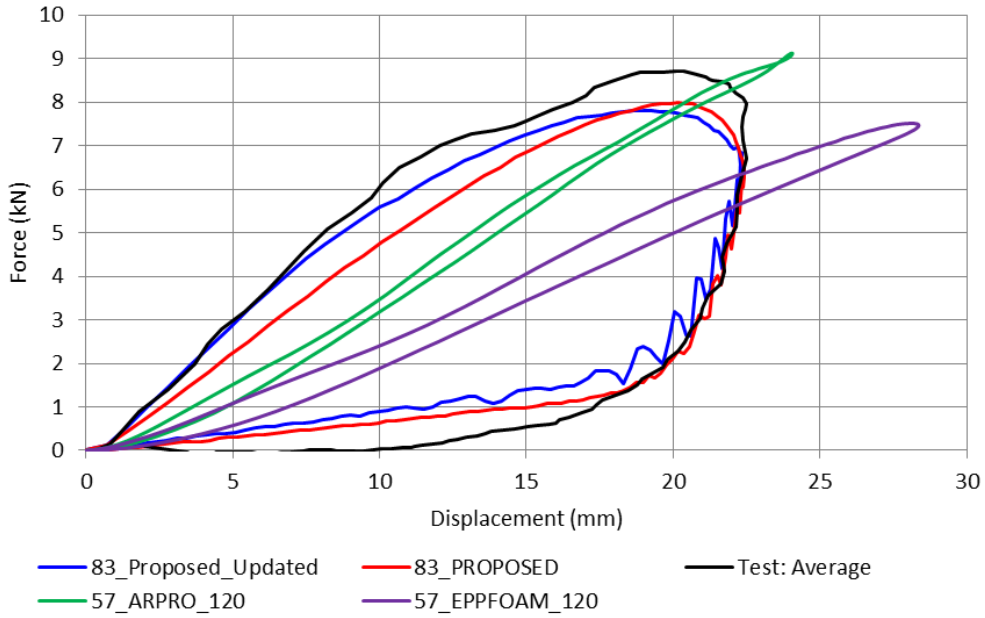

Figure 14: Simulation of Head Impact block using most recent Material 83 input

Table 4: Residual error comparison between iterations of material models

	ARPRO	**EPPFOAM**	**Updated**	**Final**
Loading Curve				
Sum of residual error (kN)	319	945	88	34
Percentage Improvement (%)	0	-196	72	89
Unloading Curve				
Sum of residual error (kN)	1518	468	18	48
Percentage Improvement (%)	0	69	99	97

There are however still inaccuracies within the simulation, this could be down to the input energy that is not being replicated in the simulation or that the input data does not represent the mateial used. The sample is fully enclosed with a skin layer, whereas the testing done by EUEPP does not include this. This thicker layer could explain the increased stiffness within the sample. The discrepancy in energy output shows the importance of record keeping and validation when testing, ensuring the repeatibility of testing is available.

3.6.1 Quantifying a Vehicles Safety

The same block simulated in section 3.6 is used to provide a Head Injury Criteria (HIC) analysis for evaluating vehicle safety. Figure 15 shows a section from the full body model, with the specific expanded polypropylene sample positioned within the interior trim. Figure 16 shows the location within a vehicle that the samples originate from.

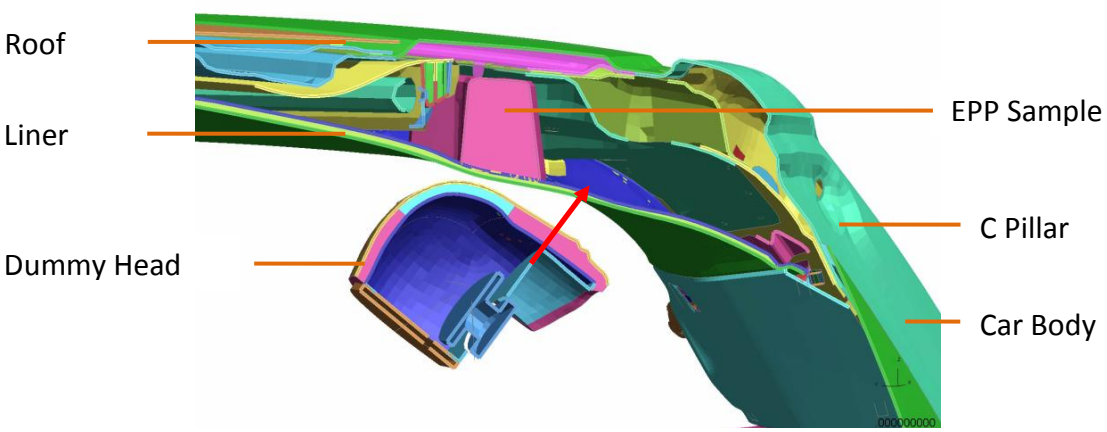

Figure 15: Cross section of a full vehicle model for HIC analysis

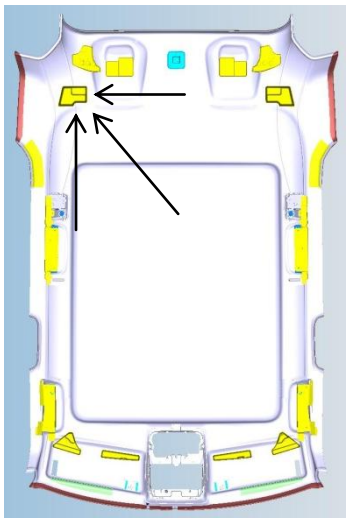

Figure 16: Block location within a Land Rover vehicle

A comparison was therefore carried out using this model on the original inputs, the updated MAT_57 and the proposed MAT_83 material definitions. Figure 17 has the test data from experimental work done by JLR and the simulations that represent it. The axes are acceleration against time, used for the HIC calculation.

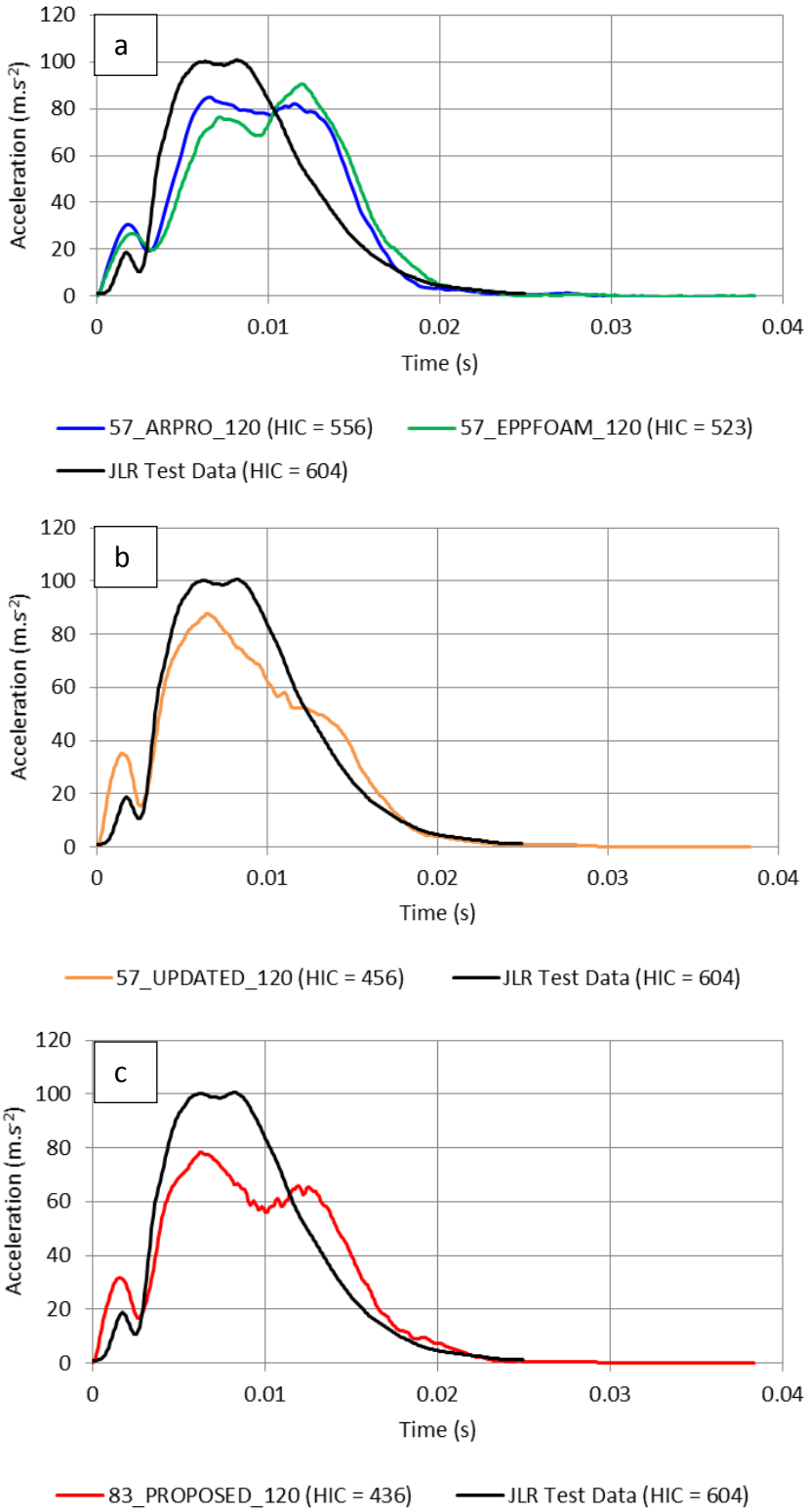

Figure 17: Comparison between a) original, b) new MAT_57 and c) new MAT_83 material definitions against the HIC test

T/HIS, an Oasys package (ARUP) for XY graphical plotting and post processing, is used to calculate the HIC value using the function provided. It is a measure of the likelihood of an injury on a passenger caused by a high speed impact (calculations are discussed in Submission Two: Section 6.2.2.1). The calculation monitors the rate of deceleration a passenger goes through during a crash. A value of 700 is the maximum permitted by the U.S. advanced airbag regulation; this sample is only present in the US Land Rover vehicles. The testing done by Jaguar has returned a HIC value of 604, which is under the maximum permissible. The values from the simulated test, Figure 17, are also within the requirement. However the updated material definitions increase the gap between test and simulation. None of the simulations meet the peak acceleration that is demonstrated during the physical test.

The original material models (ARPRO and EPPFOAM) exhibit very different mechanical responses in Figure 14, but are similar in the results shown in Figure 17a. This implies that foam model is relatively insignificant in this load case. The 57_Update has demonstrated the largest change to output shape, therefore the modulus and yield stages of compression could be the most important for this test. 83_Proposed has the least accurate result when compared to the test data, with the lowest acceleration and therefore HIC result. However based on component validation tests in section 3.6, the original 57 cards cannot be recommended for JLR's use.

It is possible that there are errors in the test data or the model used to represent it. The full body model is made up of lots of components, each exhibiting a displacement during the test. It is also possible that a magnitude of errors from other parts within the model could conceal any improvements that the new material models have contributed. This further highlights the importance of accurate and traceable coupon and component testing, as well as the material model and validation methods.

3.7 Summary

- The simulation methodologies at JLR were reviewed and updated.
- Dataset of EPP stress-strain responses acquired from a European manufacturer.

- JLR's material models were updated with new datasets, increasing the accuracy of their simulations

Having evaluated simulation procedures and the modelling choices of JLR, a new set of methodologies were created. This included formulation of geometric models and the specific material models used for simulating both Polyurethane (PU) and Expanded Polypropylene (EPP). The latter were constructed using test data sourced from a manufacturer of EPP from Europe in both MAT_57 and MAT_83.

Components sourced from a Land Rover vehicle were tested in order to validate material models. A comparison between the original JLR datasets and those updated showed a significant improvement, reducing the residual errors for loading by 89%.

The modelling capabilities were also improved with robust models that can now compress to high strain without the occurrence of calculation errors. This removed the requirement for model alteration from the user. With the new robust modelling procedures, output data can be relied upon as being an accurate representation of the intended material.

The dataset received from EUEPP then required its own authentication in order to prove the input data was as accurate as possible. It also needed to be benchmarked against alternative manufacturer's foam, as at the time EUEPP did not supply much material to JLR. The following chapter explores these concerns and discusses material test procedures used to investigate them.

4 Geometry Investigation: Stress-Strain Response of Expanded Polypropylene, Strain Rate Effect and Production Variation (Submission Three)

Having created the material inputs for simulation and shown an improvement using the new data acquired from EUEPP, it was important to show the dataset is an accurate representation of their material; as it is used to evaluate safety critical components within the vehicle. As Jaguar Land Rover (JLR) do not source all of their material from EUEPP, the material was tested to ensure the dataset represents other manufacturer's foam. There were also gaps within the data provided, as shown previously in Table 3.

This chapter is a summary of the work produced in *Submission Three - Geometry Investigation*. New methodologies were produced for characterising energy absorbing foams at a range of strain rates on three different compression testing machines. Using these methods the following testing and research was carried out to investigate the mechanical response of Expanded Polypropylene (EPP).

1. The materials behaviour when using a decelerating mass versus a constant velocity impact, therefore effecting the simultaneous strain rate of an experiment (Section 4.4)
2. EUEPP's stated foam stress-strain response versus the reality of testing samples purchased from them (Section 4.5)
3. EUEPP's foam versus the performance of UKEPP foam (Section 4.6)
4. The effect on EPP with an increase in strain rate compression (Section 4.6.1)
5. Coupon testing using a flat plate impactor versus a localised load from a cylindrical compression fixture, improving the representation of a car crash (Section 4.7)
6. The use of Digital Image Correlation to view the strain distribution during compression (Section 4.7.1)
7. The distribution of mass across a moulded part and the effect on its response (Section 4.8.1)

8. The effect of a dense skin layer that is formed during the moulding process (Section 4.8.2)
9. The mechanical response when stacking multiple layers of foam to produce a single test sample. Can the performance be tailored to reduce high stresses from occurring early on in an impact (Section 4.8.3)
10. The effect of sample size on the stress-strain output of EPP, investigating whether coupon testing can be applied to alternative samples within simulation. (Section 4.8.4)

4.1 Material Selection and Sample Preparation

All sample preparation, testing, post-processing and simulations have been done at WMG to avoid problems with missing details and traceability. Table 5 shows the material purchased for testing, both suppliers use the same raw material for creating their EPP. Therefore any differences in material performance stems from the manufacturing process. A large single block was purchased from EUEPP, whereas UKEPP supplied pre-cut cuboids, it is therefore unknown from where within the original mould they come from.

Table 5: Material Specifications for Testing

Manufacturer	**Density (kg/m^3)**	**Dimensions (mm)**
EUEPP	30, 60, 80, 120	Single Block - 1200 x 800 x 200
UKEPP	30, 50, 80	30 x Blocks - 200 x 200 x 100

Samples of density 30 and 80 kg.m^{-3} were purchased from both suppliers in order to have a direct comparison, the other densities correspond to gaps in EUEPP's supplied data as well as the 60 kg.m^{-3} that they have performed extensive testing on, as a benchmark.

Each test has been conducted three times for each variable, removing anomalous results and reducing error. The samples dimensions were collected with three points of measurement in order to achieve an average; these dimensions were then used to

calculate each sample's density and for converting results into a stress-strain output. The mass of each sample was recorded in grams to two decimal places.

Through preliminary sample preparation, methods of cutting EPP were investigated. A hotwire cutter was found to cause structural change due to melting, which was not occurring with a band saw. Through changing the surface of the material it is possible the flow of air during compression would be effected, increasing air pressure and therefore the stresses exhibited. Cutting has therefore been done using the band saw method, taking into consideration the thickness of the blade when planning sample size.

As previously discussed in Section 2.3, the number of available tests for polymeric foam is vast. A British Standard and ASTM Standard have been chosen for each loading condition, in order to consolidate the possibilities and to direct test engineers at JLR to the correct format. Uniaxial Compression is the most important method for analysing the materials energy absorption capabilities; testing for which has consequently been done based on BSENISO_3386_1_1997 (British Standards Institution, 1997).

4.2 Test Methodologies: Strain Rate Sensitivity Investigation

The following three subsections contain the test methodologies for compression testing across the three testing machines used within this project; an Instron 5800R, the Drop Tower and the VHS respectively.

These machines were chosen for their range of strain rates, from quasi-static to 100 s^{-1}. Different load cases exhibit these rates of strain when using a motor vehicle. Passenger weight on a seat can cause quasi-static compression of foam and during a crash of up to 30 mph rates can reach 100 s^{-1}. Table 3 shows the strain rates used for material characterisation by EUEPP and their corresponding impact velocities. The range is from quasi-static up to 111 s^{-1}; providing a close comparison for the validation testing required.

The Instron 5800R machine is used for quasi-static compression testing between 1.667 x 10^{-4} and 3.333 x 10^{-3} $m.s^{-1}$. The Drop Tower was used to replicate the testing done by EUEPP and to simulate the conditions during a vehicle crash; where the impact mass decelerates. In order to reinforce the simulation validation a complex load case was tested and simulated. This was achieved through a cylindrical impact shape, demonstrating a difference in stress and strain distribution across the sample. Digital Image Correlation (DIC) was used on this machine in order to view the strain distribution during a test.

The final machine used was the Very High Strain-Rate (VHS) compression machine. This machine is capable of doing a constant velocity impact, using a shear pin to disengage the system after the desired compression. This gave a true material response by removing the effect of deceleration of a falling mass. The VHS can also do quasi-static strain rates. A comparison between each machine has been conducted in Section 4.4.

4.2.1 Quasi-Static Compression Test Methodology

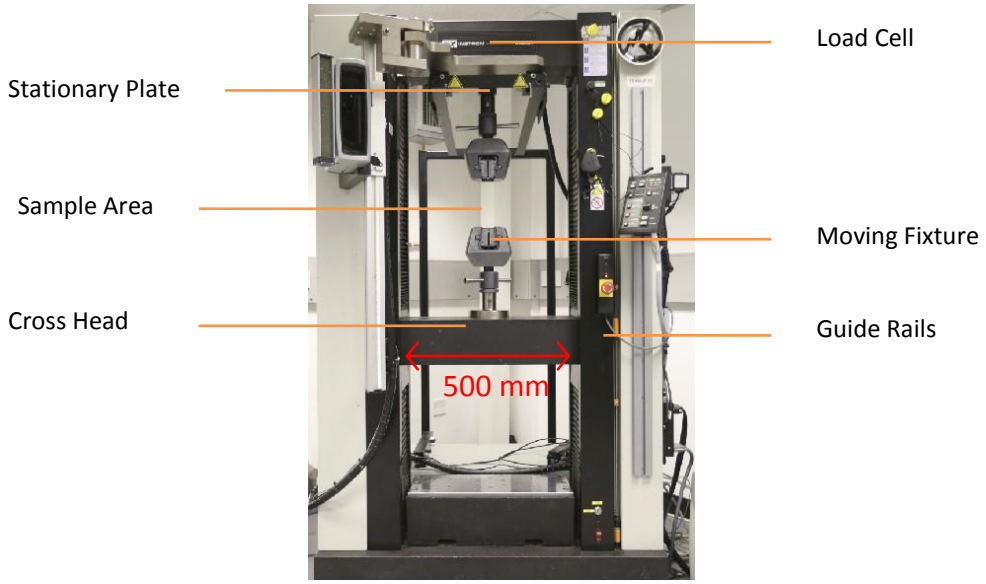

Figure 18: Instron 5800R Compression Rig

This is used for material characterisation and to evaluate joining technologies, the Instron 5800R is a quasi-static machine capable of velocities up to 200 mm.min^{-1}. In order to achieve the higher velocities the machine requires significant time and displacement due to the screw displacement mechanism; Figure 19 shows the requirement for 2 to 3 seconds of travel prior to impact. The low strain rates demonstrate material performance without viscoelastic effects. Table 6 contains a summary of the capabilities of the machine.

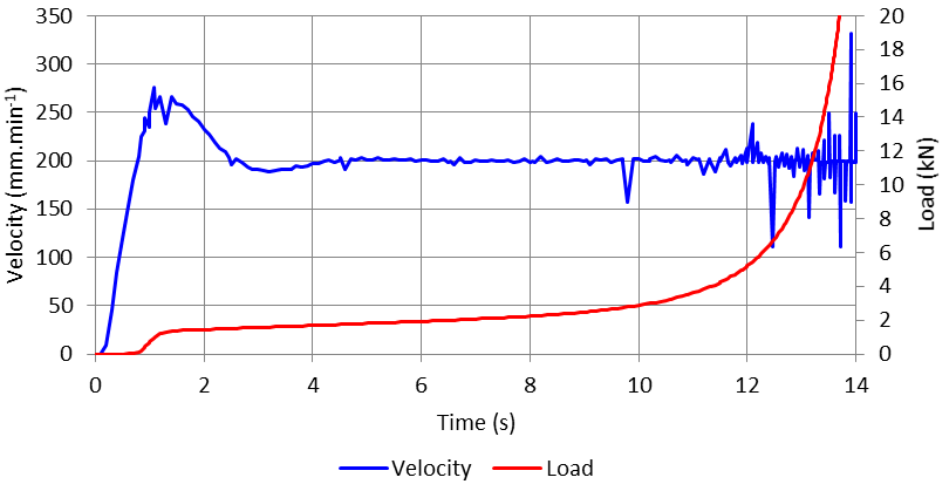

Figure 19: Velocity Profile of a 200 mm.min^{-1} compression test on the Instron 5800R

Table 6: 5800R Machine Specification

Manufacturer	Travel	Velocity	Load Cell	Fixtures
Instron	0.5 m	0.1 to 200 mm.min^{-1}	100 kN	Flat Plate

The compression fixture is designed for small samples, with a diameter of 100 mm. Figure 20 shows both the top and bottom compression plate.

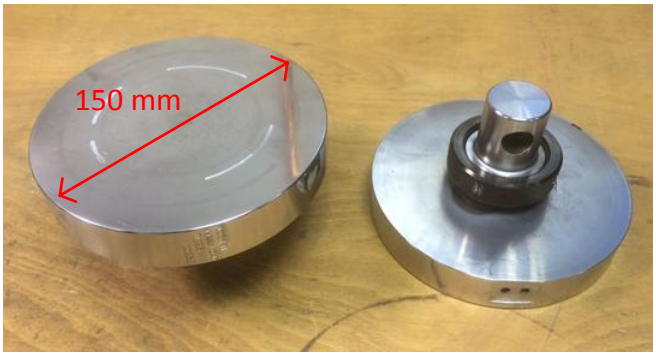

Figure 20: Compression plates for the 5800R testing rig

The sample dimensions that were used for quasi-static compression can be seen in Table 7. The high load cell capabilities allow for the strain to be tested to beyond 0.8, well into the materials densification stage.

Table 7: 5800R Sample Preparation

Samples	Material	Dimensions	Surface Finish
Cube	Expanded Polypropylene	50 mm x 50 mm x 50 mm	Band Saw

Table 8 are the test specifications used for compression testing samples. A distance of 5 mm is used to trigger the data acquisition. This accounts for the displacement required to achieve the specified velocity. A displacement and load limit can be assigned to the test; which are dictated by the load cell's capabilities (100 kN) which can be reached during the densification stage.

Table 8: 5800R Test Setup

Data Acquisition	Sample Rate	Stop Limits	Accuracy	Output
Trigger – 5 mm before sample	0.001 kHz	Load Cell	± 0.001 kN ± 0.01 mm	Load Displacement

4.2.2 Drop Tower Test Methodology

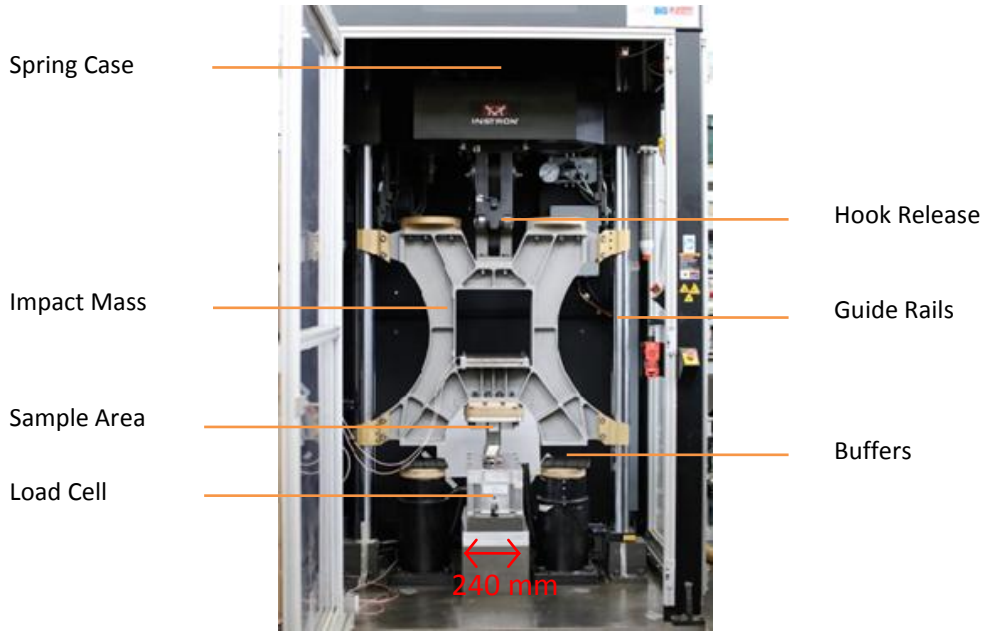

Figure 21: Instron Drop Tower

The custom built machine has a dual spring system for increasing the energy at a shorter distance to simulate a drop height of up to 14.8m. It is useful for automotive material characterisation; with space for both small and large structures. Table 9 contains a summary of the machines capabilities.

Table 9: Drop Tower Machine Specification

Manufacturer	**Travel**	**Simulated Drop Height**	**Maximum Velocity**	**Maximum Energy**	**Fixtures**	**Impact Mass**
Instron	1 m	Up to 14.8 m	17 $m.s^{-1}$	11.5 kJ	Flat Plate Cylindrical	70 to 170 kg

The fixtures have been custom built in order to satisfy the characterisation and validation needed within simulation and can be bolted to the bottom of the carriage. Figure 22 shows the flat plate used for characterisation and the cylindrical fixture used within validation. The maximum sample area is 200 mm for the former, the cylinder has a radius of 40 mm and a length of 250 mm.

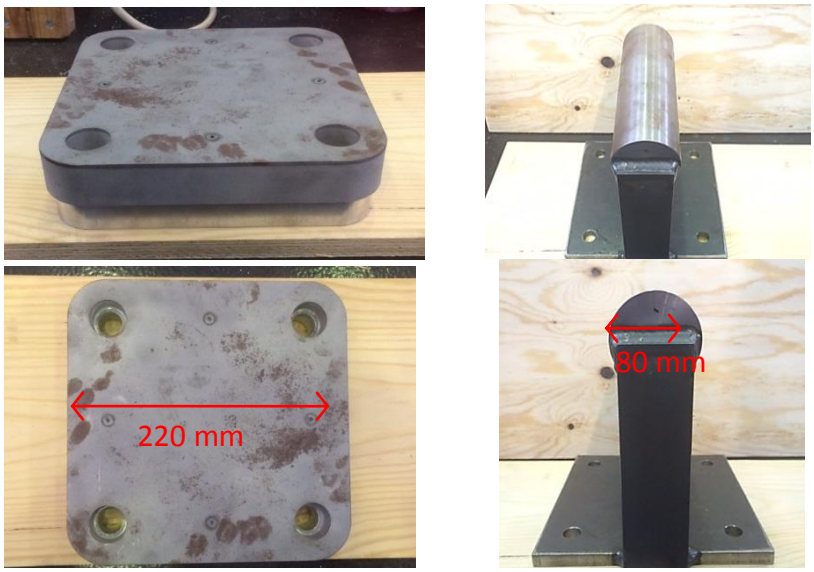

Figure 22: Custom made impactors for the Drop Tower. Flat plate (Left) and Cylindrical (Right)

The samples were cut from a large block of dimensions 200 x 800 x 1200 mm in order to remove the effect of a skin layer and reduce that of density distribution. They were cut using a band saw, which has been shown to limit the effect on surface finish within *Submission One - Literature Review*. Sample dimensions can be seen in Table 10, wider samples were used for cylindrical impact testing in order to evaluate the strain distribution across a loaded and unloaded section.

Table 10: Drop Tower Sample Preparation

Sample – Impactor	**Material**	**Dimensions**	**Surface Finish**
Cube – Flat Plate	Expanded Polypropylene	100 mm x 100 mm x 100 mm	Band Saw
Cuboid – Cylindrical	Expanded Polypropylene	200 mm x 100 mm x 100 mm	Band Saw

Buffers absorb any remaining energy before the carriage hits the load cell. Load and displacement are recorded, along with time in order to produce the output data. Table 11 show the test specifications used for testing each sample.

Table 11: Drop Tower Test Setup

Data Acquisition	**Sample Rate**	**Stop Limits**	**Accuracy**	**Output**
Trigger - 10 mm before sample	81.92 kHz	Buffers	± 1 kN ± 1 mm	Load Displacement

4.2.3 VHS Test Methodology

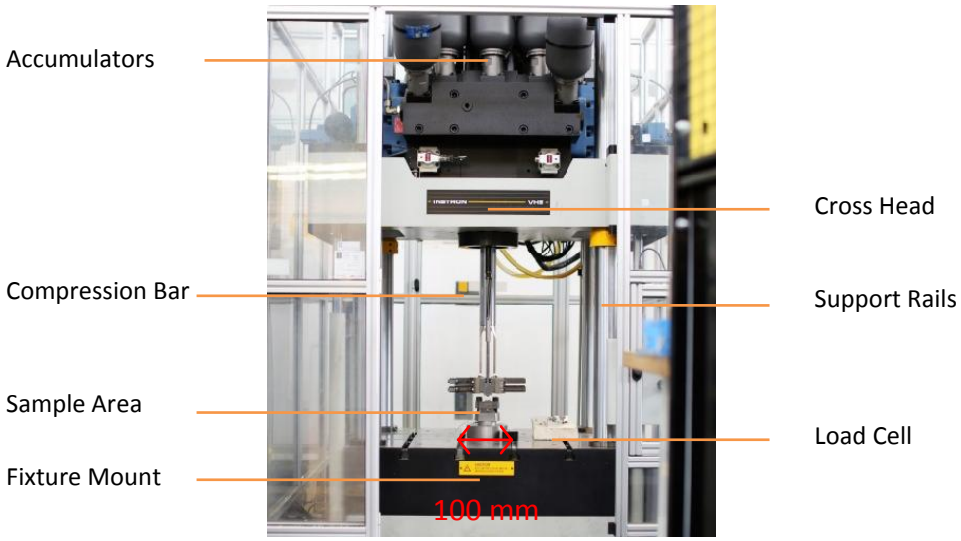

Figure 23: Instron VHS

The very high strain rate testing machine is set up for small to medium samples at a range of strain rates. It is used specifically for material characterisation and testing within WMG, focussed on lightweight materials and structures. Table 12 is a summary of the machine capabilities.

Table 12: VHS Machine Specification (Compression)

Manufacturer	Travel	Velocity	Load Cell	Fixtures
Instron	± 150 mm	0.001 m.s-1 to 5 m.s-1	65 kN	Flat Plate

Initially made for tensile testing, fixtures have been prepared for compression testing. Figure 24 shows the plates available in position; under which three load cells are attached. The surface area of the top plate is 200 mm square, however a smaller 100 mm plate is available.

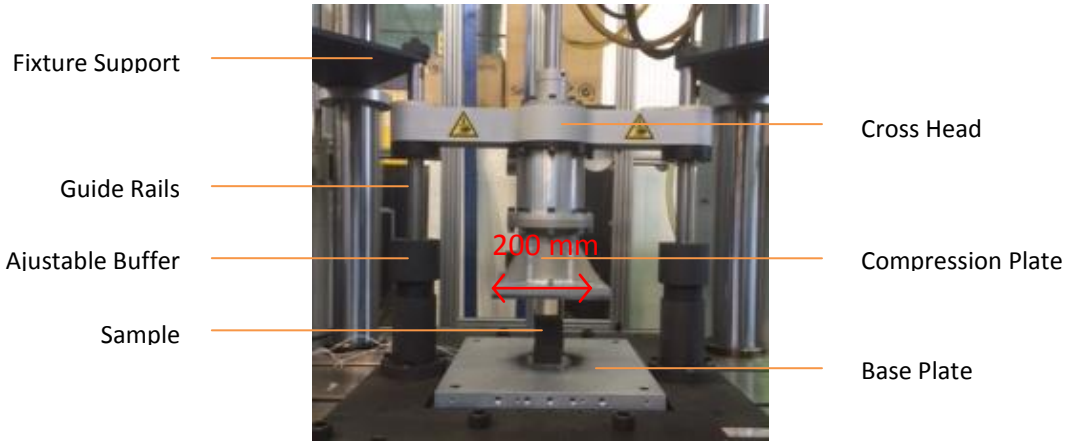

Figure 24: Compression plates on the VHS testing rig

The samples were cut from the same materials previously discussed. Taller samples have been made in order to reach greater strain if necessary, the dimensions of which are in Table 13. Two mechanisms are available on the VHS for compression, using the internal buffers, or breaking a shear pin under load in order to disconnect the frame once the desired displacement is met. The shear pin allows for constant velocity displacement. The internal buffers give some deceleration at the end of the test, similar to the Drop Tower testing. A comparison between the velocities is shown in Section 3.5.

Table 13: VHS Sample Preparation

Samples	**Material**	**Dimensions**	**Surface Finish**
Cube	Expanded Polypropylene	50 mm x 50 mm x 50 mm	Band Saw
Cuboid	Expanded Polypropylene	100 mm x 50 mm x 50 mm	Band Saw

The data acquisition is triggered based on a displacement value, 10 mm prior to the impact of a sample. The sample rate is varied based on the input velocity in order to record the whole compression with enough detail.

Table 14: VHS Test Setup

Data Acquisition	**Sample Rate**	**Stop Limits**	**Accuracy**	**Output**
Trigger - 10 mm before sample	5 to 200 kHz	Buffers	± 0.05 kN ± 0.01 mm	Load Displacement

4.3 Procedures for Data Processing

The raw data taken from testing discussed in this document has been filtered using T/HIS, software discussed in section 3.6.1, ready for validation and use within the material models in LS-DYNA. Figure 25 shows both the Load against Time and Displacement against Time curves that are exported from a typical drop tower test. A Butterworth filter is applied initially to reduce the noise; it attenuates the high frequency components of the signal. Each curve is clipped, dictated by the onset of force on the Load – Time curve and then regularised in order to reduce the data points closer to 400. This lower number of data points increases the effect of smoothing if further filtering is required, it also keeps the important features of the curves such as the Young's Modulus, yield stress and densification stage. Higher frequencies of the filter preserves features but also noise; yield is inherently a high frequency phenomenon, therefore the process can be hard to remove noise without altering the underlying signal.

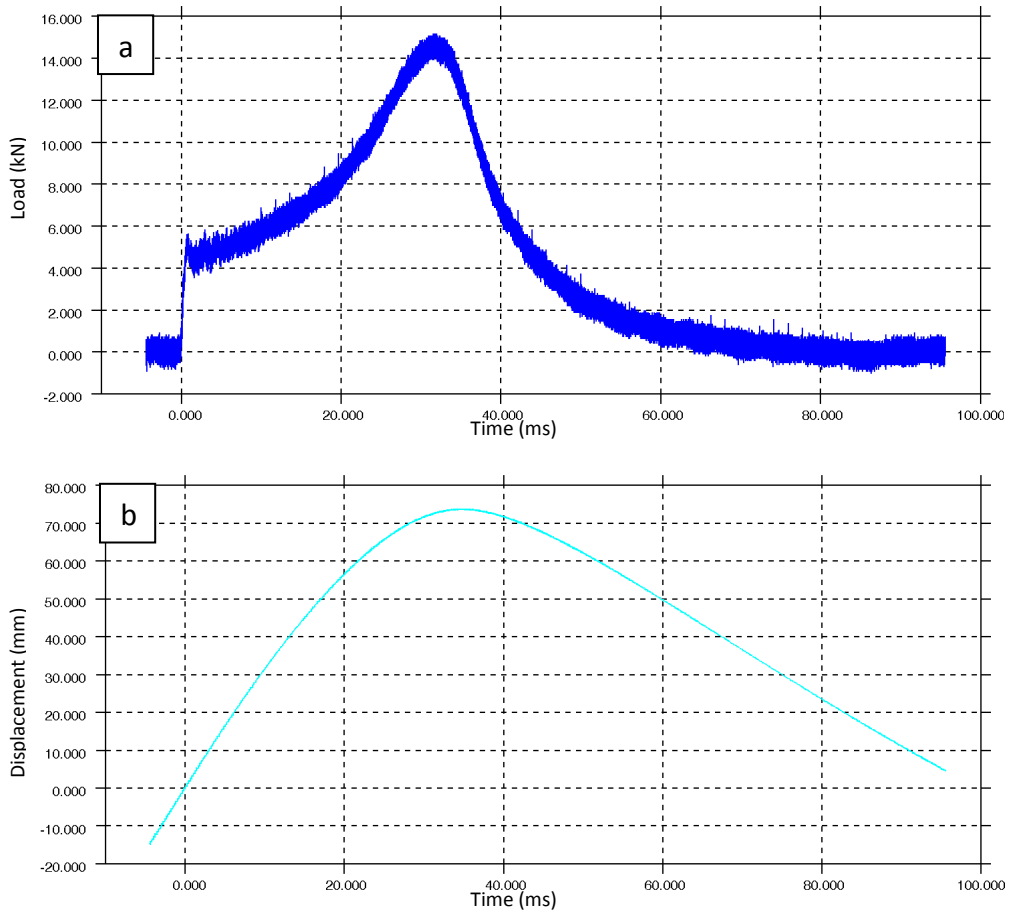

Figure 25: The a) raw Load/Time and b) Displacement/Time data from a drop tower test of 60 kg.m^{-3} EPP at 3.5 m.s^{-1}

Once filtered, as is shown in Figure 26, the data can be combined in order to produce a force – displacement curve. Which in turn produces the stress - strain curve in Figure 27 using the dimensions recorded prior to testing.

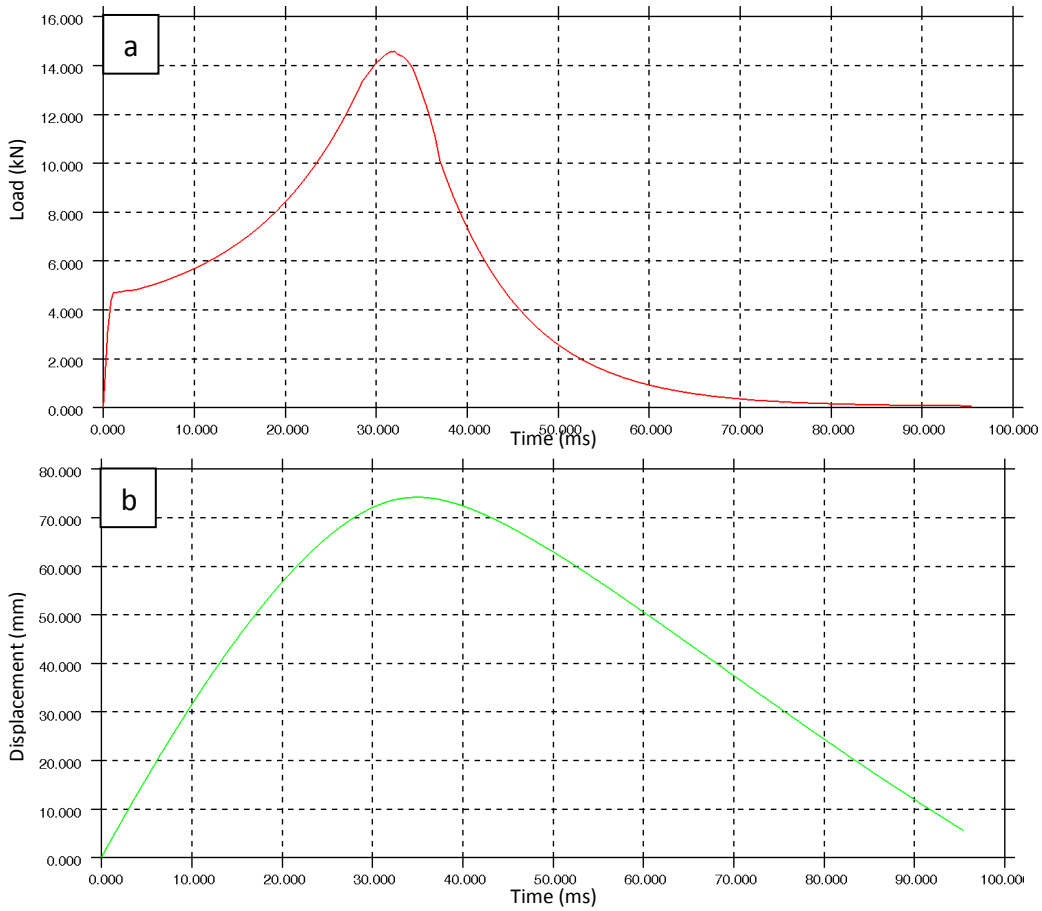

Figure 26: Post processed a) Load/Time and b) Displacement/Time data from a drop tower test of 60 kg.m^{-3} EPP at 3.5 m.s^{-1}

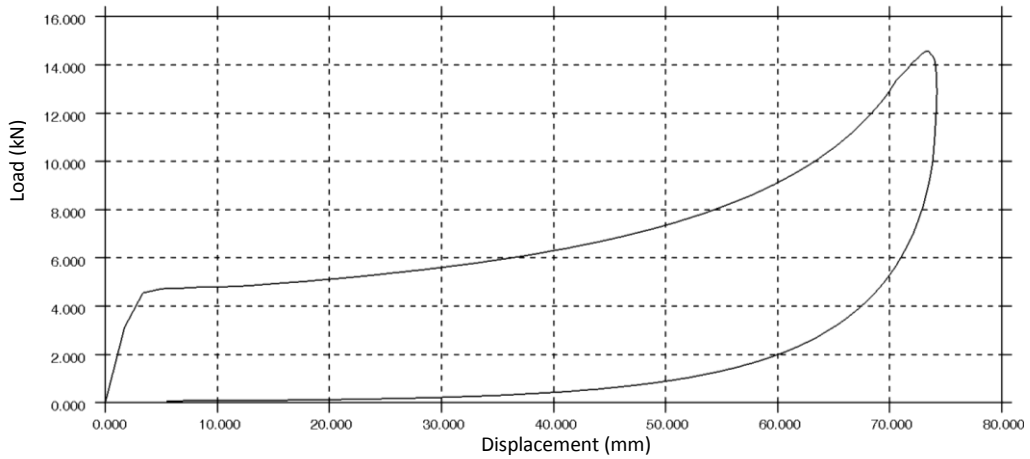

Figure 27: Load/Displacement Curve from a drop tower test having been filtered and zeroed for a 60 kg.m^{-3} EPP compressed at 3.5 m.s^{-1}

4.4 Test Specification Comparison

Two setups are available for the VHS testing rig under compression (Section 4.2.3). The first runs the compression plate into the internal hydraulics buffers, using the machine maximum extension. The second system runs the cross bar into adjustable stoppers, shown in Figure 24, which results in a peak force that shears a pin, disengaging the actuator. Figure 28 is a comparison between the two setups and that of the Drop Tower (Section 4.2.2). The velocity of the compression plate is plotted against displacement. Using the shear pin configuration with an input velocity of 5 $m.s^{-1}$, the fixture has not reached it prior to impact; due to the distance required for accelerating a stationary mass to the required velocity. This may be the cause for a reduced modulus compared to the Drop Tower test, however the plateau and densification are under the constant velocity of 5 $m.s^{-1}$. The Drop Tower and VHS buffers decelerate during the test; this is dictated by the samples ability to absorb the energy with the former and the hydraulic buffers in the latter.

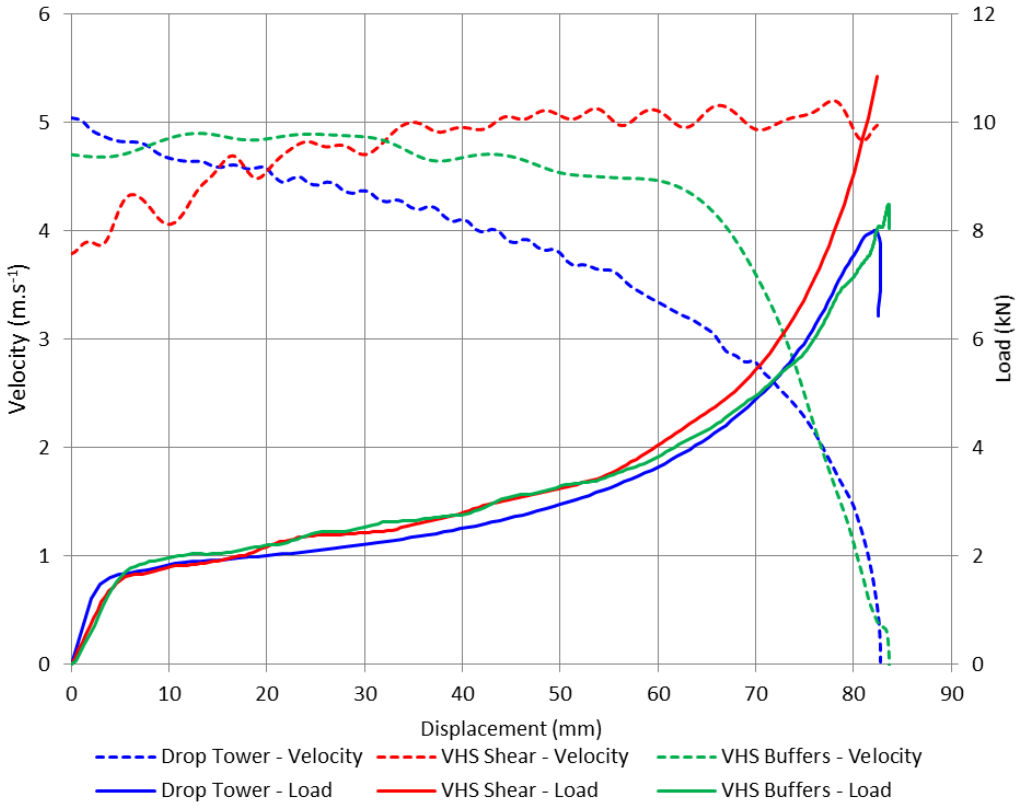

Figure 28: Velocity - Displacement and Load -Displacement for a sample of EPP 30 $kg.m^{-3}$ under the three test conditions available from the Drop Tower and VHS

The continuous deceleration of the Drop Tower, and deceleration on approach to the buffers for the VHS are shown by a decrease in velocity. The load from the buffers configuration matches that of the shear pin during plateau, but as the velocity decreases at the onset of densification, the load decreases to match that of the Drop Tower. This demonstrates the effect that velocity has on the densification stage, a higher velocity causes it to reach densification earlier. A possible reason is the reduced time for internal gas to escape, and therefore the increased pressure it applies as it is compressed. The stress-strain response for the same experiment can be seen in Figure 29, with the calculated density of each sample.

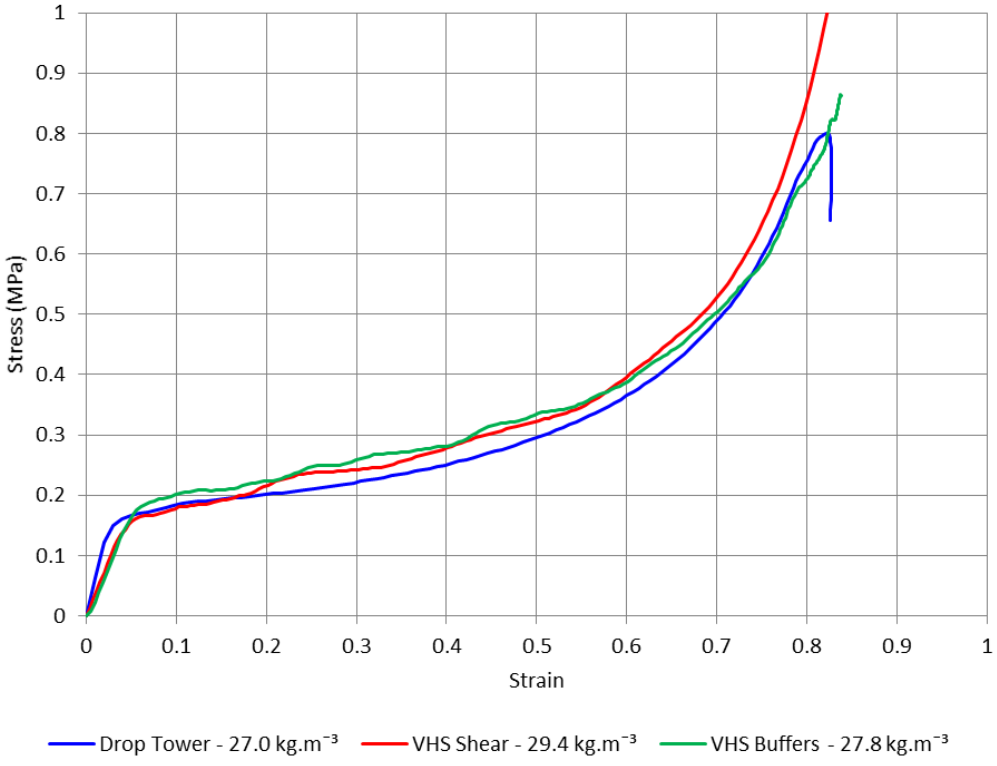

Figure 29: Stress-Strain curves for 30 kg.m^{-3} EPP at 5m.s^{-1} on the Drop Tower and VHS

The Young's Modulus, yield stress and onset of plateau are similar across all three conditions, with each variation explained by the changes in velocity as the experiment develops. The constant velocity of both the shear and buffers systems in the VHS testing shows the steady increase of stress during the compression. Figure 30 is a similar case, with a higher density block of EPP compressed at 2.5 m.s^{-1}. Using the lower velocity configuration for the VHS the compression plate has more time to reach the input value and requires less time to decelerate as the compression plates

approach the buffers. Also the decrease in velocity results in less energy for the block to absorb, this emphasises the decrease in stress as the Drop Tower mass decelerates. In Figure 30, A and B show the strains at which a noticeable deceleration occurs for the Drop Tower and VHS Buffer tests respectively.

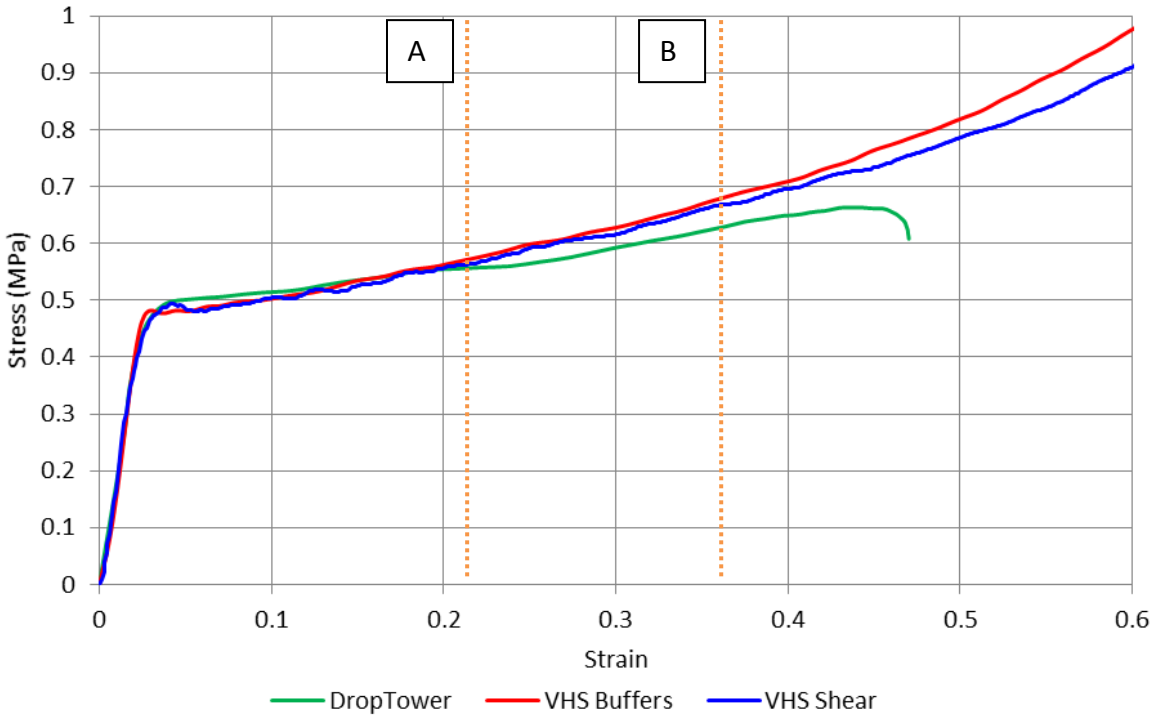

Figure 30: Stress-Strain curves for 60 kg.m^{-3} EPP at 2.5m.s^{-1} on the Drop Tower and VHS

Another cause for the change in response could be the effect of inertial loading. Once under compression, the samples resist the change in velocity of the Drop Tower and the VHS with buffers. This inertia load could contribute to the increase in stress and the apparent softening of the material close to unloading. The VHS with shear has an effective infinite inertia due to the constant velocity throughout the test. The unloading had a much sharper response on this machine as soon as the load was removed.

The inertia loading can become a concern when designing a component to absorb energy across its full strain; however the energy absorbed is consistent across all three machine specifications for the first 0.4 strain. It does not have an effect on the initial peak stress that can cause injury to the occupant.

The use of the VHS allows the material to be characterised at specific velocities to a desired strain without the reduction of stress from deceleration that is typical of a

drop tower test. Figure 33, in Section 4.6.1, demonstrates the sensitivity of a drop tower test response at different velocities.

4.5 EUEPP Dataset Validation

As was the case with all Drop Tower testing of EUEPP foam, the materials stress-strain response did not match the supplied performance. Figure 31 shows material of density 30 kg.m^{-3} impacted on a drop tower between 2 and 5 m.s^{-1} using the test methodology shown in Section 4.2.2. The yield and plateau stress of the validation tests are lower than that of EUEPP's suggested curves.

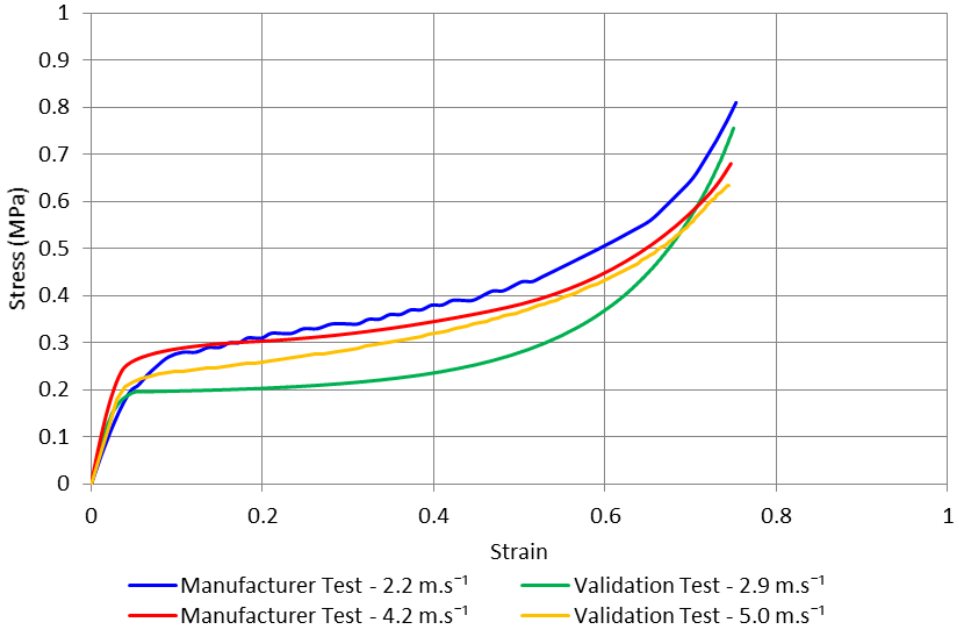

Figure 31: Manufacturer and Validation stress-strain data for 30 kg.m^{-3} EPP

An increase in impact velocity has shown an increase in stress for the yield and plateau during validation testing, but appears to only effect the Young's Modulus for the manufacturers testing. There is also a difference in the onset of densification, with both the lower rate tests reaching densification at a lower strain. The cause of this could be the microstructure of the material remaining intact during the compression at a lower rate, which then contributes more to the stress after cell collapse and as air is being expelled.

The comparison highlights the requirement for in-house characterisation for JLR. Manufacturer's data may not be applicable to other samples and test conditions, making it important to check the repeatability of a dataset.

4.6 Material Performance across Manufacturers

Figure 32 is a comparison between the two manufacturers' (EUEPP and UKEPP) EPP of density 30 $kg.m^{-3}$. Velocities of 0.1, 2.5 and 5 $m.s^{-1}$ were used to verify that a change in material mechanics occurs as the strain rate increases. The tests were carried out using the test methodology shown in Section 4.2.3.

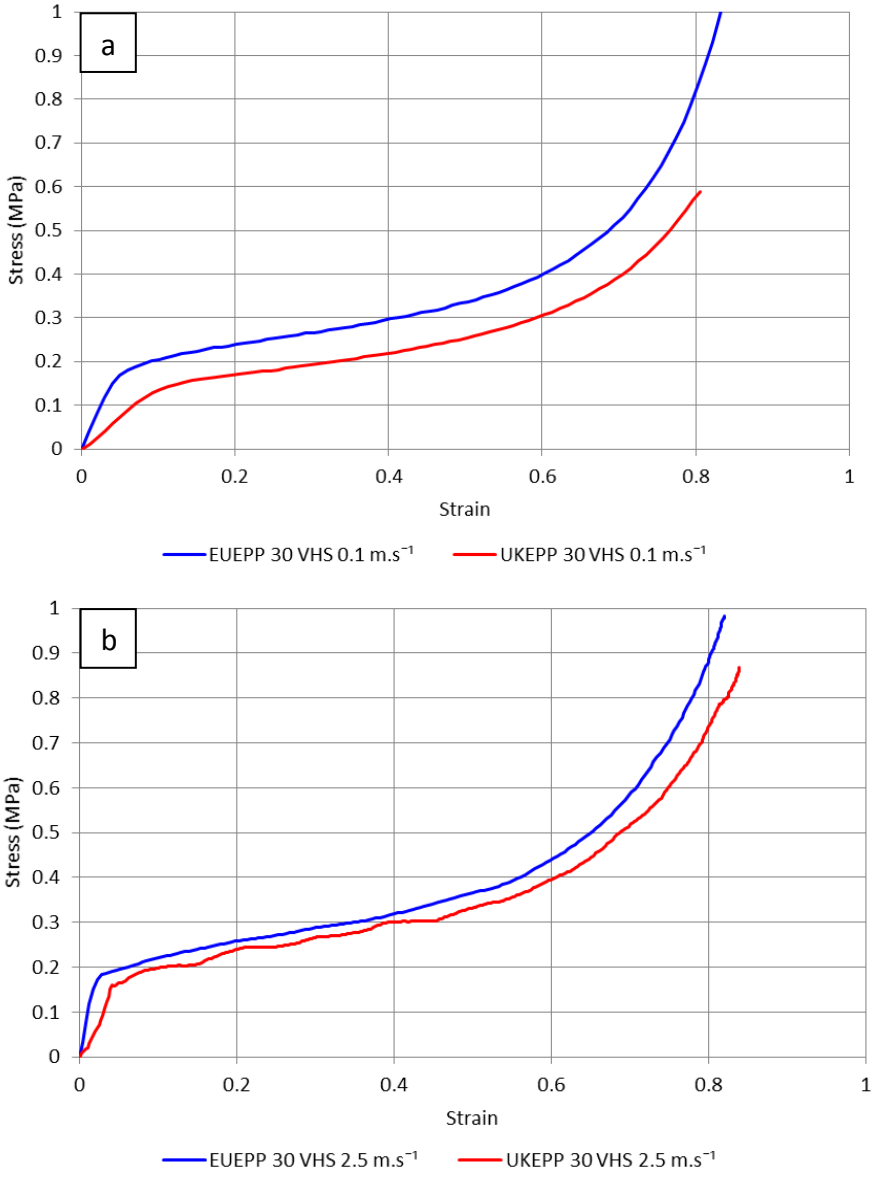

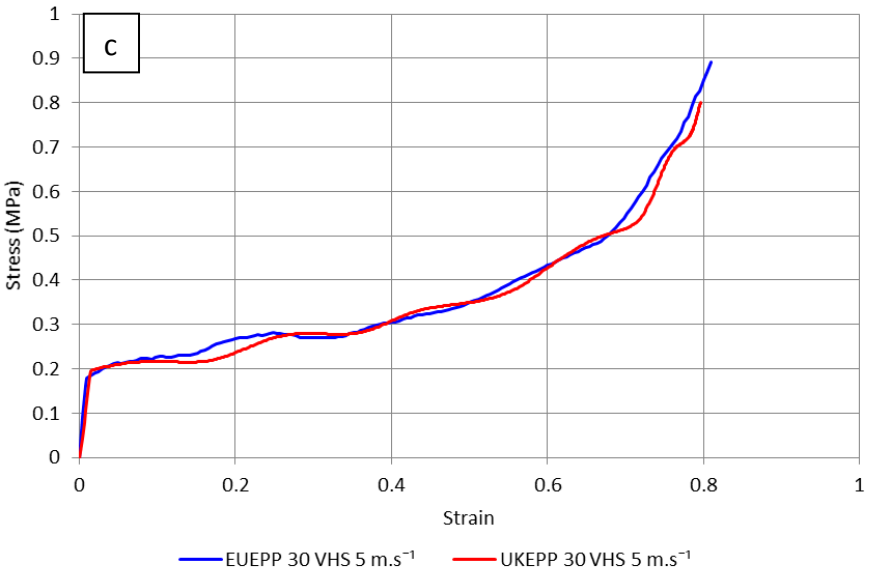

Figure 32: VHS testing of two supplier's material at three different velocities; a) 0.1, b) 2.5 and c) 5 m.s^{-1}

The modulus of EUEPP increases with the increase in strain rate, however the plateau stress does not appear to be affected. This is in contrast to the UKEPP material; a cause of which could be created during the manufacturing process. At 0.1 m.s^{-1} there is a clear difference in material performance between the two suppliers. EUEPP outperforms UKEPP exhibiting a higher Young's modulus, yield stress and plateau stress; resulting in more energy absorbed over a given displacement. The difference in material performance decreases at 2.5 m.s^{-1}, and has gone by 5 m.s^{-1}, therefore the contributing factor has been nullified at the higher velocity. At lower rates, EUEPP's foam may have a superior mechanism for absorbing energy through buckling. If, at higher strain rates, the polymer becomes brittle which results in a fracture, then the possibility for energy absorption due to buckling has been removed. This would explain the improvement in performance for a range of strain rates, which is then unidentifiable outside of such a range.

The performance trend may not apply as the impact speeds increase beyond 5 m.s^{-1} (strain rate of 100 s^{-1}). Figure 4 shows testing conducted by Bouix et al (2009), with strain rates of 0.1 s^{-1}, 200 s^{-1} and 1500 s^{-1}; demonstrating an increase in yield and plateau stress. This could be a result of the custom manufacturing process or smaller sample size adopted for the research. Alternatively as the strain rates increases a component of the stress equations may increase its contribution for rates above those investigated for vehicle impact tests.

The analytical solutions discussed in Section 2.2 split the contribution of stress into three features for foamed material; fraction of material within cell struts (A), remaining fraction within cell walls (B) and the air pressure from within the cell (C). The equations for modulus, plateau and brittle collapse are as follows:

$$\frac{E^*}{E_s} \approx \phi^2 \left(\frac{\rho^*}{\rho_s}\right)^2 + (1-\phi)\frac{\rho^*}{\rho_s} + \frac{p_0(1-2\nu^*)}{E_s(1-\frac{\rho^*}{\rho_s})}$$

A B C *Equation 5*

$$\frac{\sigma_{pl}^*}{\sigma_{ys}} \approx 0.3\left(\phi\frac{\rho^*}{\rho_s}\right)^{3/2} + (1-\phi)\frac{\rho^*}{\rho_s} + \frac{p_0 - p_{at}}{E_s}$$

A B C *Equation 6*

$$\frac{\sigma_{cr}^*}{\sigma_{fs}} \approx 0.2\left(\phi\frac{\rho^*}{\rho_s}\right)^{3/2} + (1-\phi)\frac{\rho^*}{\rho_s}$$

A B *Equation 7*

As the strain rate increases and causes a possible brittle fracture to the cells, the contribution of air pressure (C) is removed as shown in Equation 7. There is also a reduction in the contribution to stress from the cell walls (B) that were previously stretched and held in tension by the struts. In such a scenario, the defining feature for the foams modulus, Equation 5, would be the cell struts (A); which may be very similar for EUEPP and UKEPP foam. This would result in a steady approach to matched material performance as the strain rate was increased.

In order to analyse this hypothesis, computed tomography could be used to analyse post-test foam microstructure, in order to evaluate any evidence of internal brittle fracture that could take place. Quasi static testing of both manufacturers material is discussed in Section 5.

4.6.1 Strain Rate Effect

The strain rate effects are difficult to analyse for testing done on the Drop Tower (Section 4.2.2), due to the requirement to reduce energy input and therefore

displacement of the drop mass. Figure 33 shows impact velocities ranging from 1 to 3 $m.s^{-1}$ on blocks of 60 $kg.m^{-3}$ EPP. The materials Young's Modulus appears to increase with the increase in velocity, but the effect of deceleration makes the yield and plateau analysis problematic to interpret. An increase in energy into the system will initiate a larger proportion of the materials absorption mechanics; thus slowing the impact mass at a greater rate.

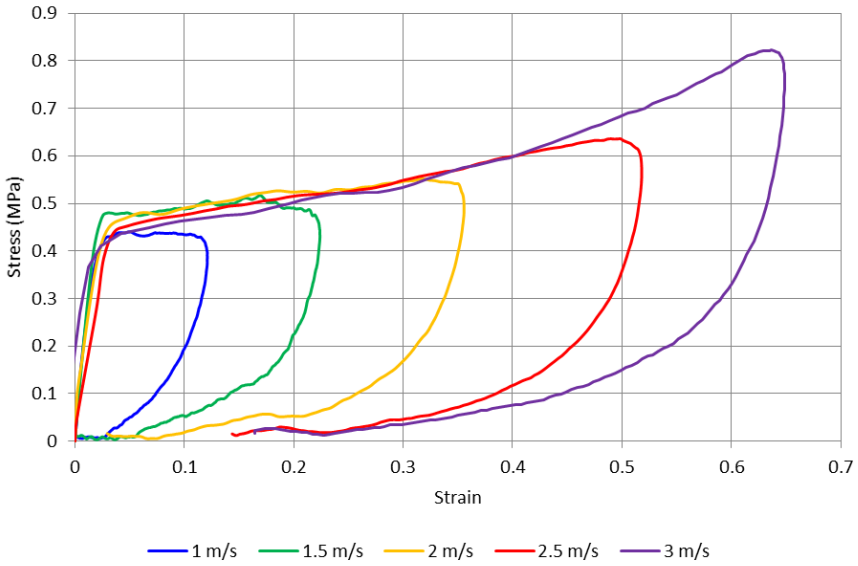

Figure 33: Drop Tower velocity outputs for 60 $kg.m^{-3}$ EPP

Figure 34 represents the stress-strain curves for 60 $kg.m^{-3}$ EPP on the constant velocity VHS (Section 4.2.3); it is representative of the densities that were tested. The strain rate possibilities are greater on the VHS, with a range of 0.001 $m.s^{-1}$ up to 5 $m.s^{-1}$, and samples that can be compressed further into the densification phase. The increase in velocity results in an increased Young's Modulus, yield stress and rise in stresses during the plateau region. As the velocities increase to 5 $m.s^{-1}$ the increase in plateau stresses appear to steady off, as discussed previously.

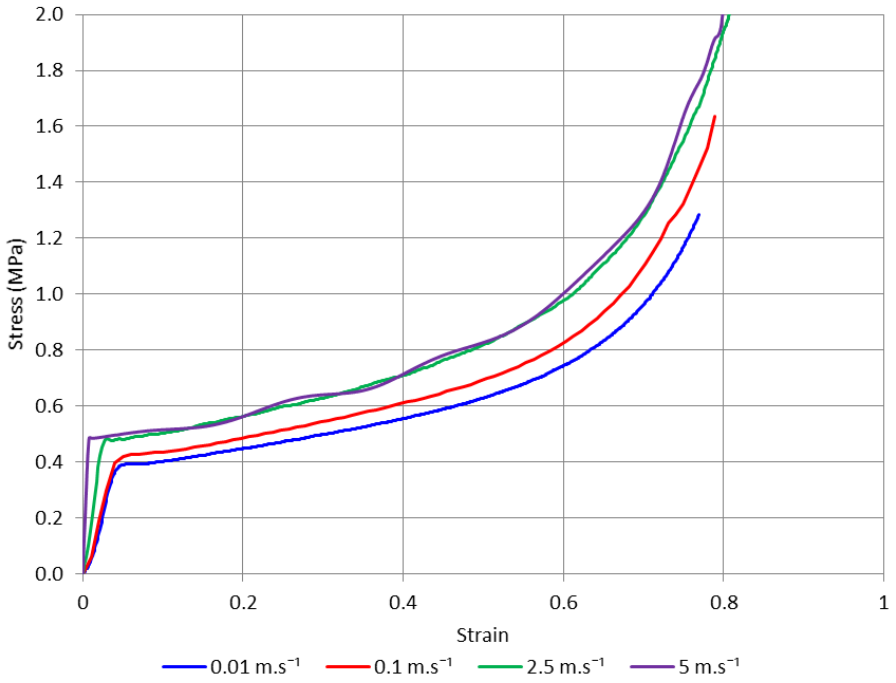

Figure 34: VHS stress-strain outputs for 60 kg.m^{-3} EUEPP EPP with an increasing velocity

Figure 35 shows the change in Young's Modulus and yield stress as the strain rate is increased. The modulus greatly increases with the increase in rate whereas the degree of change in the yield stress is reduced. Equation 5 and Equation 6, the modulus and yield stress, change with strain rate possibly due to a change in absorption mechanic. During the modulus stage of compression it is assumed the struts and cell walls are contributing to the stress response for all strain rates. If the struts are changing from a buckling to a fracture mechanism during yield as the strain rates increase, the contribution they have to stress will decrease. Again, µCT could be a means to investigate this further.

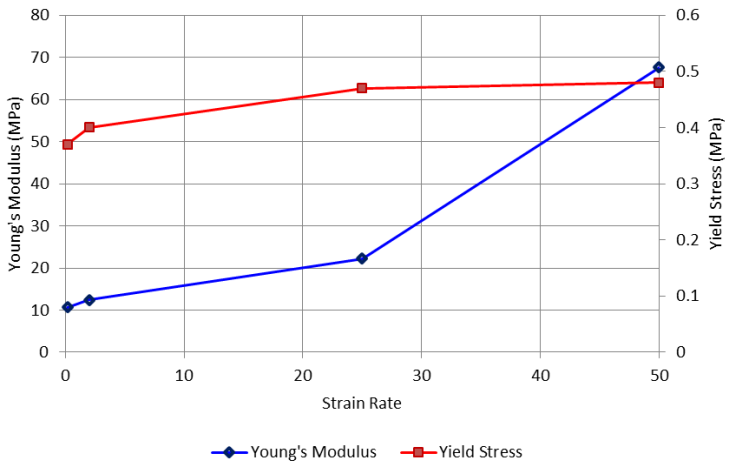

Figure 35: Materials Young's Modulus and Yield Stress with an increase in Strain rate for 60 kg.m^{-3} EUEPP EPP

4.7 Final Review of Material Models with Validation

The coupon simulation, that was formulated for *Submission Two - Simulation Development* and discussed here in section 3.2, was used for the validation of flat plate testing in LS-DYNA. The addition of a cylindrical impact model represents the Drop Tower load case using the test methodology shown in Section 4.2.2. The models are shown in Figure 36.

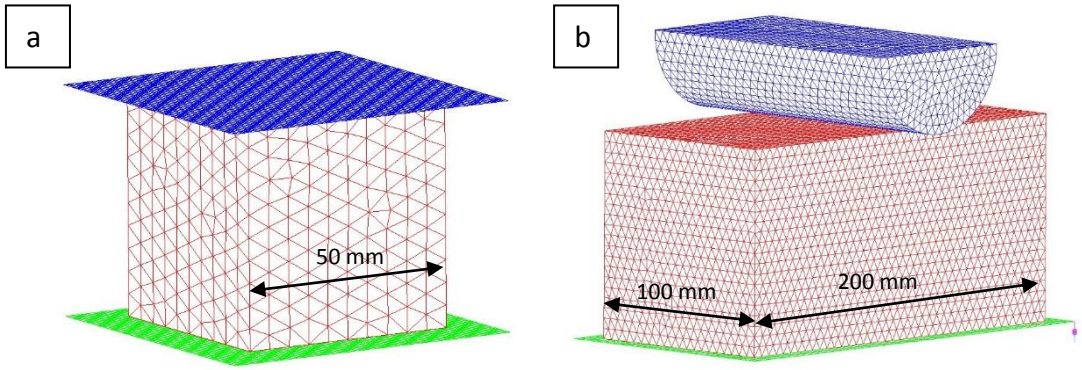

Figure 36: FEA models used for testing and validating test data; a) Coupon and b) Cylindrical Impactor

Using the Drop Tower data with a flat plate impactor, an updated material model was created, inputting a validated stress-strain curve. The new material model was then used to simulate the cylindrical impact test, to demonstrate that LS-DYNA can predict the samples response under a different load case. Figure 37 shows the material model input curves that have changed over the project. The original JLR model, the updated model using EUEPPs dataset and the validated model created within WMG.

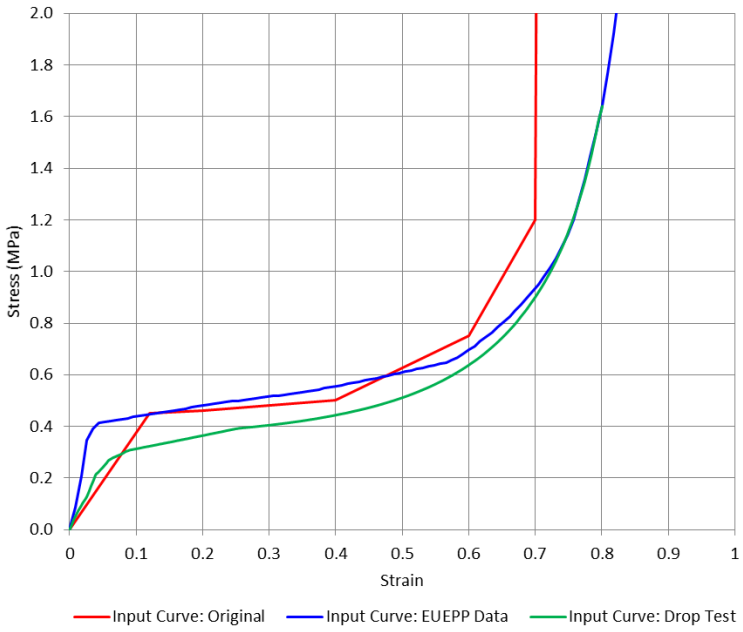

Figure 37: Material Model input curves used to compare the cylindrical impact simulations

Figure 38 shows the material response from the cylindrical testing with the simulated counterparts, demonstrating an improvement in simulation predictability that is now available to JLR. The results from this validation have fit the physical testing very well, with a residual error reduction of 93% when comparing the Drop Tower data model to the original JLR material model. Due to the peak stress during yield, the EUEPP data created an increase in residual error.

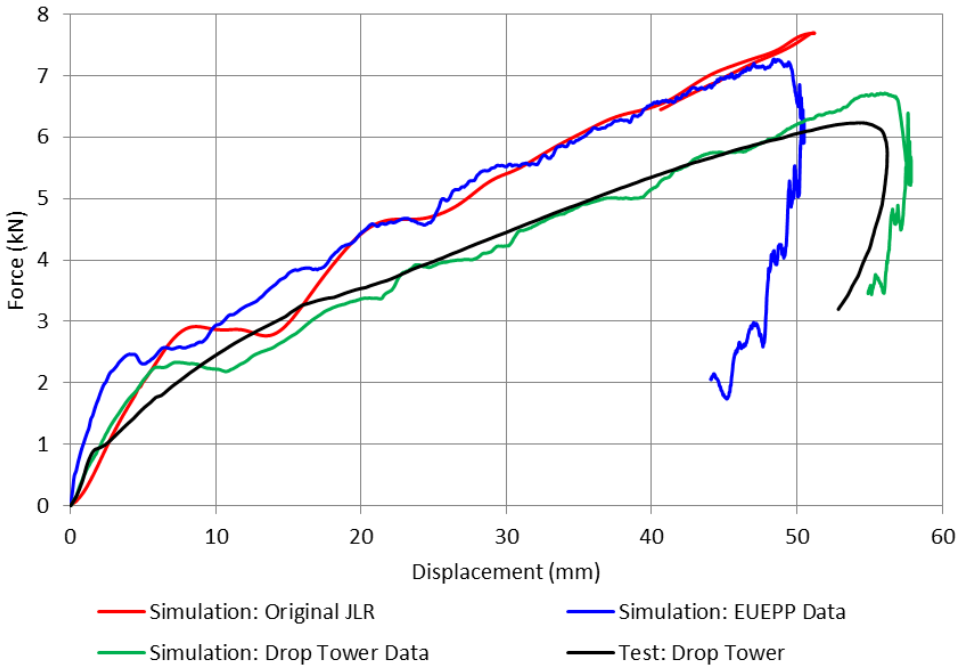

Figure 38: Cylindrical impact response from testing and simulation of 50 kg.m^{-3}

Further details on the FEA model can be found in *Submission Four – Geometry Investigation*. Cylindrical impacts have been tested and simulated on all of the sample combinations available with similar results. Without the testing uncertainty that was present in the previous validation work, Section 3.6.1, the simulation fidelity could be fully incorporated; demonstrating the importance for tractability and record keeping from testing.

4.7.1 Strain Distribution using Digital Image Correlation

Digital Image Correlation (DIC) was used to verify the models were representing the strain distribution correctly, based on the distribution of mass that can occur in cellular solids. Using the test methodology previously discussed, a 100 mm cube sample of EPP was compressed using the Drop Tower (Section 4.2.2). The same test setup was simulated using LS-DYNA, and the strain pattern from both is displayed in Figure 39. The simulation is a homogenous material that provides the global response of a foamed part. The strain distribution is therefore spread equally across the entire sample, whereas the testing shows nonuniform distribution. There is a band of higher strain upon impact directly under the compression plate. At 20% compression, bands of material have begun to strain quicker than others; suggesting weaker points in the material are susceptible to yielding first. Computed Tomography could reveal what the cause of this effect is and where in the material it is stemming from (see Section 5).

DIC is limited to a 2 dimensional image, therefore movement of the sample towards the camera would not be detected. Based on observations it is assumed that the sample does not move horizontally or bulge during compression. This is due to the vertical collapse of cells and the expulsion of gas.

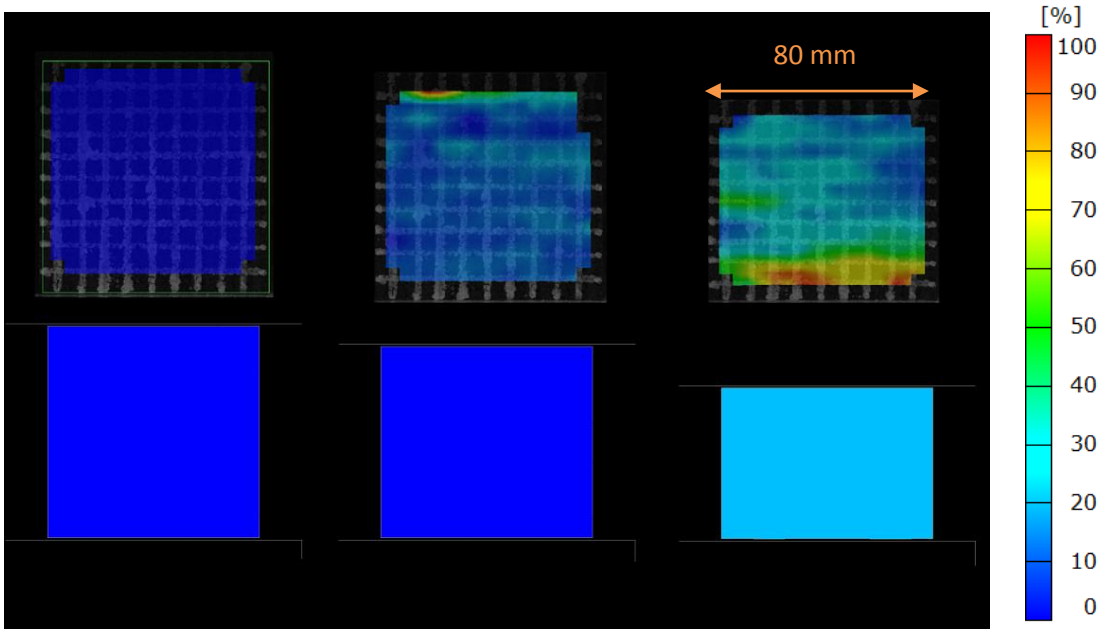

Figure 39: Strain distribution from a compression test using DIC (top row) and the simulated test in LS-DYNA (bottom row); at 0, 10 and 20 % engineering strain.

Larger samples, 200 x 100 x 100 mm^3, were used to validate a localised impact on EPP. Figure 40 and Figure 41 are the DIC and simulation plots, respectively, for a cylindrical impactor test on the Drop Tower. The images show compressions at 0, 20, 30 and 50 mm of displacement.

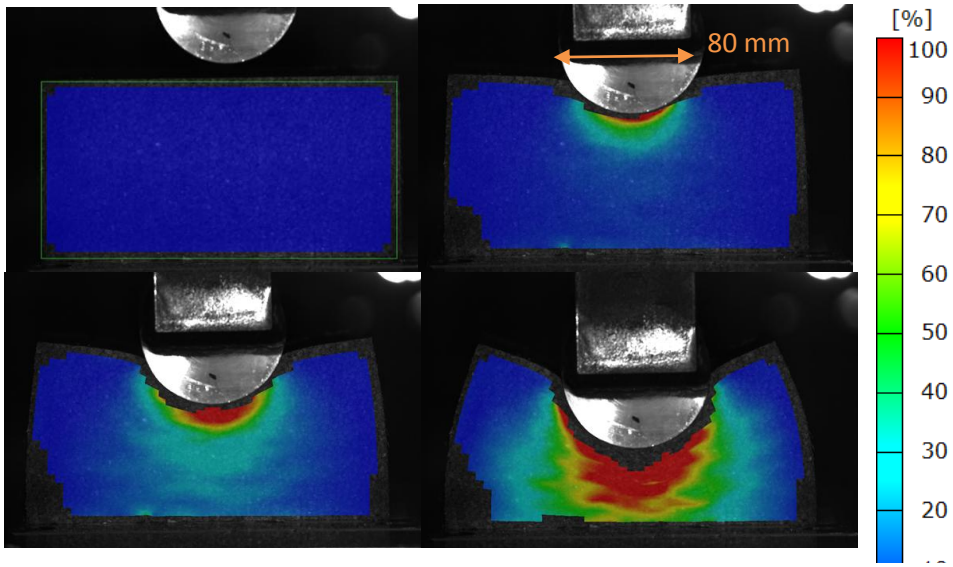

Figure 40: Strain mapping using DIC for a cylindrical impactor on EPP with an initial energy of 100J

The strain has originated from the point of contact and radiated outwards in a spherical shape in both cases. The banding that was exhibited by the samples under a flat plate compression fixture has largely disappeared in the more complex load case due to the high strain gradient.

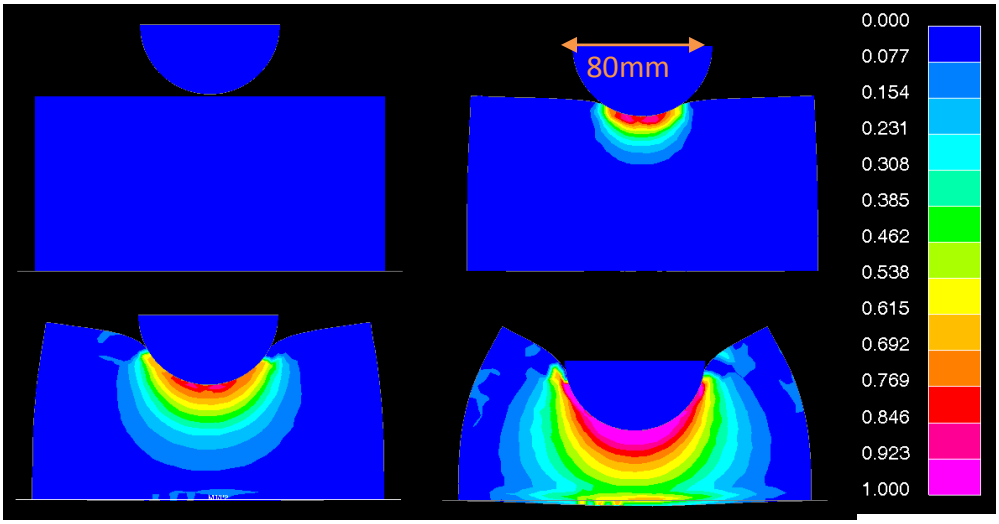

Figure 41: Strain mapping from LS-DYNA for a cylindrical impactor on EPP

The simulation matches closely to the test apart from a band of elements directly under the impactor and above the base plate that have been cut off due to the limitations of the technique used.

Both simulation and testing demonstrates the effect of tension across the top surface of each sample. There is also an element of shear as the sample resists the compression outside of the impactor's surface area. MAT_83 incorporates tension but not shear. Based on simulation validation this has not been an issue for the testing carried out; however if JLR design samples specifically for shear loading it should be investigated further.

4.8 Effect of Production Methods

Production of expanded polypropylene includes a pressure chamber to increase the volume of the beads and a mould that compacts them into the correct shape, before injecting heat through the surface as hot air in order to fuse the beads together. This process produces a skin layer on the surface of a sample and a resulting variability in density across a part; the effects of which has been investigated.

4.8.1 Density Distribution

Moulded samples are supplied with a skin layer; which is often desirable for aesthetic purposes. The material is denser within and in close proximity to this skin layer due to the compaction of the moulding process. The variation in density was therefore investigated in order to identify the change in material properties caused by it. One implication could arise if JLR request a part based on simulations using a homogenous density, but in reality receive something different. It is worth noting that the contribution to density variation caused by a skin layer on a vehicle component may have a greater effect than in the large block of material used here; however the thickness of the skin layer will be smaller in that scenario.

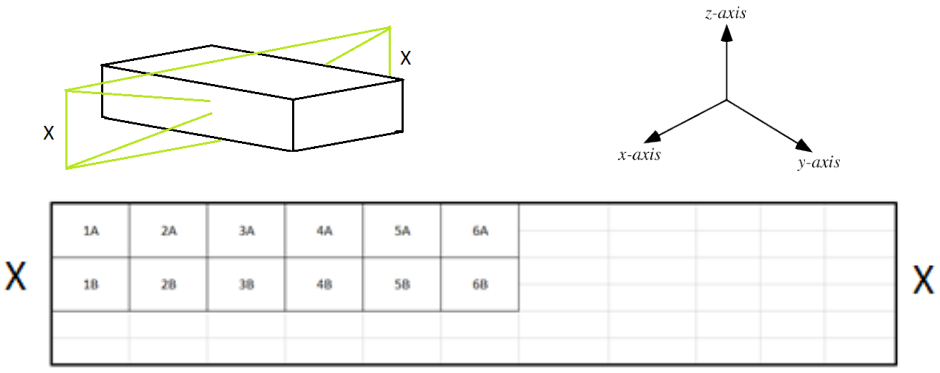

Figure 42: Cross section of 20 kg.m^{-3} part with samples taken from the corner to the centre of the block

Figure 42 shows that the samples came from the centre of a moulded block. Each one had dimensions of 50 mm cube; with the original block purchased at roughly 150 x 500 x 800 mm^3. The mould for this block was made across the shortest length. Therefore beads are compacted in the y-axis; causing the greatest density variation in that direction. The greatest density is found where two skin layers meet, as is the case for sample 1A. The material was specified as a 20 kg.m^{-3} block of EPP as shown in Figure 43; the average densities are 23.1 and 21.6 kg.m^{-3} for layer A and layer B respectively. The smallest density is still 6% higher than that purchased.

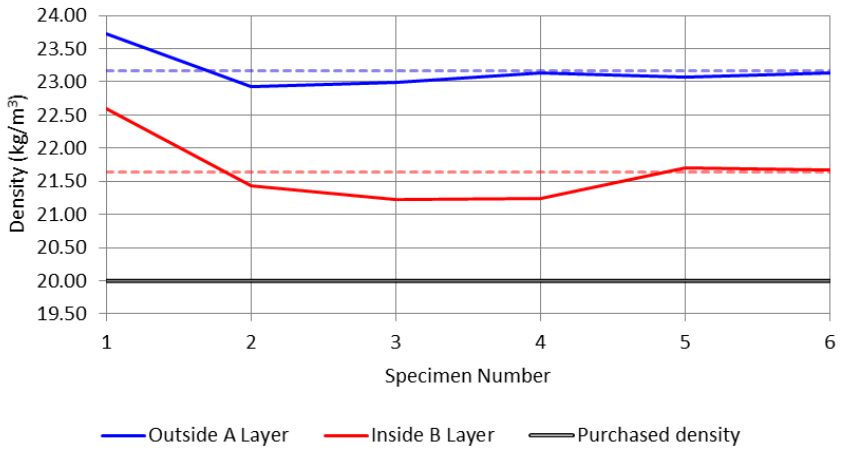

Figure 43: Density variation within a block of foam. The dotted line represents the layers average density

Figure 44 shows the difference in stress-strain response between the two layers. The concern was that samples designed based on required stress levels or strains in which a specific energy is absorbed may perform differently with this density distribution; however the comparison shows little variation in the results. The average response from layer A had a lower yield stress, but the blocks reached densification at a lower strain due to the skin layer that is already compacted; reducing the effective gauge length. The plateau stress remains the same across both layers.

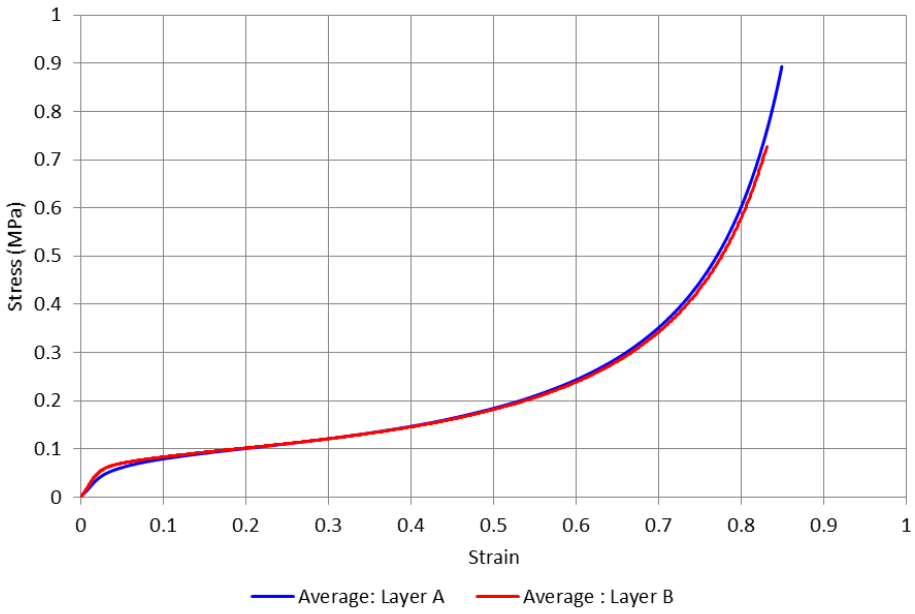

Figure 44: Average Stress-Strain response of Layer A and Layer B

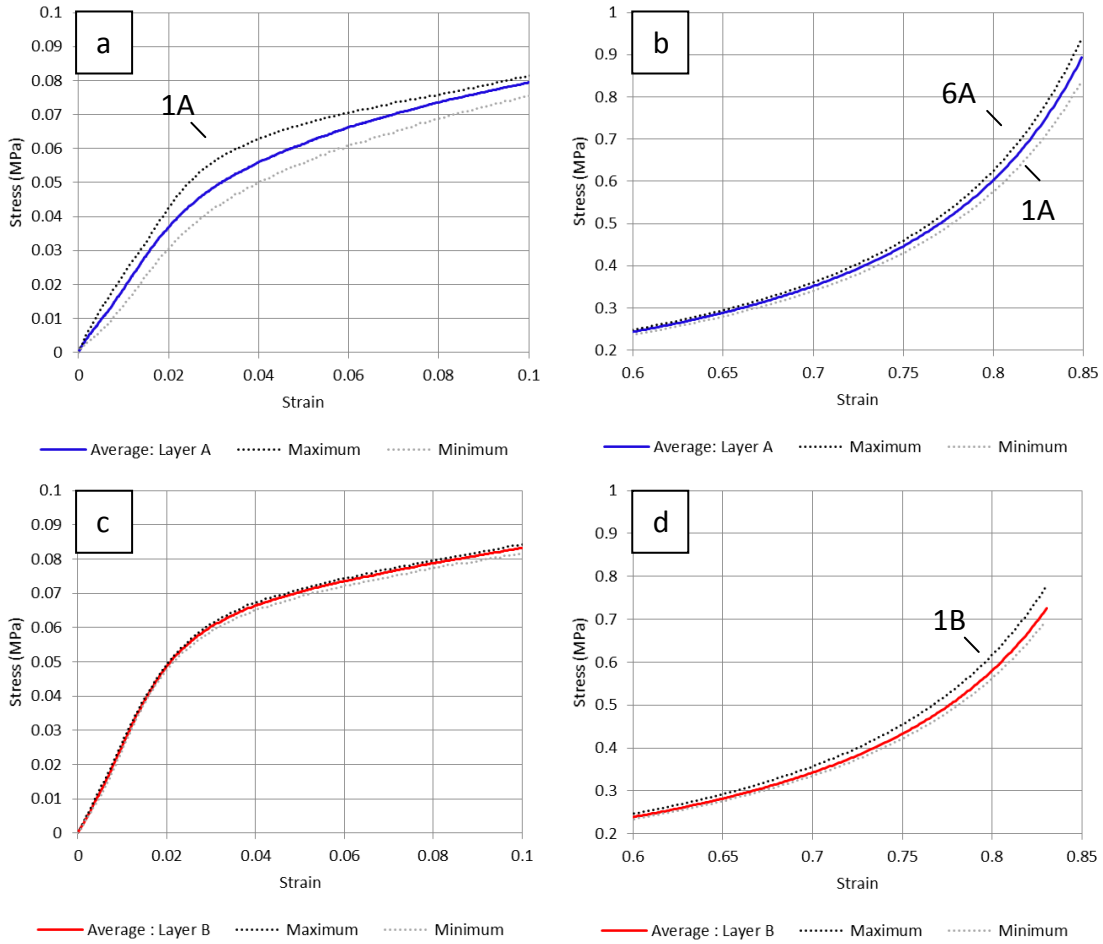

Figure 45: Yield and Densification stage of Layer A and Layer B showing the maximum and minimum responses. a) Yield of Layer A, b) densification of Layer A, c) yield of Layer B, d) densification of Layer B.

Figure 45 has been split into four graphs, showing the yield and densification of both the top and middle layer of material. Figure 45a and b are the stress-strain responses under compression of the top layer of specimens. The specimen from the corner, 1A, which has two skin layers from the mould has the highest yield stress. However it does not have the largest Young's modulus or plateau stress, 6A, which suggests this is determined by foamed structure and not affected by the thick wall within the height. 1A is also subject to densification at a later strain. Figure 45c and d shows the data from specimen layer B, of which only one sample has a skin layer and it is tangential to the direction of compression. The yield stress and Young's modulus are very similar with little variation. The foam block with a skin layer, 1B, undergoes densification sooner as is expected, due to less material available to compress.

The effect of density distribution is minimal, having little influence on energy absorption; it is therefore not a concern for JLR. Parts should be designed with a safety factor of stress levels in order to avoid injury to an occupant during an impact.

4.8.2 Exterior Skin Layer

The early onset of densification shown in Figure 44 is due to the already dense and compressed skin layer. Figure 46 shows the testing done on a homogenous foam, stacked layers of foam and a sample with a 3 mm skin layer. Additionally the strain calculation for the latter has been done to disregard this extra 3 mm, resulting in a material response that is closer to the other two, however the onset of densification still occurs at a lower strain. This suggest the gradient of density is higher towards the skin layer and therefore effected by the moulding process.

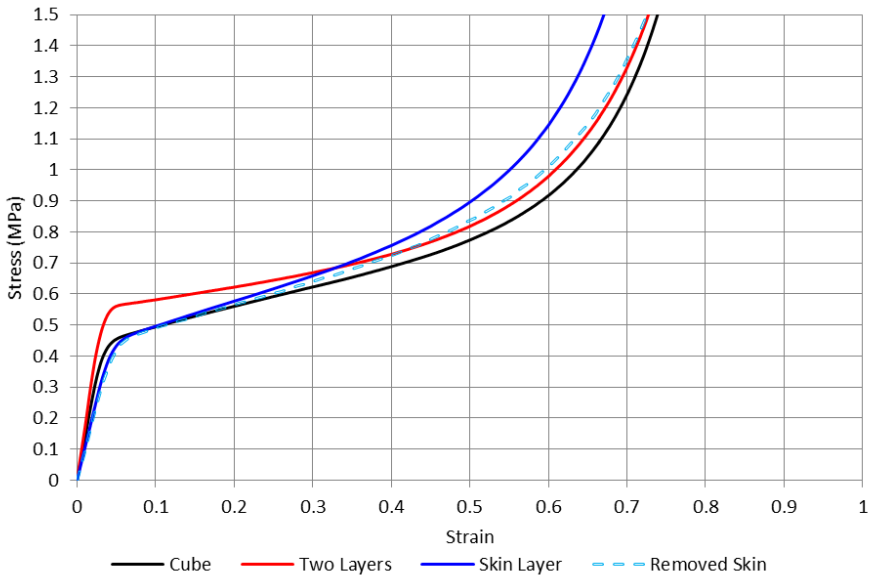

Figure 46: Strain calculations for the skin layer taking into account only the foamed material

4.8.3 Multiple Layers of Material

Structures within vehicles are often made with layers of different foams and or densities, for example the head rest which contains both energy absorbing EPP and comfort PU. This is to achieve different behaviour based on the load case the object is

being subjected to. Stacking multiple layers of a single foam is also an option, and can be incorporated into the moulding process. An investigation was done into the interaction between different densities of EPP; Table 15 shows the combinations of layers that were tested under quasi static conditions; highlighting the equivalent homogenous density they represent.

Table 15: Specifications for an investigation into the effect of stacked material

Densities within stack ($kg.m^{-3}$)	**Equivalent homogenous density ($kg.m^{-3}$)**	**Available Density used for comparison ($kg.m^{-3}$)**
30 + 30	30	EUEPP 30
30 + 60	45	UKEPP 50
30 + 80	55	EUEPP 60
30 + 60 + 80	56.67	EUEPP 60

Each sample has dimensions 50 x 50 x 25 mm^3, and are stacked with the shorter length as height. The tested combinations of stacked samples were as follows; two layers of 30 $kg.m^3$, 30 and 60 $kg.m^3$, 30 and 80 $kg.m^3$ and a three layered stack of 30, 60 and 80 $kg.m^3$. Using the volume of each stack and the average density it represents a comparison to an equivalent homogenous sample was possible.

Figure 47 is the comparison between a stack of 30 and 80 $kg.m^{-3}$ against the equivalent homogenous block with a density of 60 $kg.m^{-3}$ (chosen based on the availability). The average response from the stack is similar to that of 60, however there is a lower initial stiffness and a slightly earlier densification once the layer of 80 yields, between 0.3 and 0.4 strain. The material has a similar energy absorption across the full compression for a potentially better initial stress that is transferred onto the occupant. This could be used to customise EPP response within the space that is available.

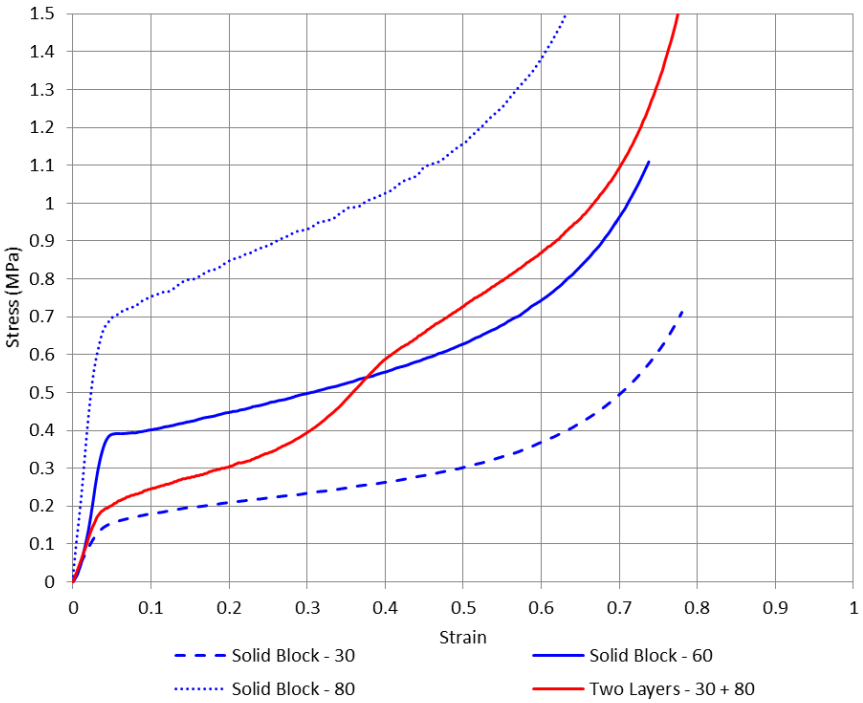

Figure 47: Stress-strain response for a block of 60 kg.m^{-3} and a layered equivalent

The three different stacks and three base homogenous densities are shown in Figure 48. They appear to have the same response for the first 0.15 strain, where the 30 kg.m^{-3} layer is being compressed. A 'step change' in stress occurs when there is a big difference in the base densities and therefore materials yield stress. Smaller gaps in density as well as the contribution of more layers results in a 'blended' stress-strain curve that smoothly ramps the plateau stage. This could help improve such quantitative analysis of vehicles as the HIC calculation (Section 3.6.1), in which accelerations must be extended over a larger time period for the passenger.

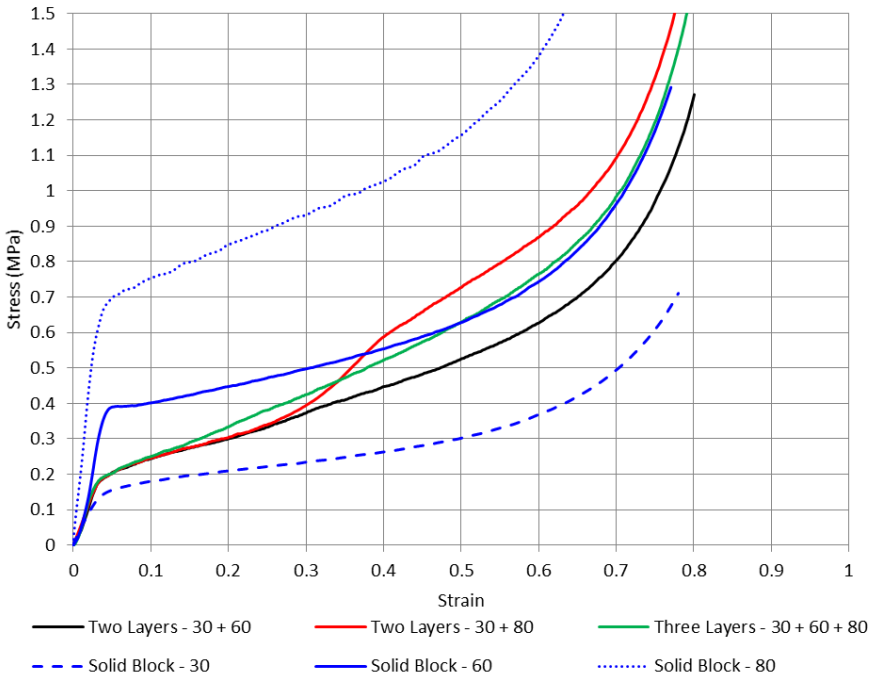

Figure 48: Stress-strain response for each layered combination

Simulation of a stack of homogenous blocks is possible, however the unloading effects may need investigation at different compressive strains in order to evaluate the models hysteretic mechanics and the interaction between each layer.

4.8.4 Sample Size

Under the recommendations of BSENISO_3386_1_1997 (British Standards Institution, 1997); characterisation is done on cubes or cylinders with a height less than the width as to avoid buckling. The effect of material size has been investigated in order to identify any change in material response, including the taller samples. Figure 49 shows the stress-strain curves for samples of 60 $kg.m^{-3}$, with dimension 50 x 50 x 100 mm (Tall) and 100 x 100 x 100 mm (Cube). The decrease in densification strain has previously been attributed to the VHS setup rather than the sample. The results suggest the samples shape and size does not affect the mechanical output in regards to stress against strain.

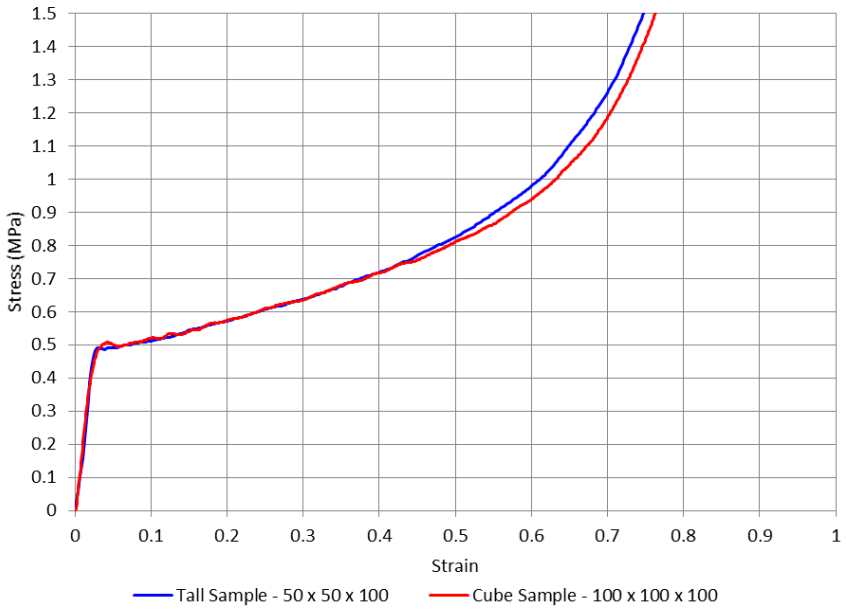

Figure 49: Sample variation for a block of 60 kg.m^{-3} EPP at 2 m.s^{-1}

4.9 Summary

- New test methodologies have been created and implemented into JLR for a range of strain rates across three machines.
- Validation of manufacturer's material showed discrepancies with their reported capabilities.
- A comparison between two manufacturers material showed vastly different performances for the same design specification.
- The addition of a skin layer does not have a significant effect on the materials stress-strain response.
- Materials absorption capabilities can be customised using a stack of varied densities.
- Further development of material models reduced residual error by 93%

The work shown in this chapter has led to the development of new energy absorbing test methodologies for JLR on three different machines, detailed in Section 4.2. Each of these used to create a different test condition, but all applicable for characterising foamed materials. The Instron 5800R and Drop Tower are commonly used for polymeric foam for quasi static to high strain rate testing. The VHS has a custom built

compression fixture that simulates a constant velocity impact, a test condition that previously was not well reported in the literature. A comparison between the two demonstrated the advantage of the VHS setup, with a greater range of strain rates and accurate velocities that can be used to characterise EPP. Some limitations were identified when testing at the high end of velocities, the configuration requires extra displacement to reach the specified speed.

The dataset acquired from EUEPP did not match the validation tests carried out on their material. This puts into question both the test method and conditions used, also whether they are manufactured at a different scale or potentially different parameters. Therefore it is recommended JLR do their own material characterisation when developing a new material model, rather than accepting the manufacturers data. A single set of material models in not enough for modelling foam materials, each manufacturer requires their own dataset based on their foams performance.

The material acquired from EUEPP and tested in house has been shown to be stiffer than the UKEPP performance, which is useful when designing for energy absorption over a smaller strain. For JLR this means more care must be taken in purchasing EPP from manufacturers, evaluating their capabilities to meet a material performance, rather than specifying simply the density required. Foam should not be treated as a commodity due to the variation in outputs that they exhibit, therefore the supply chain should be managed differently in order to improve the supply of these safety critical components.

The strain rate sensitivity of the material has been demonstrated on the VHS for strain rates ranging from 0.2 and 50 s^{-1}. There is a clear difference in manufacturers foam performance at lower rates, demonstrating the effect of production methods. A hypothesis has been created relating the mechanical response back to the analytical solutions created by Gibson and Ashby (1997). The contribution of air pressure is increased with strain rate, and an assumed cell failure or brittle behaviour explains an eventual drop off in stress plateau.

The effect of manufacturing methods were investigated. A density distribution is present in samples, with moulded blocks showing regions containing a 19% increase in

specified density of relatively large samples. The skin layer has little effect on the material performance, but does imply a density gradient towards the skin layer that is created by the moulding process and should be considered when creating a component. Layers of material can be used to customise a components response.

Using the updated dataset a validation test demonstrated an improvement in simulation outputs, with a residual error reduction of 93%.

The following chapter will now look at the manufacturing differences that have been demonstrated through testing, by evaluating the foams on a microstructure level, to help identify the cause. This includes analysing the interactions between foam beads, the size of cells and the material distribution across each component.

5 Micromechanics of Expanded Polypropylene: Computed Tomography and 3D Simulation (Submission Four)

The previous chapter highlighted the different energy absorption performances that EUEPP and UKEPP achieve under compression and the change in response caused by an increase in density of a foam. This chapter explores the possibilities of using micro computed tomography (μCT) for characterising foam materials. The use of this technology was identified in the literature review and allows a materials internal structure (Section 5.1) to be viewed and evaluated, without causing damage to the sample. Through imaging the microstructure of the two manufacturer's foam (Section 5.5), it was hoped that the cause of performance change could be identified. The aim was also to conduct a dynamic test on each sample during the scanning process (Section 5.6). Using the images a 3D mesostructural model could be produced to simulate and predict the mechanic response of the material (Section 5.7), showing the characterisation possibilities that were available to Jaguar Land Rover (JLR).

JLR do not have in house access to X-ray facilities and are therefore unable to utilise μCT capabilities readily. There are a number of research facilities around the UK that provide the opportunity for using μCT, usually from scanning through to post processing. The specification of the machines, including X-ray source and detectors dictates what the options are. Two types of facilities have been used here as a comparison; Warwick University, WMG and the central European Synchrotron Radiation Facility (ESRF), Grenoble (Section 5.2). This research is essentially a feasibility study for JLR on the use of X-ray technology for material characterisation (Section 5.8).

5.1 Internal Structure of EPP

The key features to view within a sample of expanded polypropylene (EPP) are the beads and their internal cell structure. The phases of compression, including the initial linear elastic response, yield, plateau and densification, are caused by the morphology of a foam. Evaluating the internal structure may highlight the structure mechanics that create the stress-strain response from a cellular solid. Computed tomography can

provide slices of the sample, which in turn can be converted into a three dimensional volume and reconstructed within a software package. This is a state-of-the-art process and is explained in more detail in *Submission Five – International Placement*.

5.1.1 Predicting the Effect of Material Distribution

The mechanisms for absorbing energy are paramount to the materials performance and applicability to a situation. Using X-rays the three key features can be visualised; they include bead wall buckling, cell strut buckling and cell wall resilience to air pressure.

$$\frac{E^*}{E_s} \approx \phi^2 \left(\frac{\rho^*}{\rho_s}\right)^2 + (1-\phi)\frac{\rho^*}{\rho_s} + \frac{p_0(1-2\nu^*)}{E_s(1-\frac{\rho^*}{\rho_s})}$$

A B C

Equation 8

Using Equation 8 (Gibson and Ashby 1999) along with values for 60 kg.m^{-3} EPP foam, a comparison between two fractions of solid within a cells struts was evaluated; shown in Table 16. Two extremes of material fraction 0.9 and 0.1 were implemented; demonstrating the swing from one stress contributor to another. However this does not take into consideration the effect of bead size/formation for polymeric foam with expanded beads.

With more material in the edges (ϕ = 0.9) the largest contribution to the Young's modulus is equation segment A, which has resulted in a reduced modulus compared to a structure with more material in the cell walls (ϕ = 0.1). In the latter case, the pressure and cell edge have almost equal weighting.

Table 16: Comparison between contributing foam features with different fractions of material within cell edges

Foam Density	Polymer Density [Modulus]	Air Pressure	Poisson's Ratio	Fraction of solid in edge	Resultant Foam Modulus	Dominant Component
60 kg.m^{-3}	947 kg.m^{-3} [1.5 GPa]	0.1 MPa	0.33	0.9	13.4 MPa	A
				0.1	81.1 MPa	B

As discussed in Chapter 4, the manufacturer's material has produced different stress-strain responses when created to the same density specification. Therefore, using this theory, the distribution of material from both EUEPP and UKEPP was evaluated. By identifying cell edge and wall contributions it is possible to explain the differences between each material and why at lower strain rates the material performance varies.

Through rearranging the equation to make ϕ the subject within a quadratic, it is possible to predict the materials solid material within a cell's edge using the Young's modulus from a low strain rate test, as shown in Figure 32a. The test was carried out on a sample of EPP from EUEPP and UKEPP; the results from the VHS compression test for a block of 80 $kg.m^{-3}$ EPP at a strain rate of 1 s^{-1} showed a modulus of 21 MPa and 14 MPa respectively.

The value of ϕ for EUEPP was found to be 0.906 and for UKEPP 0.970. This suggests that more material is held within the struts for a sample of UKEPP foam, whereas EUEPP material has thicker cell walls. The increase in cell wall thickness may be the cause for an increase in modulus, as the cell resists collapse. Using X-ray tomography it was possible to view the internal structure of each manufacturer's material, with the intention of viewing these distributions of mass. However, as mentioned, the equations do not consider the bead morphology, nor the voids that exist between them; which may be the leading cause for a change in material performance between the two. The output is also an approximation, using assumptions that will vary in practice. The three main features based on the beads that could affect the stress-strain response are the bead and internal structure, bead to bead joining and void space that remains outside of each bead.

5.2 Computed Tomography at WMG

The resolution of data acquisition is important for a material such as expanded polypropylene, where a bead can be have a diameter on the scale of 1 mm, and internal features that are as small as 10 μm. Using the WMG Nikon CT system, a

'volume pixel' or voxel size of 50 µm was achieved, on a sample of 30 x 10 x 10 mm^3 EPP with a density of 80 $kg.m^{-3}$, slices of which can be seen in Figure 50.

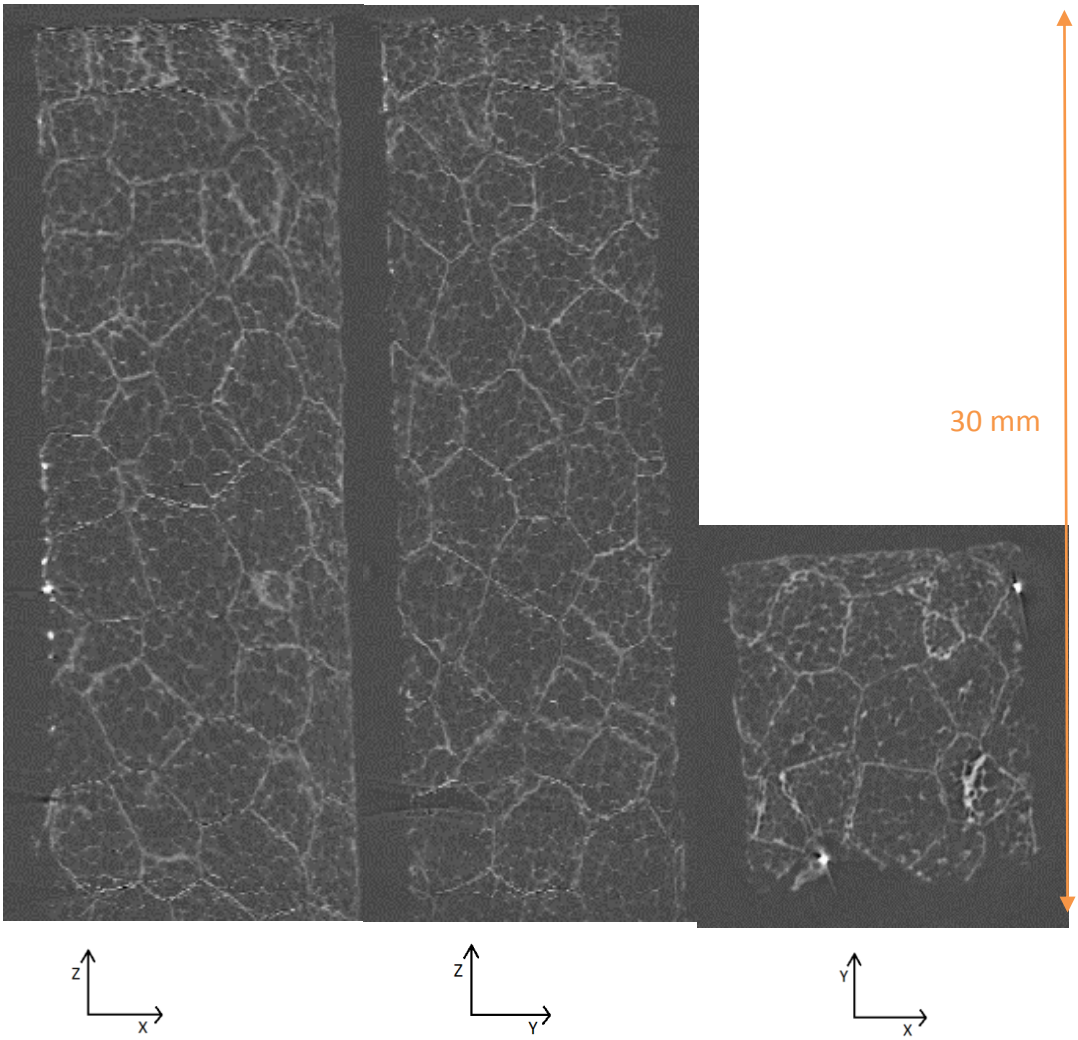

Figure 50: X, Y and Z axis cross section of a sample of 80 kg.m-3 EPP using the Nikon CT system with a 50 µm voxel resolution

Although the thicker bead walls were readily observed, the internal cell features were blurred and undefined. In theory, resolution can be improved by reducing sample size. However in order to detect the features on WMG's facilities it would require a sample at least 5 times smaller, reducing it to a length of 2 mm. This would remove the possibility for bead interactions as well as internal structure analysis. Multiple scans could be used to isolate specific areas, but could not incorporate all of them at once. In practice for lab-based machines resolution is limited to 10's of µm for moderately large specimens.

The effect of compression within the same type of lab-based machine requires a staged approach, as the time for a full rotation scan can take several minutes, requiring no motion to occur during this time. Even with a staged compression, relaxation during each stop results in some movement, which can affect the scan quality due to blurring.

In order to achieve an in-situ compression scan the beam quality, acquisition time and detectors must be of much higher ability. A facility using synchrotron radiation as its source opens up these possibilities.

5.3 International Placement: ESRF (Submission Five)

The international placement was an opportunity to experience industrial work or research outside of the United Kingdom as part of the EngD programme. The choice was made do this with the European Synchrotron Radiation Facility, as a means to expand on the material characterisation through computed tomography. It also helped to develop contacts for JLR and explore the feasibility of using such a facility for industrial research. The specific group hosting the placement was ID19, a beamline specialising in microtomography.

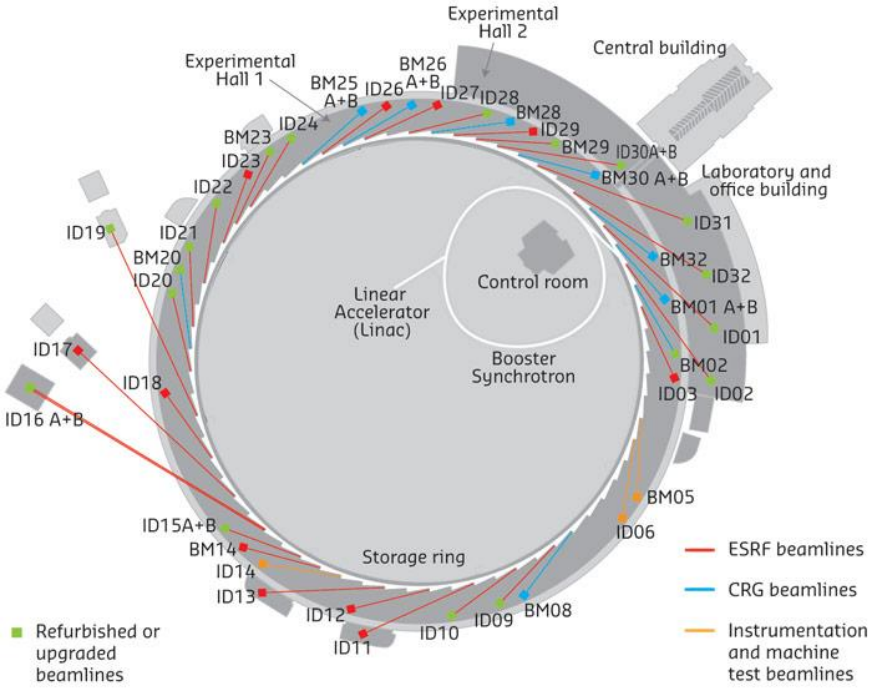

Figure 51: Schematic of the building layout; showing the individual beamlines (ESRF, 2016)

The schematic of the facility, Figure 51, illustrates the key features of a synchrotron X-ray complex. The accelerator, synchrotron booster and storage ring circulate and accelerate the electrons to just below the speed of light. Electrons are bent at magnets and emit X-rays which are then detected within each beamlines experimental hutch. ID19 is a satellite building, meaning it is situated outside of the central circular complex, in order to achieve a beam length of 145 m. This distance provides a highly collimated beam, giving the highest resolutions.

ID19 specialises in microtomography, the method of imaging a volume with high resolution, with a particular interest in in-situ experimental work and industrial collaboration. The beamline has a tuneable photon energy range of 6-120 keV with maximum beam dimensions of 45 x 145 mm^2.

The team has a range of high speed cameras, lens magnifications and detectors available for customising the images that are required for each experimental case.

5.4 X-Ray Technology and its Utilisation

During the placement a variety of academic and industrial users were allocated beam time, each using a variety of X-Ray technologies, including radiography, computed tomography and laminography.

X-Ray computed tomography allows for the internal structure of a sample to be viewed. The method avoids damaging the sample while creating the images, keeping the full structure intact. This was an attractive prospect for viewing the mechanical response of polymer foam during compression; to assist in the understanding of each phase that a foam undergoes, from onset of yield to densification. This also helps to demonstrate the differences between manufacturers material, highlighting where manufacturing improvements can be made.

The intensity of the beam available at the ESRF allows for rapid data collection, opening up the opportunity for dynamic scanning.

5.5 Experimental Procedure for the use of Synchrotron Radiation

The compression fixture used for the in-situ experiment is shown in Figure 52. An in-situ experiment was carried out for a compression rate of 2 µm.s^{-1} and 10 µm.s^{-1}, which equated to a strain rate of 6.67x10^{-5} s^{-1} and 3.33x10^{-4} s^{-1}, up to three factors smaller than the standard quasi static rate (3x10^{-2} s^{-1}) investigated for *Submission Three - Geometry Investigation*.

The focus of the experiment was on observing the yield, plateau and densification phases during compression of EPP foam. Sensors recorded the displacement, load and time from each test during loading and unloading.

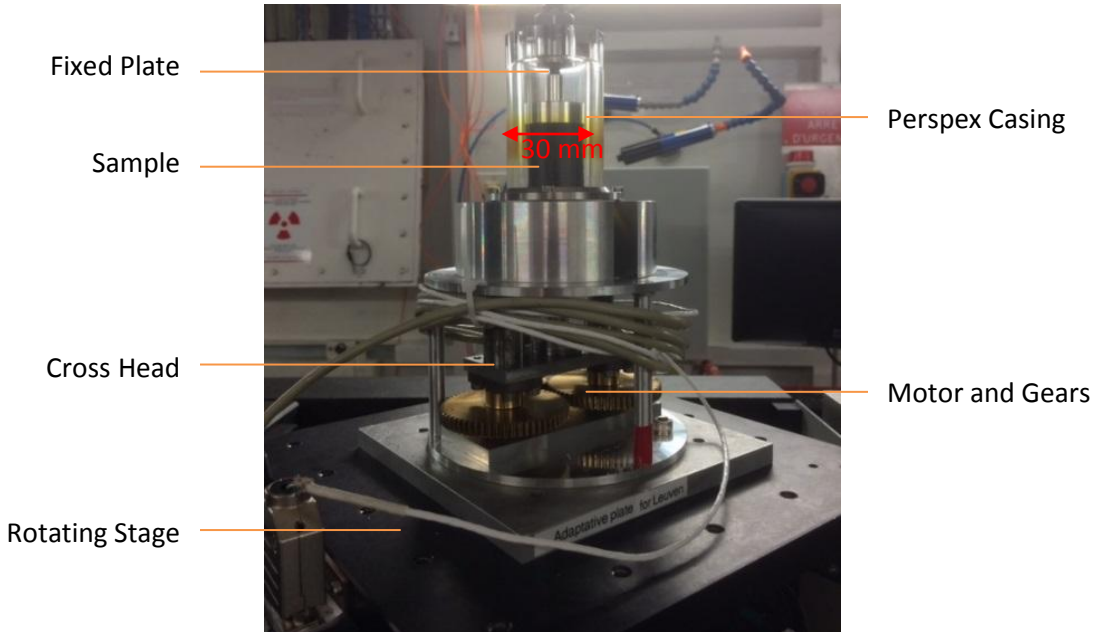

Figure 52: Novitom5K Compression Fixture on ID19

A beam energy of 35 keV was chosen to obtain the best possible image contrast upon advice. The resolution was set to 2016 x 2016 with a voxel size of 5.2 µm; this resulted in a sample volume of 10.48 x 10.48 x 10.48 mm^3. This size of sample was desired in order to see the interaction between a bead and all of its adjacent beads.

A scan was completed within a rotation of 180 degrees, taking 2 seconds for each full 180° scan. Table 17 is a summary of the experimental conditions used in order to scan each sample at the required strain, illustrated in Figure 53. The samples scanned range from 30 to 80 kg.m^{-3} and were taken from samples of EUEPP and UKEPP foam.

Table 17: Experimental Procedures created for executing the required scan conditions

Experimental Procedure Name	Compression Percentage (%)	Time interval [Start Time] (minutes)	Number of rotations (turns)	Compression rate (µm.s^{-1})	Sample Size (mm)
Scan2s (Initial)	0	N/A	N/A	N/A	30 and 25
Scan2sa (Plateau A)	5, 20, 35, 50, 65	7.5 [2.5]	112.5	10	30
Scan2sb (Plateau B)	20, 40, 60, 80	8.333 [8.333]	125	10	25
Scan2sc (Yield)	1, 2, 3, 4, 5, 6, 7, 8, 9, 10	2.5 [2.5]	35	2	30

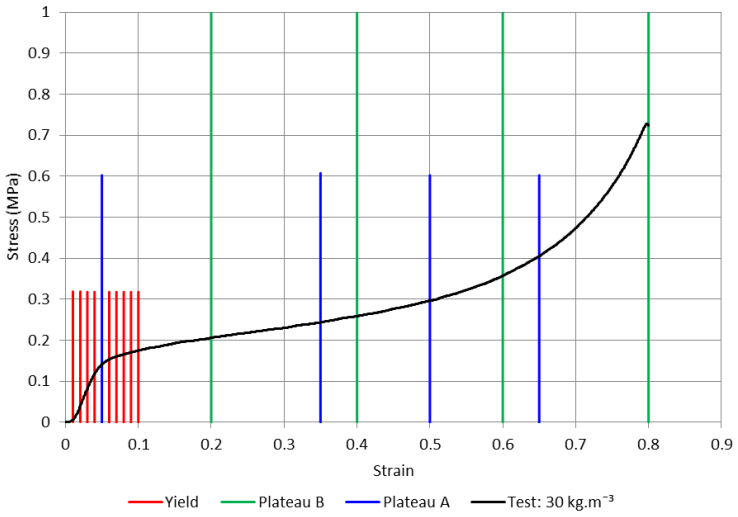

Figure 53: Scans during experimental procedures that show the corresponding strain during each compression test

5.6 Differences between Manufacturers Foam

The initial scan data were analysed to produce images of each sample prior to compression. Figure 54 is a comparison between the two manufacturer's samples with a density of 80 kg.m^{-3}. The UKEPP material has larger voids when multiple beads meet, which could be a result of a lack of compaction prior to moulding. This lack of force created during compaction has produced an apparent weakness where the beads meet, not producing the polyhedral shapes that are clear for a few of the EUEPP beads. It is worth noting that this is one slice in a collection of 2016 from a small sample of EPP, but it is indicative of the general trend.

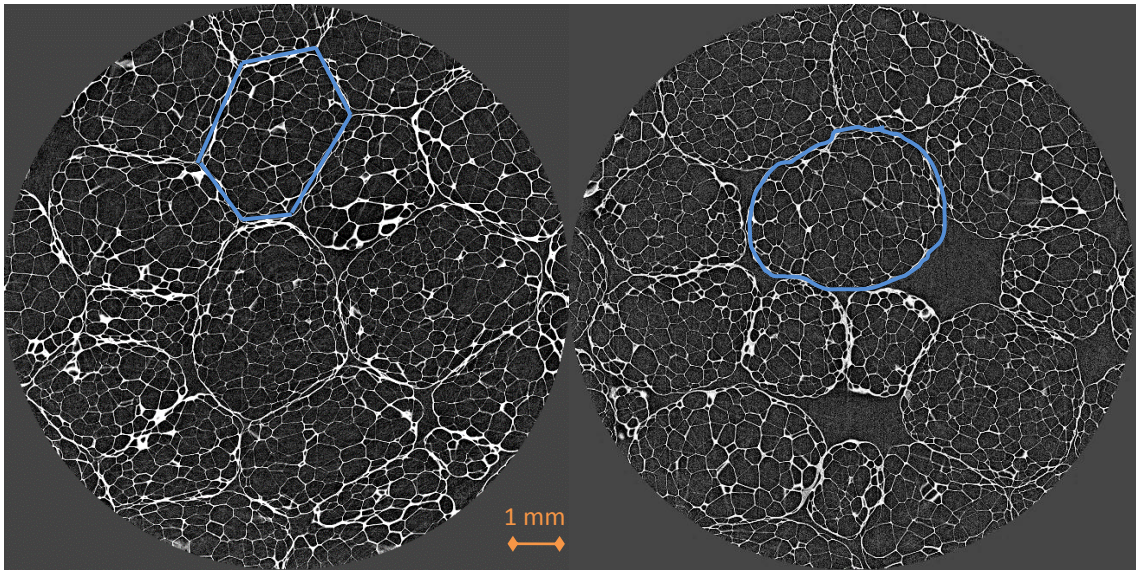

Figure 54: XY slice from a sample of unloaded EUEPP (left) and UKEPP (right) 80 kg.m^{-3} EPP

Based on the testing shown in Figure 32 and the equation discussed in Section 5.1.1, the fraction of material within the struts of a sample of UKEPP could be greater than that of EUEPP, explaining the reduced modulus. Figure 55 shows the internal structure of a bead from both manufacturers foam; some cells within the EUEPP foam show thicker cell walls and the thickness of each cell feature is relatively equal, there also appears to be more cells within the same area. Whereas the EUEPP sample seems to thin as the distance from each node is increased. As discussed previously, a fraction of material in the struts of 0.9 reduces the Young's modulus of the material, which agrees with the compression testing.

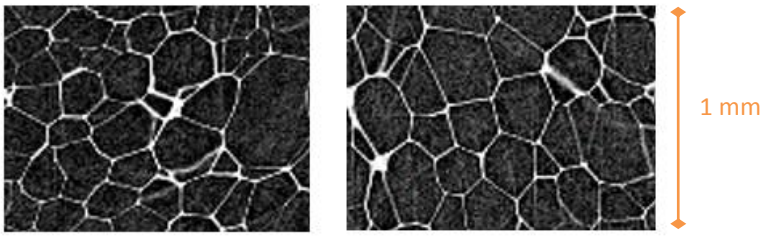

Figure 55: Cell Structure of an unloaded EUEPP (left) and UKEPP (right) 80 kg.m^{-3} EPP

In order to quantitatively analyse the data a linear intercept method could be used to count the number of cell walls and measure their thicknesses for both samples. Statistical analysis of the void sizes could give better information, an area that can be explored further.

5.7 In-situ Compression of Foam

Figure 56 a) shows the compression response of a sample of 80 $kg.m^{-3}$ EUEPP foam at a rate of 10 $\mu m.s^{-1}$. The following images, Figure 56 b - f, are XZ axis slices with strains from 0 to 0.8 in increments of 0.2. At a strain of 0.2 (c) the plateau phase is under way, meaning the cells have begun to collapse and the bead interactions are optimised. Some void space still remains as bead walls resists collapse. By a strain of 0.4 (d), towards the end of this samples plateau, bands of cell collapse have occurred which stem from the remaining voids; this suggests the voids are a point of weakness. The mechanism for cell collapse resembles the elastic plastic buckling, rather than the yield hinge shown in Figure 3. At the onset of densification, 0.6 (e), some beads still remain intact, showing the density distribution and therefore strength is attributed to a beads microstructure. Towards full densification little air space remains within the structure.

Figure 57 is a focus on the linear elastic region of EPP compression for a sample of EUEPP with the same density as the sample previously discussed. It shows a sample of 80 $kg.m^{-3}$ EUEPP foam that was compressed at a rate of 2 $\mu m.s^{-1}$ using the experimental procedure “Yield” - Table 17; it captured the first 10 percentages of strain. A strain of 0, 0.02, 0.05, 0.07 and 0.1 are shown, as well as the stress-strain response across those intervals. At 0.02 (c) strain the foams modulus is still resisting the yield, some displacement has occurred from the beads, but there is little sign of cell failure. At 0.05 (d) the material has yielding and is transitioning into the plateau, the image shows bands of cell collapse, and voids are beginning to fill. At 0.07 (e), where the plateau is almost reached, weaker bead walls are collapsing, still focussed around the bands of weakness; other areas have not begun to collapse. This remains the case at a strain of 0.1, demonstrating the collapse of cell walls occupies the plateau stage of compression.

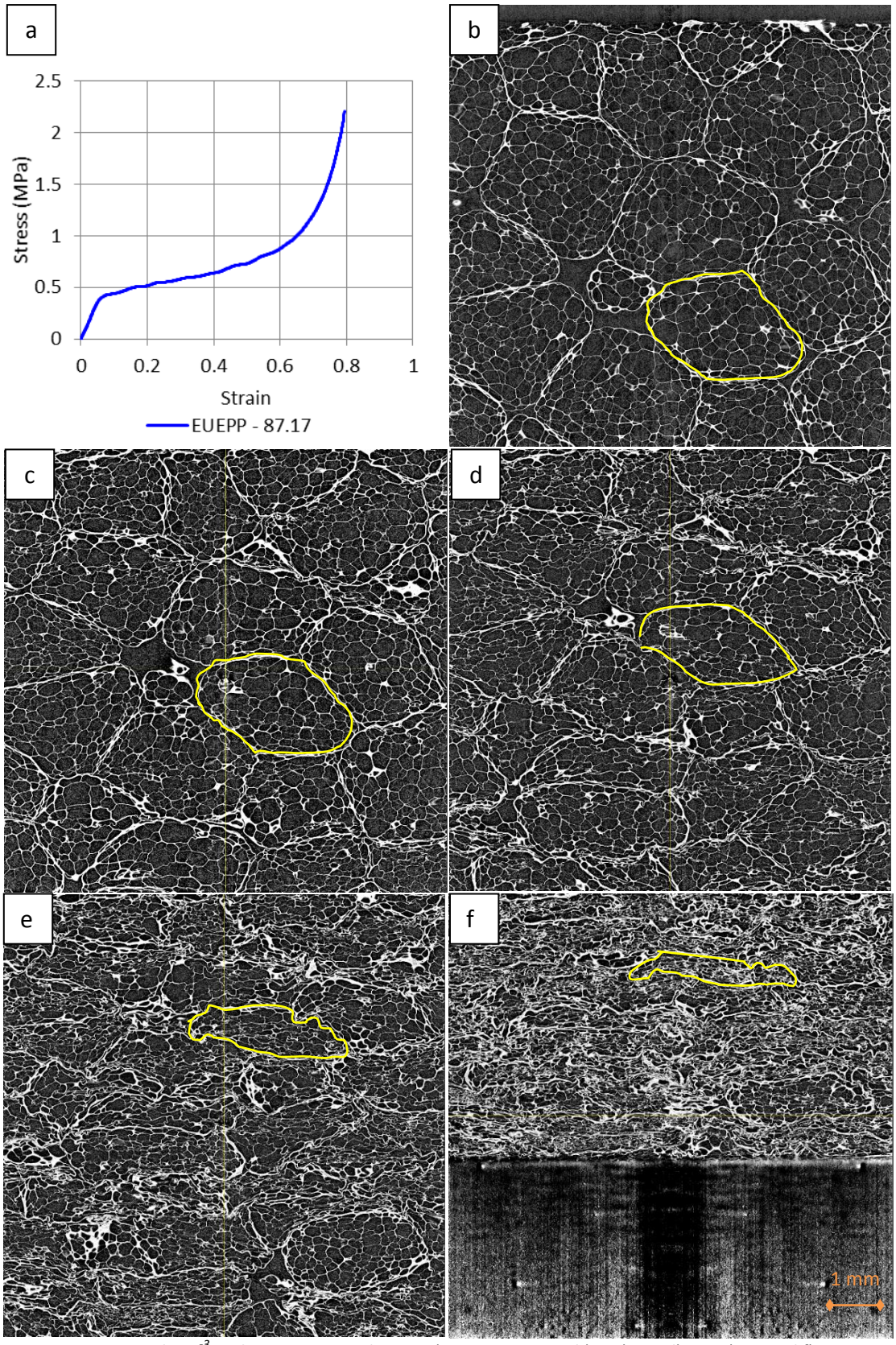

Figure 56: EUEPP 80 kg.m^{-3} under Macro B conditions: a) Stress Response b) 0, c) 0.2, d) 0.4, e) 0.6 and f) 0.8 strain. Highlighting the displacement and collapse of a bead (yellow)

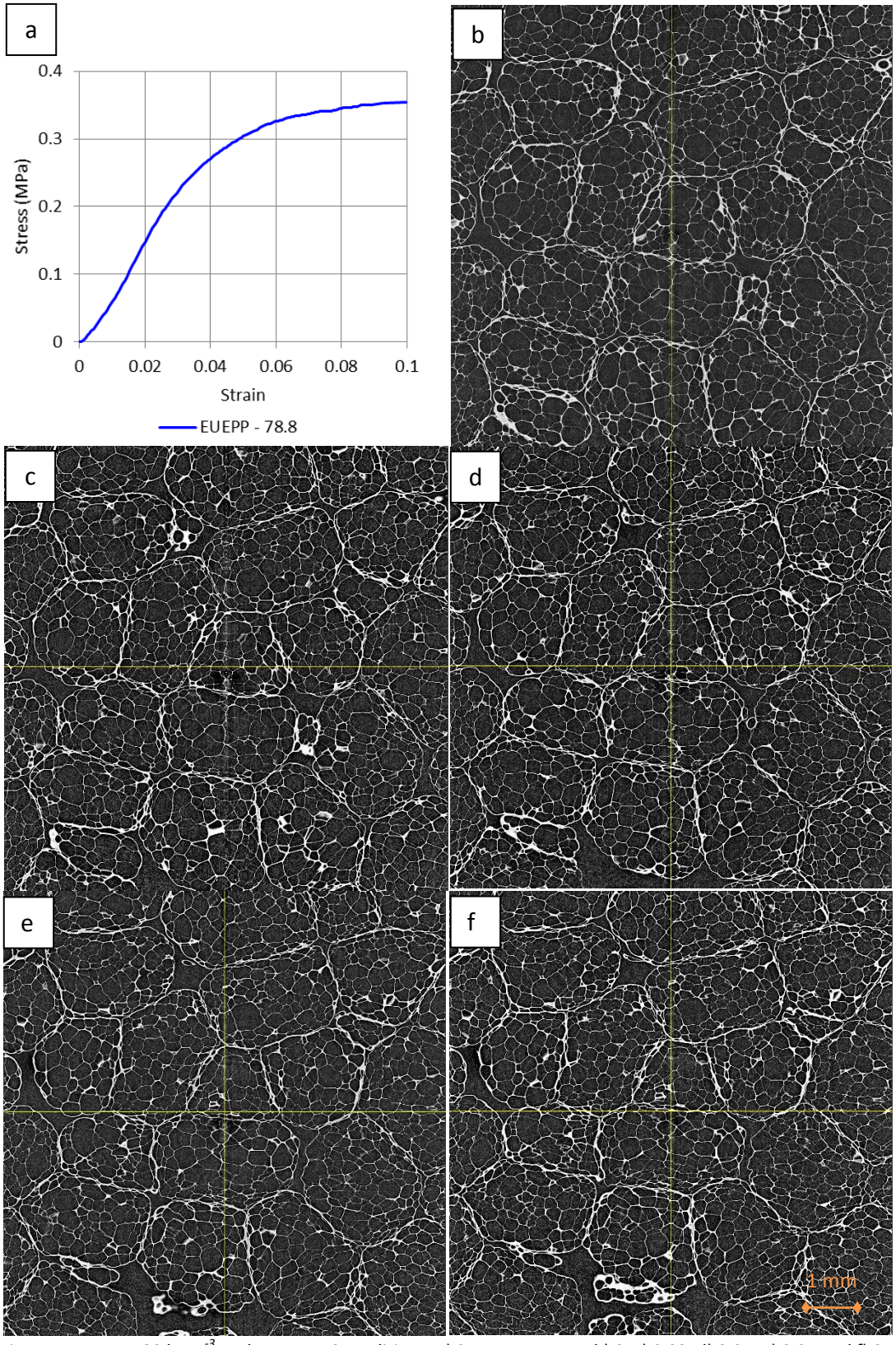

Figure 57: EUEPP 80 kg.m^{-3} under Macro C conditions: a) Stress response, b) 0, c) 0.02, d) 0.05, e) 0.07 and f) 0.1 strain.

From the images it is apparent that the struts bend during collapse, supporting Gibson and Ashby's equation assumption. However the assertion that foam is a homogenous

collection of cubic cells is not applicable to EPP foam. It is therefore recommended that the equations for modulus and yield be modified to incorporate a 4^{th} and 5^{th} term that represents the bead and void space morphologies respectively. Using the same approach as Gibson and Ashby, the equation to determine corresponding constants could be determined from the testing of the material. The new model would represent the contribution that each material characteristic has on the stress output during a compression.

5.8 3D Mesostructural Simulation

The cell structure of a bead of EUEPP 80 kg.m-3 was imported as a stack of TIF files into Simpleware ready for meshing. Simpleware is a commercial software that visualises and provides analyses of volumetric scans. It can read stacks of raw output or post-processed images including the previously discussed TIF format. Once the volume is rendered, Simpleware outputs a full 3D mesh, ready for FEA analysis. Some post processing was required, including threshold selection where the contrast of material was selected and transferred into a solid mass. Noise reduction was used to remove loose material or artefacts that appeared through scanning. Cell wall filling is a function used to join any remaining gaps that appear within the cell walls.

A fine tetrahedron mesh was used on the surface of the volume, small enough to contain two elements across the thickness of each cell wall (roughly 5 μm). This resulted in a model containing approximately 9 million elements (ELFORM 10). Using LS-DYNA, the meshed volume of the foam was compressed under similar conditions to that of testing.

The material was allocated the properties of a monolithic polymer material polypropylene. Three contacts were used; between the foam and each of the two plates and a final contact to prevent the foam passing through itself. The polymer definition used to represent the monolithic foam is MAT_PIECEWISE_LINEAR_PLASTICITY. The material model requires five property inputs; Density (RO), Young's Modulus (E), Poisson's Ratio (PR), Yield Stress (SIGY) and a load curve (LCSS). Tensile testing was carried out on the VHS for polypropylene

dogbones in order to produce a stress-strain curve. Digital Image Correlation (DIC) was utilised to obtain the strain response from each sample.

Figure 58 shows the two models, with a clear difference in structure. The laboratory scan shown in A appears like a block with holes in, however B shows a closed cell cellular structure that was previously shown in Figure 2b.

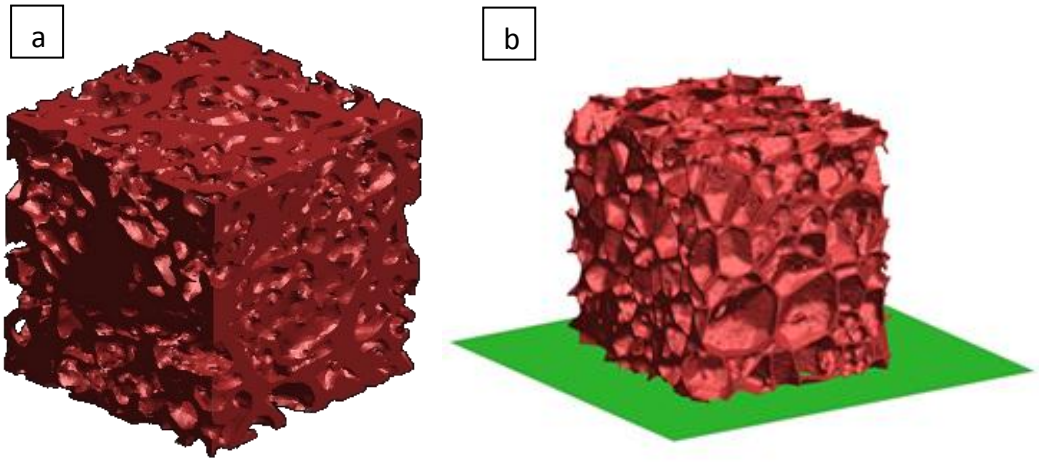

Figure 58: FEA models from a a) 50 micron resolution scan and b) a 5 micron resolution scan

Figure 59 is a size comparison between the volumes that were taken from each scan. The high resolution ESRF scan, in red, is smaller due to the computing limitations that a detailed mesh requires. It is clear in both comparisons that the cell structure has been lost almost completely with a resolution of 50 µm voxels.

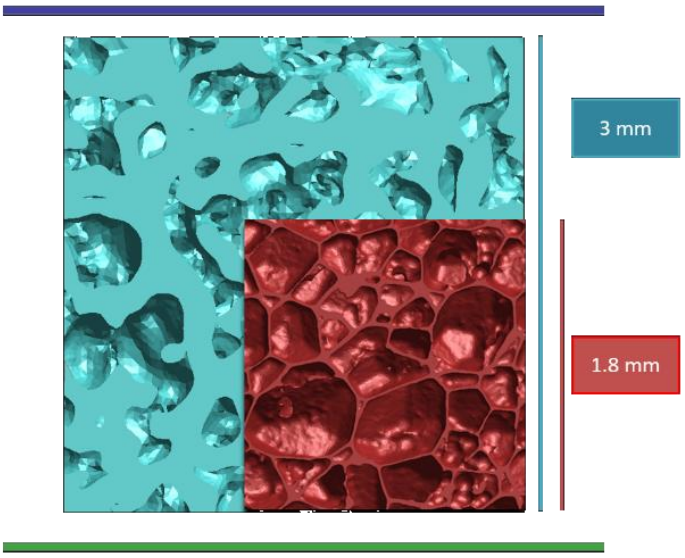

Figure 59: Size and resolution comparison between the two scans; ESRF - red, WMG - blue

The ESRF model has been used to predict the materials performance using a monolithic material definition of polypropylene, created using tensile data taken from testing done on the Instron 5800R. Figure 60 shows the different stages of compression, with yield and eventual densification. Figure 61 shows the strain contours from a slice taken from the same model. The model represents the buckling, instead of yield, as was seen within the µCT images. The plot shows that strain initiates across bands that are weak, and predominantly across cell walls rather than struts. Even under large displacements the strain within the struts is minimal.

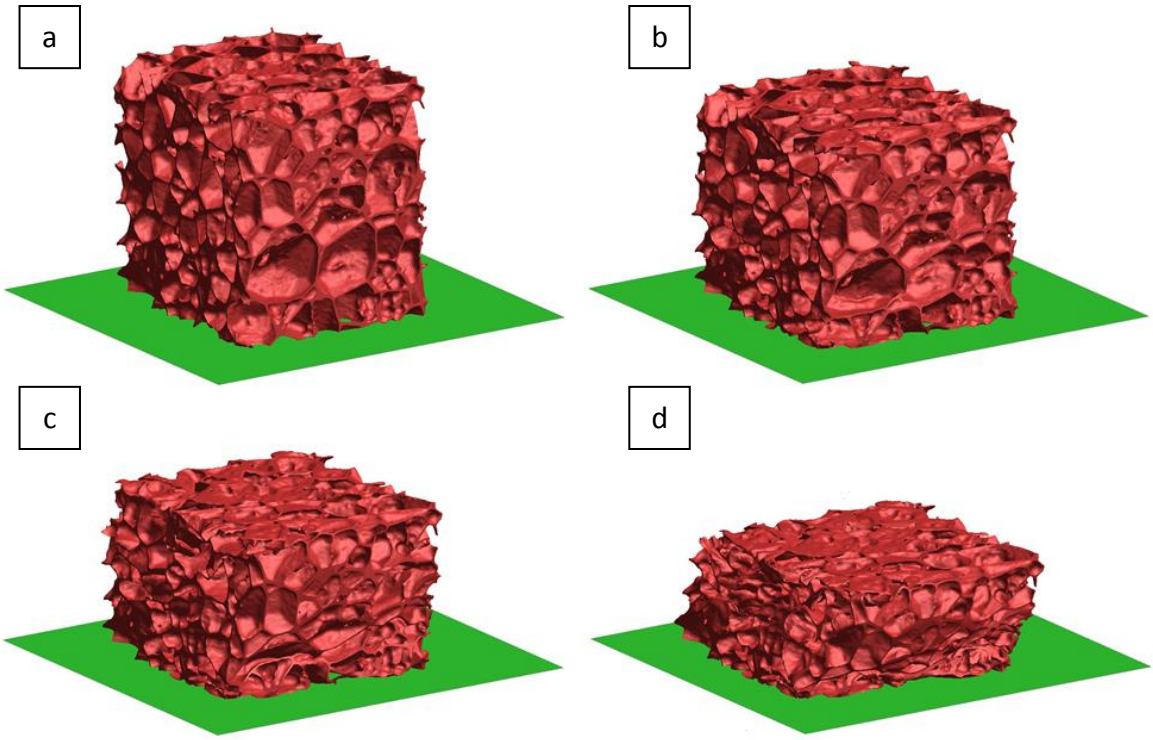

Figure 60: LS-DYNA Model of 80 kg.m^{-3} EPP at a) 0, b) 0.2, c) 0.4 and d) 0.6 Strain

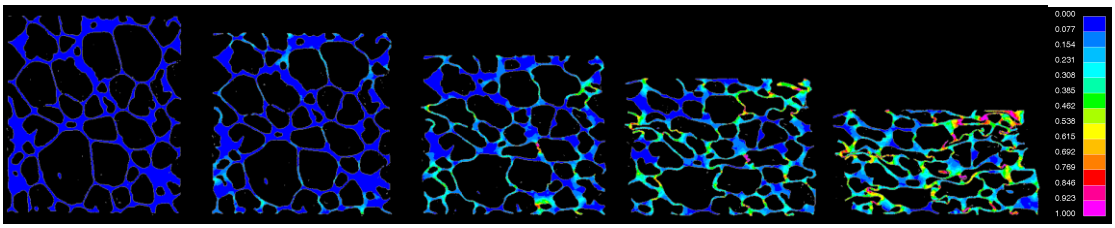

Figure 61: Strain distribution for a slice of 80 kg.m^{-3} EPP compressed in LS-DYNA

5.9 Summary

- A feasibility study has been conducted into the use of µCT to characterise material for JLR.
- Synchrotron radiation was used to view the in-situ compression of EPP; visualising the stages of compression a cell foam undergoes.
- High resolution images were converted into a mesh ready for FEA analysis.
- The DYNA model demonstrated the same buckling mechanism as the experimental tests.

A comparison has been made between the types of µCT that are available in the WMG laboratory and the synchrotron radiation accessible at the ESRF. There are great differences between the two; a lab source is commonly available but has a low resolution. A central facility such as the ESRF, has a very high resolution and high flux reducing the time required for each scan. The satellite building occupied by beamline ID19A uses a collimated beam; producing a very fine resolution which is ideal for microtomography.

The ESRF scans that yielded the best results had a resolution of 5.2 µm per voxel; the camera setup was 2016 x 2016 pixels sampling a specimen length of 10.48 mm. A beam power of 35 keV provided the greatest contrast from the imaging and a scan time of 2 seconds, 180 degree revolution, allowed for in-situ compression without creating image artefacts.

Differences between the manufacturer's foam microstructures were identified. A larger compaction force appears to be used by EUEPP, possibly with beads of a lower density to increase the number of beads that can be fitted into a mould. This results in a homogenous density that matches that of UKEPP. This is supported by the finding of Bouix et al, 2009, who found a sample with smaller cell sizes produced an improvement in material performance. Further analysis is required to understand other features effects on absorption mechanisms, for example the cell shape, bead wall thickness and cell strut thickness.

Simulation effort was limited by computing power in the time available, as the mesh preparation was all done in RAM. Therefore a small sample, 1.8 mm tall, was analysed. A resolution of 50 µm was found to be too large for producing an accurate FEA model, however 5.2 µm captured each feature in its entirety. The general behaviour of the model matches the CT images; a strain distribution also represent the theoretical analysis done. Currently the model is too unstable to predict the mesostructural stress-strain response and therefore further work is required.

The feasibility study has shown that JLR could utilise the µCT X-ray technology for material characterisation. Computed tomography is useful for viewing the internal structure of a material, which in turn aids in the characterisation of it. This can be coupled with a tensile or compression fixture for in-situ experimental responses with the use of facilities such as the ESRF. Circuit boards within the vehicles can be analysed using laminography in order to check the manufacturing process or post impact integrity. Radiography is a useful tool for viewing liquids and flow mechanics within components.

Contacts have been established in both the ESRF beamline team and the communications and publishing departments. They have expressed a desire to stay in contact with JLR and would appreciate hosting further research from them. An article centred on the placement has been published within the ESRF news, a publicly available document that highlights work and collaborations across all departments and beamlines.

The next chapter will highlight where the research has been adopted by JLR as well as the impact it could have.

6 Review of Research Impact

The work presented in this portfolio has been used by both Jaguar Land Rover (JLR) and other parties that have been involved across the project. This section discusses where work has been incorporated into each organisation, and how it has been useful to them.

6.1 Research within Submissions

The Material Characterisation and Technical Specialist, whom has supported the development of the project from within JLR, identified the JLR's requirement for this project. It is through this group that the datasets, material models and background information will be disseminated into the organisation for the employees use. Each submission has been tailored to document the processes used and summarise the findings; the information from them is therefore useful for the department to contribute through future work and discussions across the organisation.

The same department has created a new material database system within JLR and is the central location for all material data that the organisation uses. This database, covering testing, post processing and simulations (of which are discussed in Section 3 to 5) will be the location for all of the work provided to JLR, so that each user can see where the data has come from and how it was acquired. This is key to overcoming previous issues with traceability, such as the inability to find sources, replicate test methodologies and therefore validate data. With a robust source of information the testing is more reliable and the simulations are robust and consistent. Which in turn saves costs on physical testing and assists in designing products that keep the passenger safe within the vehicle.

6.2 Informative Documentation

The lack of traceability and repeatability of the data available to JLR was a starting point when the project specification was created. Therefore the key findings from each

submission has been split into more concise documentation for disseminating the information. This includes test methods, data processing and simulation output; each displayed on a one page document. This reporting system highlights where the material, data or model has come from, how it was used and all the prior information required to replicate it. By attaching these documents to JLRs database, it is simple for the user to quickly access information about the simulation they are running or to discover more about the material in general. This helps the end user select an appropriate material model from the database, with validation to back it up. The dataset available to JLR has been consolidated, with all Expanded Polypropylene (EPP) material models now represented by a single prefix. Each density also contains multiple strain rate input curves, reducing the requirements for model selection. By restricting the choice to a few robust and validated material models, each employee is modelling and producing output results using the same input; which is now accurate.

6.3 Material Testing and Database

JLR did not have an up-to-date test methodology for characterising energy absorbing materials. A new method, as well as the raw, processed and implemented test data has been supplied to them.

6.3.1 Test Methodology

The test methodology has been summarised across a double sided A4 sheet, similar to the previously discussed documentation. There is one for each machine used within the project; the Instron 5800R quasi-static rig, the Drop Tower and the VHS. The test methods are transferable to alternative machines, depending on which are available to the company. It also includes sample preparation for each. Each test machines specification is listed in Section 4.2.1 to 4.2.3.

6.3.2 Expanded Polypropylene Test Data

The raw data from EPP testing has been kept, as well as being converted into a format ready for simulation. The data from each density and manufacturer will therefore be supplied within spreadsheets, which can be attached to their internal material database. The procedure to convert raw data into an input curve ready for simulation has been discussed in Section 3.4.3.

Across the two manufacturers the range of densities tested are 30 to 120 $kg.m^{-3}$ at a range of quasi static to 100 s^{-1} strain rates. Previous data, shown in Table 2, contained inputs for 30 to 170 $kg.m^{-3}$; but were inaccurate and not assigned to a strain rate.

6.4 Simulation of Foam

The original purpose for this project was to improve the simulation capabilities and accuracy of JLRs models for energy absorbing materials. The focus has been put on EPP for passenger safety due to its isotropic and hysteretic properties and the lack of a peak yield stress. The modelling and material definitions used by JLR for this foam has therefore been analysed.

6.4.1 LS-DYNA models

The models created for coupon level validation and cylindrical testing have been supplied to JLR. They will be assigned to the database for access from the CAE department. Along with the models are the recommendation for simulating EPP, from mesh size and element choice to appropriate contact definitions. This information is essential for an engineer or end user to take material data from the database and create a safe and accurate model with it.

6.4.2 Material Models for Simulation

The simulation and research departments have access to all of the material definitions that have been created for EPP. This was done as a two stage process, initially replacing JLR's material models for MAT_LOW_DENSITY_FOAM with the same model type. The second stage followed full analysis of the material model MAT_FU_CHANG_FOAM, which is the final choice for simulating EPP. This new model adds capabilities that they were not using previous, such as strain rate effects and accurate hysteresis.

6.5 Spreadsheet for Data Extrapolation

Compression testing of foams becomes difficult during the densification stage due to the high forces that are experienced and the limitations a machines load cell has. Therefore it is typical to test the sample to a strain of 0.8. In order to enhance the data used for simulation, a review into extrapolating this incomplete curve was done. A spreadsheet has therefore been created to extend a materials stress-strain curve up to a strain of 1, keeping its original curvature during densification.

Some stress-strain data has exhibited intersections between the strain rate changes, noticeably on the drop tower testing. The same spreadsheet can be used to separate the curves, as is necessary for numerical stability during simulation.

6.6 Additional Contributions outside of Jaguar Land Rover

Outside of the project work presented, there have been contributions to external parties that were involved in the project. The following sections discuss what they were and how they were incorporated into the organisations.

6.6.1 ESRF User Documentation

While on the placement with ESRF, the organisation required documentation to be created for a compression fixture that is available for ID19. The user documentation illustrates each component within the press and how to operate it both mechanically and through the software. Having created the file, it has been made available to staff and users through the companies intranet page. A copy of the guide has been attached to the Appendix of *Submission Five - International Placement*.

The work with the ESRF has also led to discussions involving JLR and the possibilities for further research in Grenoble. It has served as a route for JLR to conduct research within this field.

6.6.2 EUEPP Data validation

It was agreed with EUEPP to provide feedback on their materials performance having tested it under different test conditions. They were specifically interested in the performance under a constant velocity compression test, opposed to the drop tower scenario they had previously investigated.

7 Conclusions and Recommendations

The aim of the research developed jointly with Jaguar Land Rover (JLR) were as follows:

- Research and deliver improved material characterisation and CAE techniques for simulating the behaviour of energy absorbing foams when subjected to high deflection, dynamic loading, specifically those that occur during vehicle crash events. (Chapter 2, 3, 4 and 5)
- Understand JLRs current foam material usage and functionality, CAE methodology and foam material models. (Chapter 2 and 3)
- Understand the important characteristics of current foams and identify weaknesses in current CAE methods. Investigate processing and environmental variability. (Chapter 3 and 4)
- Using DYNA CAE code, improve current modelling methods and develop a correlation test to validate improvements. (Chapter 3 and 4)

The key outcomes of the research are an improved virtual analysis capability, new test procedures and data analysis standards (ready for TPJLR format), a CAE dataset of validated EPP foam and a correlation test with the corresponding validated CAE model.

Through comparing computed tomography capabilities that were previously unknown to JLR, the characterisation possibilities for analysing the microstructure of foams have been presented (Chapter 5). From which an international placement took place.

The business opportunities that are available from the research include reduced occupant protection development time, improved and optimised designs which reduces package requirements, reduced issues within virtual prototype tests, fewer late changes based on validation tests and a development towards the introduction of new energy absorbing materials into the business.

The following sections summarise each evaluated subject area, broken down for clarity into characterisation, simulation, testing and computed tomography of EPP.

7.1 Characterisation

Chapter 2 summarises *Submission Two - Literature Review*, a review of energy absorbing materials. The following areas were identified for investigation:

- Manufacturing methods and the effect they have on sample orientation, density distribution and microstructure.
- Analytical solutions used to predicting a foams compressive stress output. The contribution of stress was attributed to three main cell structure features, the cell struts, the cell faces and the pocket of air within each cell.
- Testing conditions with a specific look at the effect strain rate has on a foams performance.
- Simulations within the FEA package LS-DYNA for representing foam as a continuum model, using the appropriate material models.
- The possible use of computed tomography for evaluating a foams structure and therefore potential performance during compression.

Polymeric foams became the leading material with suitability for passenger safety; this included Rigid Polyurethane (PUR), Expanded Polystyrene (EPS) and Expanded Polypropylene (EPP). These materials are relatively isotropic when compared to an alternative honeycomb sheet. PUR is affected slightly by expansion direction, whereas the beaded material are fully isotropic. PUR and EPS exhibit fracture damage and material expulsion during compression testing, unlike EPP. UKEPP advertise their material as having “good recovery” and the material returned to 90 percent of its original shape after near full compression.

EPP was being used by JLR, however the characterisation methods were not being utilised, resulting in a lack in confidence for simulation predictions. Prior to the research this required physical testing of a component for head impact evaluations, each test using a fresh body shell; which has limited availability and is expensive.

7.2 Simulation

Chapter 3 was a summary of the work presented in *Submission Two – Simulation Development*. With a focus on EPP foam, the CAE capabilities, methods and results of modelling such a material were reviewed. The following stages of research were undertaken:

- Evaluation of JLRs geometric and material models, identifying what the cause is for inaccurate FEA outputs. In some cases the stress-strain curves lacked detail and the material properties did not match the sample being simulated.
- Simulation methods developed from literature and coupon simulations. The use of 5 mm mesh in the element formulation 10: 1 point tetrahedron element type provided the best results for EPP foam.
- Comparison between JLRs previous material model, MAT_57, and a recommended, MAT_83, model showed the improvement in EPP simulation; incorporating strain rate sensitivity.
- Manufacturers of EPP were consulted, supplying a dataset ready for simulation and validation.

A review was performed into JLRs datasets within their CAE simulations of polymer foam, specifically on the material models for EPP. Having confirmed issues within the models it was identified that a new dataset was required. A collaboration was formed with a European manufacturer (EUEPP) of EPP, a company that already supplied raw polypropylene beads to a second tier supplier (UKEPP). An analysis was done to show the differences between EUEPPs test data and those used for JLRs simulations. Figure 62 shows the input curves from both, as well as material testing done on the Drop Tower testing machine. The original data had few data points and therefore missed key features within the stress-strain response, including the yield and densification stage.

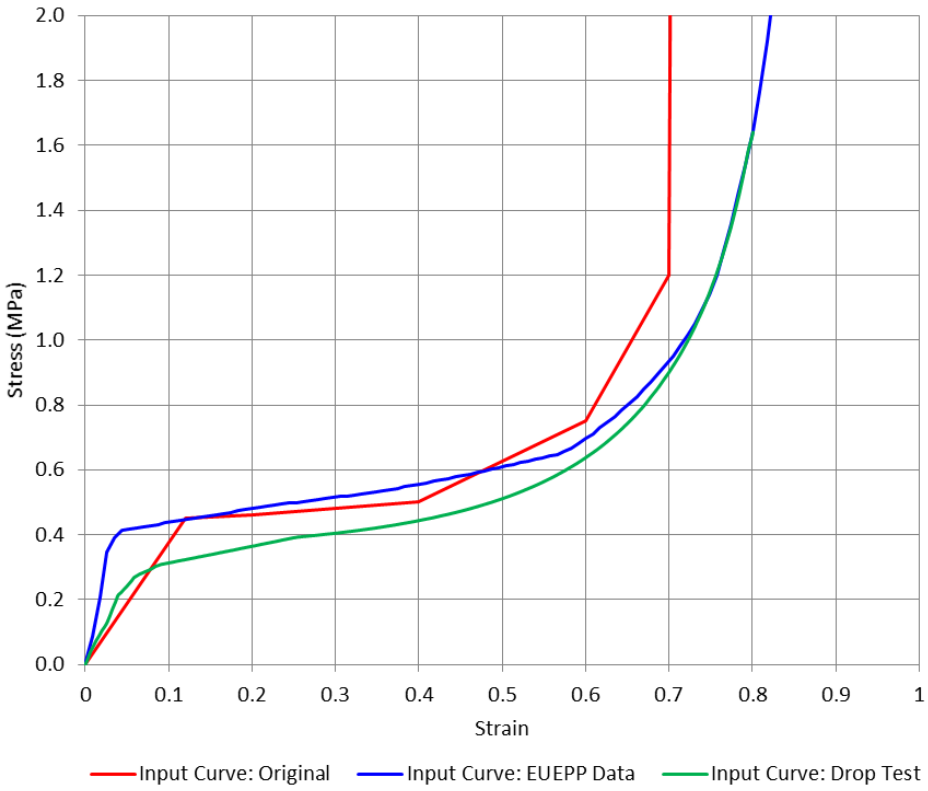

Figure 62: Material Model input curves used to compare the cylindrical impact simulations

A direct replacement of JLRs material models was proposed and quickly used within the organisation for modelling their EPP. However the material model choice required an upgrade to a more appropriate model that required validation. All methods and solutions have been documented for JLR use.

The simulation procedures and geometric models were reviewed in order to identify improvements within their simulation methodologies. A full modelling method has been proposed, suggesting element, mesh and contact properties; along with the results to justify each decision.

With the new modelling capabilities, an upgraded material dataset was validated, utilising a material models strain rate capabilities. The new material models have shown clear improvements when compared to physical and simulated validation tests, as shown in Figure 63. The new material models have reduced the residual error by 93% compared with the original JLR dataset.

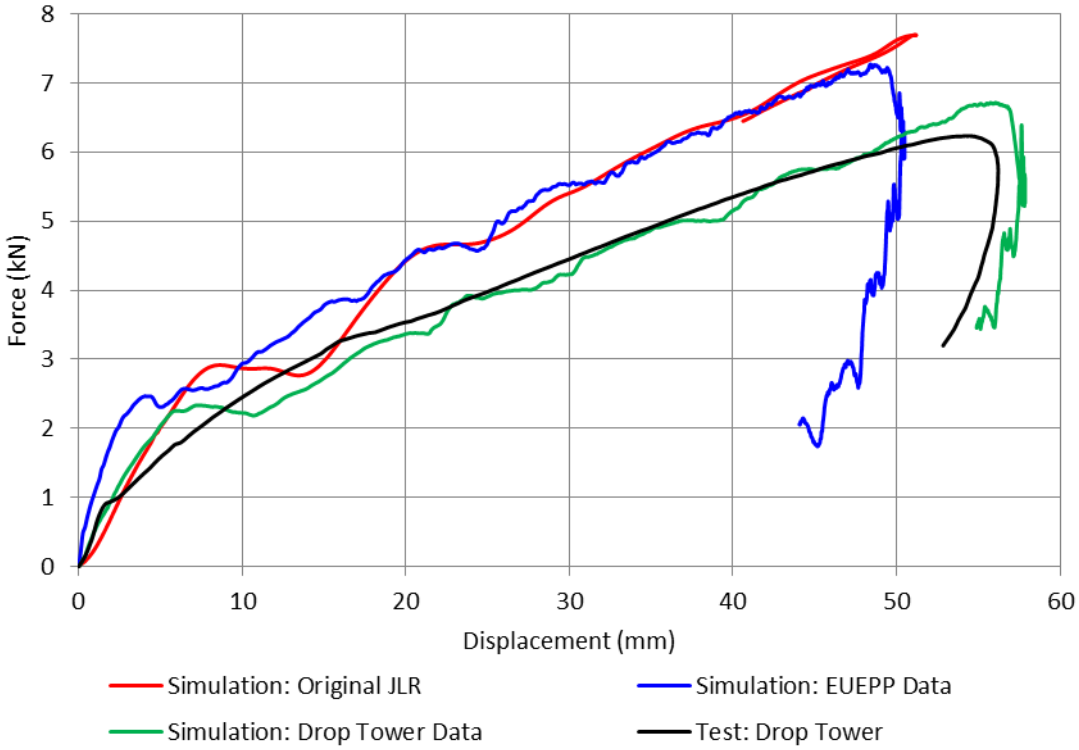

Figure 63: Comparison between material models used for cylindrical impact simulations of 50 kg.m^{-3} EPP; created using Original JLR Data, ARPRO Data and Validation Data

The change in material model has provided an increase in virtual prototype reliability. Something that had been diminishing, and resulted in an increase in full vehicle physical tests. An increase in reliability of results saves on development time and cost.

7.3 Material Testing

Chapter 4 contains the work presented in *Submission Three – Geometry Investigation*. Having created simulation models for EPP and obtained material from two manufacturers, research into the following areas was done:

- Sample selection and preparation ready for both coupon testing and component validation.
- Test methodologies on three test machines that provide different load cases for compression testing. Quasi-static, Drop Tower and VHS, all of which can be converted into a TPJLR ready for use.
- Data processing for converting the raw data into a format ready for CAE analysis.

- Evaluation of EUEPP datasets previously used to support simulation.
- The differences in manufacturers foam at different strain rates, investigating the possibility of performance change due to processing methods.
- Updated material models and the validation of previous simulation iterations plus the use of Digital Image Correlation to view the distribution of strain across a sample.
- A focus on sample density was done by analysing the production methods that result in density distribution, skin layer and multiple layers of foam.

The physical testing required to both validate the datasets previously implemented and to characterise future energy absorbing materials have been supplied as separate documents. They cover sample size, preparation methods, data acquisition and post processing. Test methodologies have been created for three testing machines, a low strain rate Instron 5800R, an impact test Drop Tower and a constant velocity Very High Strain rate (VHS) testing rig. The change in load cases were used to replicate different loading conditions on the material. A deceleration in drop tower mass results in a decrease in stress, usually beyond the yield point.

Using each machine the effect of strain rate on EPP was investigated. The results demonstrated that up to a speed of 5 $m.s^{-1}$, the materials Young's modulus, yield stress, plateau stress and the strain at which densification begins all increased. The strain for densification decreases.

A comparison between manufacturers, EUEPP and UKEPP, demonstrated the difference in performance that two samples of EPP with the same density can exhibit, this was also supported by µCT analysis. It highlights the implications of receiving EPP as a second or third tier material; and that it should be designed based on a manufacturers capabilities. The conclusion drawn was that JLR should not treat foam components as a commodity item, instead managing supply chains to check delivered items match the simulated counterpart. The production process also creates a density distribution, with a higher impact as a samples size increases.

A skin layer that is produced by the internal surfaces of a mould has been shown to increase the samples stiffness. The larger the mould, the thicker this layer becomes,

but it does not have a significant effect on the compressive response. However the slight increase in yield stress should be accounted for when designing components.

EPP is not effected by the size of a sample, all of which comply with the British Standard ISO 844. A range of cube and rectangular samples produces the same stress-strain compression response. Dimensions tested were 50 x 50 x 50 mm^3, 100 x 100 x 100 mm^3, 200 x 200 x 100 mm^3 and 100 x 50 x 50 mm^3.

The difference between a decelerating mass and a constant velocity compression plate has been analysed using the Drop Tower and VHS. The deceleration results in a decreasing strain rate over strain, and therefore reduces stress towards the end of a compression, this is important when designing a component that will reach strains greater than 0.6.

The Drop Tower was used to investigate the strain rate of samples, however there was a large amount of crossover in results. Also an increase in strain rate meant more energy within the system and therefore a change in compression percent.

Using the test methodology on the VHS, a study was performed on the effect of stacked material under varying strain rates, with large density change across each layer. It has been shown that the initial pulse of stress curing a compression can be reduced, which is a contributing factor to the Head Injury Criteria used to quantify a vehicles safety. The materials response can be customised in order to reduce initial stress, but increase the gradient of the plateau. This can also be used within smaller spaces, such as interior trim.

7.4 EPP Microstructure

Chapter 5 was a summary of the µCT work carried out on two types of X-ray sources; the laboratory equipment available at WMG and the central facility ESRF. The work is supported by *Submission Four – Micromechanics of Polymer Foam using Computed Tomography* and *Submission Five – International Placement*. The research was divided between:

- The internal structure of EPP and the mechanisms for absorbing energy that arise from the microstructure.
- The international placement that took place at the ESRF in Grenoble, from which the use of synchrotron radiation was developed.
- In-situ scanning available due to high divergence and flux produced from a synchrotron source. As well as the experimental procedures used to scan the three main stages of compression within a foamed material.
- The differences between manufacturers foam on a microstructural scale, to help understand the consequent compressive behaviour variation.
- The development of a mesostructural 3D simulation to help predict the mechanical response of EPP

The feasibility of using µCT has previously not been explored by JLR. Two facilities were investigated, both locally and internationally; with a range of X-ray source energies. The best results were produced using synchrotron radiation at the ESRF. Using a beam energy of 35 keV and a resolution of 5.2 µm, detailed images of expanded polypropylene were captured. For the first time, unidirectional compression of two manufacturers EPP foam was scanned during an in-situ compression test using synchrotron radiation.

An in-situ experimental setup equated the materials visual response to the load that is being applied and the percentage of compression reached. This demonstrated the mechanisms that EPP uses to absorb energy and were related back to the analytical solutions discussed in the literature. The information can be used to improve manufacturing processes, to enhance the EPP performance and can assist in the development and understanding of EPP research. This includes the yielding criteria; it was observed that EUEPP has a higher modulus, yield and plateau stress, which can be related to the noticeable increase in material within each foam.

The images were also converted into a mesh, ready for FEA analysis. Buckling occurred in bands of weakness during the plateau phase of compression.

The use of synchrotron radiation has been demonstrated as a feasible option for JLR. Alternative uses to computed tomography were also discussed. Non-destructive

scanning can be used to inspect supplier's material, so a required microstructure can be checked, rather than a density.

7.5 Summary of Key Achievements and Contributions to Innovation

The following is a list of the key achievements accomplished through the research presented in this report. It also highlights where the contributions have been made to JLR and therefore provided the company with a source of innovation.

- Documentation has been assimilated into JLR through their material database for testing and simulation procedures. They are accessible by engineers employed at JLR to test and model EPP consistently
  - Methodologies for testing have been established for three compression test machines: Instron 5800R, Drop Tower and VHS
    - This improves traceability of results and repeatability of testing to ensure the data can be reviewed and kept up to date
  - Methodology for geometric and material modelling within LS-DYNA have been produced
    - Validation models are available for checking simulation correlation
  - A collaboration with a foam manufacturer has led to further use of EPP within JLR vehicles
    - An EPP working group was consequently formed to guide the use of the material forward
- The use of polymeric foams in the automotive industry has been investigated. A full characterisation of EPP has been carried out for JLR
  - Production methods have been studied to improve on JLRs material understanding
    - Larger samples than those analysed in the literature have been tested; which are more suitable for automotive application
    - The degree to which density can vary across a sample has been investigated for both large and small samples, related to the location within a mould

        - The possibility of stacking multiple layers of EPP was checked, it revealed a change in yield stress and plateau mechanic can occur. The customisation of a materials stress-strain output is possible
    - Procedures are in place for characterising new energy absorbing materials; as alternative foams or structures become available
- The mechanical response of both coupon and component tests of EPP on a range of test machines were presented
    - A dataset of results, from raw to processed data, is available to JLR within the database and their material models
    - The research produced a review of two current EPP suppliers to JLR
        - Material responses change with production methods; the consequence of which was demonstrated. Possible reasons for this were discussed with the aid of computed tomography
    - Different load cases on foam were compared; a constant velocity impact exhibited a decrease in densification strain
        - Comparison was done with a commonly used drop tower test that exhibits deceleration of the drop mass during compression
        - The VHS was used to evaluate the effect of strain rate change to a samples mechanical response; the rate was related to analytical solutions and can be explored further using µCT
- Simulation of EPP within LS-DYNA
    - Material models have been evaluated for the modelling of EPP
        - Replacements to JLRs old material models are now in use within the organisation; the new models contain strain rate effects which improved model accuracy
        - A reduction of residual error by 93% was shown with validation tests, improving reliability and confidence in simulation fidelity
    - Digital Image Correlation has shown that strain distribution is accurately calculated within simulation for complex load cases
- Computed Tomography has been used to analyse the microstructure of EPP under a unidirectional compressive load
    - A review of µCT facilities available to JLR has been made

    - In-situ compression scans are now available for an in depth foam analysis
- A Mesostructural model been used to enhance failure understanding
    - It highlighted the possibilities for material characterisation that stems from it

7.6 Further Work

The following section discusses the restraints and limitations that were put on this project, which will lead into where it can be expanded upon and developed further. It has also created questions within polymer foam characterisation which could be further explored.

7.6.1 Material characterisation

JLR have the supply chain in place for ordering EPP components; which made it the focus for simulation fidelity. Using the characterisation methods presented to them, alternative foamed material can be investigated; including the use of synthetic foam that allows for a microstructure to be created and enhanced.

The contribution of comfort foam to energy absorption has also not been investigated, for example soft PU that is used within the headrest and seating may have a high air pressure contribution to stress levels when encased in a sealed leather casing. This can also be related to the multiple layered study discussed in Section 4.7.3, with an avoidance of peak stresses during the onset of yield.

7.6.2 Utilising EPP

Coupon testing has been fully evaluated for EPP, as well as a component used within a JLR Vehicle. Often components are designed to fill a space that is provided, instead of shaping the material based on desired mechanical response. An investigation of sample shape could be taken further, including the use of bored holes and surface geometry. The stress-strain response, coupled with layers of stacked density could be

customised further. Changing the compression curve of the material could lead to improvements in the Head Injury Criteria values that are used to characterise a vehicle. A safer part may require less space, which can reduce costs for production and be used for alternative components.

Some parts are moulded around structural materials, for example the head rest and the steel bar that holds it in place. The effect of a harder component through the object has not been tested. Although simulations are in place at JLR to represent this.

7.6.3 Material Testing

The capabilities of the VHS were limited to a velocity of 5 $m.s^{-1}$, which equates to a strain rate of 100 s^{-1} for the smaller samples used. An investigation into the effect of greater strain rates could reiterate the change of collapse mechanism that the foam undergoes. Components as thin as 10 mm will undergo a strain of 500 s^{-1} under the same velocity impact.

Samples sizes that comply with standards and the testing conditions used by EUEPP were evaluated. However samples below 50 x 50 x 50 mm^3 and above 200 x 200 x 100 mm^3 were not. Although an effect of sample size did not affect the response at this level, outside this range may show otherwise, especially as the material size increase and increase the required time for air to escape. The sample size may influence which collapse mechanism is exhibited.

7.6.4 Production

The manufacturing process could be replicated on a smaller scale in order to evaluate the effect of mould shape, compaction load, air injection temperature and mould temperature. The effect this has on test samples and a closer look at the microstructure could produce a manufacturing methodology for improved material performance. The analytical solutions have shown that the fraction of material within

the cell struts and that within the cell walls contributes to the materials modulus, yield stress and plateau stress.

7.6.5 Simulation

Due to the materials hysteretic effect the damage decay feature was not used within simulations. It is recommended that the function be evaluated in case an algorithm can be assigned that increase material decay as a function of strain rate.

The material models used are homogenous, creating a continuum component. This does not consider the effect of a skin layer, unless the stress-strain input data was tested using it. A coating could be applied to the geometry models with the adjustable thickness values that would represent a moulded component, improving the stiffness of the material. It should be investigated whether the air pressure calculation would be affected, due to a thicker barrier reducing expulsion. There is also a compromise between detailed material response and computation power required to run such a model.

7.6.6 Computed Tomography

In-situ compression of polymer foam was limited by the strain rate at which a sample could be scanned without causing image artefacts. Alternatively the sample can be tested at a high strain rate prior to using µCT and would not require the use of synchrotron radiation. An evaluation of the internal structure may then show the cause for change in performance, possibly showing the strut fracture oppose to buckling.

Further analysis of the computed tomography images can be done using volumetric and quantitative methods. Measuring the void count, number of cell wall thicknesses and strut volume which would show clearly the effect of density distribution on the smaller samples used for testing. As well as the difference between manufacturers methods.

It is apparent in the images that three main features are the cause of energy absorption for EPP, these are the interaction between bead walls, and the voids that remain outside of them as well as the internal cellular structure. The analytical solutions could be adapted for EPP as a function of these three mechanisms.

A mesostructural model has so far evaluated the internal cellular structure, which was limited by the computing power available. By utilising a cluster, each of the three features discussed could be modelled, with a larger model incorporating all three. This would improve on the stress-strain response that is output by the model in compression.

The same test method can be applied to a range of energy absorbing materials, from in-situ scanning to 3D modelling and simulated compression.

7.6.7 Review for Jaguar Land Rover

The testing used for evaluating Head Impact Criteria modelling was conducted by JLR. The data presented highlighted the need for an assessment of this method. Also the full body model incorporates noise from the surrounding modelled components, which in turn require evaluation for material model accuracy. The test methods applied could therefore be used on a bilateral appraisal of alternative materials used within their vehicles.

Using the collaboration established with EUEPP, JLR can explore alternative uses of EPP around the vehicle. Assisted by EUEPPs automotive contributions with alternative suppliers.

Through the proposed research of manufacturing processes, it would be possible to collaborate with UKEPP to develop the procedure and produce a full scale demonstrator, as well as improving their methods and therefore materials performance, beneficial to both themselves and their customers.

References

Alkhader, M., Vural, M., 2008. Mechanical response of cellular solids: Role of cellular topology and microstructural irregularity. International Journal of Engineering Science. 46, 1035-1051.

Andena, L., Caimmi, F., Leonardi, L., Ghisi, A., Mariani, S., Braghin, F., 2016. Towards Safer Helmets: Characterisation, Modelling and Monitoring. Procedia Engineering. 147, 478-483.

Ashby, M.F., 2006. The properties of foam lattices. Philosophical Transactions of the Royal Society A: Mathematical, Physical and Engineering Sciences. 364, 15-30.

Avalle, M., Belingardi, G., Ibba, A., 2007. Mechanical models of cellular solids: Parameters identification from experimental tests. International Journal of Impact Engineering. 34, 3-27.

Borazjani, S., Belingardi, G., 2017. Development of an innovative design of a composite-sandwich based vehicle roof structure. Composite Structures. 168, 522-534.

Bouix, R., Viot, P., Lataillade, J., 2009. Polypropylene foam behaviour under dynamic loadings: Strain rate, density and microstructure effects. International Journal of Impact Engineering. 36, 329-342.

British Standards Institution, 1997. BSENISO 3386 1 1997 Polymeric materials cellular flexible - stress strain characteristics in compression.

British Standards Institution, 2009. BSENISO 844 2009 Rigid cellular plastics - determination of compression properties.

Brydon, A., Bardenhagen, S., Miller, E., Seidler, G., 2005. Simulation of the densification of real open-celled foam microstructures. Journal of the mechanics and physics of solids. 53, 2638-2660.

Chakravarty, U.K., 2010. An investigation on the dynamic response of polymeric, metallic, and biomaterial foams. Composite Structures. 92, 2339-2344.

Croop, B., Lobo, H., 2009. Selecting material models for the simulation of foams in LS-DYNA. 7th European LS-DYNA Conference.

Cronin, D., Ouellet, S., 2016. Low density polyethylene, expanded polystyrene and expanded polypropylene: Strain rate and size effects on mechanical properties. Polymer Testing. 53, 40-50.

De Pascalis, F., Nacucchi, M., Scatto, M., Albertoni, R., 2016. Quantitative characterisation of low-density, high performance polymeric foams using high resolution X-ray computed tomography and laser confocal microscopy. NDT & E International. 83, 123-133.

Di Prima, M., Gall, K., McDowell, D. L., Guldberg, R., Lin, A., Sanderson, T., l Campbell, D., Arzberger, S. C., 2010. Deformation of epoxy shape memory polymer foam. Part I: Experiments and macroscale constitutive modelling. Mechanics of Materials. 42, 304-314.

Di Prima, M.A., Gall, K., McDowell, D.L., Guldberg, R., Lin, A., Sanderson, T., Campbell, D., Arzberger, S.C., 2010. Deformation of epoxy shape memory polymer foam: Part II. Mesoscale modelling and simulation. Mechanics of Materials. 42, 315-325.

ESRF, 2016. Find a Beam Line. [Online] Available at: http://www.esrf.eu/UsersAndScience/Experiments/Beamlines. [Accessed 17 July 2016]

Fernandes, F.A.O., Jardin, R.T. Pereira, A.B. Alves de Sousa, R.J., 2015. Comparing the mechanical performance of synthetic and natural cellular materials. Materials & Design. 82, 335-341.

Gibson, L.J., Ashby, M.F., 1999. Cellular Solids: Structure & Properties. 2nd Ed. Cambridge University Press.

Guo, Y., Hossieny, N., Chu, R., Park, C., Zhou, N., 2013. Critical processing parameters for foamed bead manufacturing in a lab-scale autoclave system. Chemical Engineering Journal. 214. 180-188.

Jiang, B., Zhu, F., Jin, X., Cao, L., Yang, K., 2013. Computational modeling of the crushing behavior of SKYDEX® material using homogenized material laws. Composite Structures. 106, 306-316.

Jin, H., Lu, W., Scheffel, S., Hinnerichs, T., Neilsen, M K., 2007. Full-field characterization of mechanical behavior of polyurethane foams. International Journal of Solids and Structures. 44, 6930-6944.

Kabir, Md E., Saha, M. C., Jeelani, S., 2006. Tensile and fracture behavior of polymer foams. Materials Science and Engineering: A. 429, 225-235.

Koohbor, B., Ravindran, S., Kidane, A., 2017. Effects of cell-wall instability and local failure on the response of closed-cell polymeric foams subjected to dynamic loading. Mechanics of Materials. In Press.

Lachambre, J., Maire, E., Adrien, J., Choqueuse, D., 2013. In situ observation of syntactic foams under hydrostatic pressure using X-ray tomography. Acta Materialia. 61, 4035-4043.

Maheo, L., Viot, P., 2013. Impact on multi-layered polypropylene foams. International Journal of Impact Engineering. 53, 84-93.

Mills, N.J., 2007. Polymer Foams Handbook: Engineering and Biomechanics Applications and Design Guide. Butterworth-Heinemann.

Ouellet, S., Cronin, D., Worswick, M., 2006. Compressive response of polymeric foams under quasi-static, medium and high strain rate conditions. Polymer Testing. 25, 731-743.

Ozturk, U., Anlas, G., 2011. Finite element analysis of expanded polystyrene foam under multiple compressive loading and unloading .Materials & Design. 32, 773-780.

Pask, R., Blair, G. R., Weierstall, M., 2007. The Time is Right for Harmonization of Foam Standards. [ONLINE] Available at: http://www.moldedfoam-ip.com/linkedpdf/Technical%20Info%20-%20The%20Time%20is%20Right%20for%20Harmonization%20of%20Foam%20Standards%20(final).pdf. [Accessed 18 April 13].

Raps, D., Hossieny, N., Park, C.B., Altstädt, V., 2015. Past and present developments in polymer bead foams and bead foaming technology. Polymer. 56, 5-19.

Sambamoorthy, B., Halder, T., 2001. Characterization and component level correlation of energy absorbing (EA) polyurethane foams (PU) using LS-DYNA material models. 3rd European LS-DYNA Conference.

Semerdjiev, S., 1982. Introduction to Structural Foam. Society of Plastics Engineers Incorporated (SPE).

Serifi, E., Hirth, A., Matthaei, S., Mullerschon, H., 2003. Modelling of foams using MAT_83 – preparation and evaluation of experimental data. 4th European LS-DYNA Users Conference.

Sun, Y., Li, Q.M., 2015. Effect of entrapped gas on the dynamic compressive behaviour of cellular solids. International Journal of Solids and Structures. 63, 50-67.

Thiyahuddin, M.I., Gu, Y.T., Thambiratnam, D.P., Thilakarathna, H.M., 2014. Impact and energy absorption of portable water-filled road safety barrier system fitted with foam. International Journal of Impact Engineering. 72, 26-39.

Viot, P., Maheo, L., Mercier, A., 2011. Behaviour of polymeric multiscale foam under dynamic loading -study of the influence of the density and the walls of beads. International Journal of Research and Reviews in Applied Sciences. 7. 1-19.

Weiβenborn, O., Ebert, C., Gude, M., 2016. Modelling of the strain rate dependent deformation behaviour of rigid polyurethane foams. Polymer Testing. 54, 145-149.

Wijnands, S. 2010. Volumetric behavior of polymer foams during compression and tension. [ONLINE] Available at: http://www.mate.tue.nl/mate/pdfs/12240.pdf. [Accessed 25 April 13].

Yang, X., Xia, Y., Zhou, Q., 2011. Influence of stress softening on energy-absorption capability of polymeric foams. Materials & Design. 32, 1167-1176.

Zhang, L., Gurao, M., Yang, K H., King, A I., 2011. Material characterization and computer model simulation of low density polyurethane foam used in a rodent traumatic brain injury model. Journal of Neuroscience Methods. 198. 93-98.

Zhang, X.F., Andrieux, F., Sun, D.Z., 2011. Pseudo-elastic description of polymeric foams at finite deformation with stress softening and residual strain effects. Materials & Design. 32, 877-884.

Zhou, Y.J., Lu, G., Yang, J.L, 2015. Finite element study of energy absorption foams for headgear in football (soccer) games. Materials & Design. 88, 162-169.